

1982

Atmospheric anisotropy and its effect on the delay power spectra of tropospheric scatter radio signals

Hosny Mohammed Ibrahim
Iowa State University

Follow this and additional works at: <https://lib.dr.iastate.edu/rtd>

 Part of the [Electrical and Electronics Commons](#)

Recommended Citation

Ibrahim, Hosny Mohammed, "Atmospheric anisotropy and its effect on the delay power spectra of tropospheric scatter radio signals " (1982). *Retrospective Theses and Dissertations*. 7507.
<https://lib.dr.iastate.edu/rtd/7507>

This Dissertation is brought to you for free and open access by the Iowa State University Capstones, Theses and Dissertations at Iowa State University Digital Repository. It has been accepted for inclusion in Retrospective Theses and Dissertations by an authorized administrator of Iowa State University Digital Repository. For more information, please contact digirep@iastate.edu.

INFORMATION TO USERS

This reproduction was made from a copy of a document sent to us for microfilming. While the most advanced technology has been used to photograph and reproduce this document, the quality of the reproduction is heavily dependent upon the quality of the material submitted.

The following explanation of techniques is provided to help clarify markings or notations which may appear on this reproduction.

1. The sign or "target" for pages apparently lacking from the document photographed is "Missing Page(s)". If it was possible to obtain the missing page(s) or section, they are spliced into the film along with adjacent pages. This may have necessitated cutting through an image and duplicating adjacent pages to assure complete continuity.
2. When an image on the film is obliterated with a round black mark, it is an indication of either blurred copy because of movement during exposure, duplicate copy, or copyrighted materials that should not have been filmed. For blurred pages, a good image of the page can be found in the adjacent frame. If copyrighted materials were deleted, a target note will appear listing the pages in the adjacent frame.
3. When a map, drawing or chart, etc., is part of the material being photographed, a definite method of "sectioning" the material has been followed. It is customary to begin filming at the upper left hand corner of a large sheet and to continue from left to right in equal sections with small overlaps. If necessary, sectioning is continued again—beginning below the first row and continuing on until complete.
4. For illustrations that cannot be satisfactorily reproduced by xerographic means, photographic prints can be purchased at additional cost and inserted into your xerographic copy. These prints are available upon request from the Dissertations Customer Services Department.
5. Some pages in any document may have indistinct print. In all cases the best available copy has been filmed.

**University
Microfilms
International**

300 N. Zeeb Road
Ann Arbor, MI 48106

8224225

Ibrahim, Hosny Mohammed

**ATMOSPHERIC ANISOTROPY AND ITS EFFECT ON THE DELAY POWER
SPECTRA OF TROPOSPHERIC SCATTER RADIO SIGNALS**

Iowa State University

PH.D. 1982

**University
Microfilms
International**

300 N. Zeeb Road, Ann Arbor, MI 48106

PLEASE NOTE:

In all cases this material has been filmed in the best possible way from the available copy. Problems encountered with this document have been identified here with a check mark .

1. Glossy photographs or pages
2. Colored illustrations, paper or print
3. Photographs with dark background
4. Illustrations are poor copy
5. Pages with black marks, not original copy
6. Print shows through as there is text on both sides of page
7. Indistinct, broken or small print on several pages
8. Print exceeds margin requirements
9. Tightly bound copy with print lost in spine
10. Computer printout pages with indistinct print
11. Page(s) _____ lacking when material received, and not available from school or author.
12. Page(s) _____ seem to be missing in numbering only as text follows.
13. Two pages numbered _____. Text follows.
14. Curling and wrinkled pages
15. Other _____

University
Microfilms
International

Atmospheric anisotropy and its effect on the delay
power spectra of tropospheric scatter radio signals

by

Hosny Mohammed Ibrahim

A Dissertation Submitted to the
Graduate Faculty in Partial Fulfillment of the
Requirements for the Degree of
DOCTOR OF PHILOSOPHY

Major: Electrical Engineering

Approved:

Signature was redacted for privacy.

In Charge of Major Work

Signature was redacted for privacy.

~~For the Major~~ Department

Signature was redacted for privacy.

For the Graduate College

Iowa State University
Ames, Iowa

1982

TABLE OF CONTENTS

	Page
DEDICATION	iv
I. GENERAL INTRODUCTION	1
II. REVIEW OF TROPOSPHERIC BEYOND-THE-HORIZON PROPAGATION AND THE RAKE SYSTEM	4
A. Introduction	4
B. Scattering Theory	5
1. The correlation function	7
2. The structure function	8
3. The spectral density function	8
C. Reflection Theory	14
D. The RAKE System	16
E. Anisotropic Spectral Densities	20
III. A SIMPLIFIED MODEL FOR EXTRACTING THE ANISOTROPY COEFFICIENT FROM THE DOPPLER SPECTRUM	23
A. Introduction	23
B. Development of the Simplified Model	24
1. Crawford model	24
2. Birkemeier's anisotropic model	28
3. Developing the simplified model	30
C. Experimental Verification of the Simplified Model	34
1. The isotropic component of the argument a_{Ij}	34
2. The crosspath wind speed	40
3. The coefficient B_j	41
4. Illustrative examples	46
IV. THE EFFECT OF ANISOTROPY ON THE DELAY POWER SPECTRA AND MULTIPATH SPREAD OF TROPOSCATTER SIGNALS	62
A. Introduction	62

B.	The Description and Calculations of Delay Power Spectra Based on an Anisotropic Model	63
1.	Bello's model for calculating the delay power spectra	65
2.	Delay power spectra based on an anisotropic model	67
C.	Anisotropy Profiles and Their Effect on the Delay Power Spectrum	69
1.	Linear increase of anisotropy with delay	70
2.	Exponential increase of anisotropy with delay	71
3.	One elevated layer	71
4.	Two-layer model	72
D.	The Effect of Anisotropy on Intermodulation Distortion and Error Probability of Binary Communication Systems	78
1.	Intermodulation distortion	79
2.	Effect of anisotropy on the error rate of a binary communication system	81
E.	Measurement of the Multipath Characteristics	88
V.	CONCLUSION	97
VI.	BIBLIOGRAPHY	100
VII.	ACKNOWLEDGMENTS	103
VIII.	APPENDIX A: PARAMETERS OF THE ISU-UW TROPOSCATTER LINK	104
IX.	APPENDIX B: WATFIV COMPUTER PROGRAM FOR CALCULATING THE DISTRIBUTION OF THE DIFFERENTIAL ISOTROPIC SCATTERED POWER VS CROSSPATH DISTANCE	114
X.	APPENDIX C: WATFIV COMPUTER PROGRAM FOR CALCULATING THE DELAY POWER SPECTRUM BASED ON AN ANISOTROPIC SCATTERING MODEL	129

DEDICATION

TO NAGWA AND THE MEMORY OF MY FATHER

I. GENERAL INTRODUCTION

The effect of the anisotropy of the scattering in the atmosphere on the multipath spread of the forward scattered signals is studied in this thesis. It is found that the shape of the delay power spectra and its corresponding statistics are very dependent on the profile of the average anisotropy coefficient. Several theoretical profiles and their corresponding delay power spectra have been studied. The corresponding effect on the bit error rate (BER) of binary communication systems is also presented.

Several different propagation theories have been proposed for interpreting signals received on transhorizon radio paths. Prominent among these are: 1) the "reflection from stratified layers" model developed by Friis et al. [1], and 2) the "scattering from isotropic turbulence" model developed by Booker-Gordon [2] and Tatarski [3]. However, atmospheric turbulence always contains large scale components which are far from being isotropic, while reflection by layers is dominant only when there are temperature inversions. Thus, interpreting transhorizon signals on the basis of an anisotropic turbulence model is more representative of the true nature of the atmosphere. In addition, the degree of anisotropy is very closely related to the dynamic stability of the atmosphere [4]. Birkemeier [4] has indicated that the degree of anisotropy affects the multipath spread of the forward scattered signals. Bello et al. [5-7] have developed a mathematical model based on the statistics of the delay power spectra. They have shown that the multipath spread is a basic parameter that affects the irreducible bit

error rate, produced by frequency selective fading.

Data taken from the Iowa State University - University of Wisconsin RAKE radar system are used in the present study. This system operates over a 406 km path at 940 MHz. The RAKE receiver effectively splits the common volume into time delay shells. The system uses a pseudorandom code modulation of 5 or 10 MHz which provides a delay resolution of 0.2 or 0.1 microseconds. A microprocessor based data acquisition and analysis system, designed for the tropospheric project calculates the Doppler spectra of each time delay shell. These spectra are further processed to extract the anisotropy coefficient and its variation with height.

Direct measurements of atmospheric anisotropy have not been attempted due to the difficulties associated with measuring small scale refractivity fluctuations in three dimensions simultaneously in time and space. This thesis utilizes a simple model that is capable of characterizing the anisotropy of the scattering process. The model combines the "reflection by layer" theory and a "scattering by anisotropic turbulence" model developed by Birkemeier et al. [8]

The simplified model offers definite advantages for the process of extracting the anisotropy coefficient from the Doppler frequency distribution of the received signals.

Chapter II presents an overview of the theories of the troposcatter propagation; both the reflection theory and turbulence theory are reviewed together with the anisotropic correlation functions and their corresponding spectra. The forward scatter radar geometry and the coordinate system of the RAKE receiver are also presented. Chapter III

presents the simplified Gaussian shaped anisotropic model. A computer program is developed to calculate the theoretical received power as a function of the cross-path position of the scatterers for the different time delay shells of the RAKE receiver. These are further processed to extract the anisotropy coefficient. Several experimental data are presented which verify the ability of the model to characterize the anisotropy. Chapter IV presents the effects of the anisotropy variations on the shape of the delay power spectra and their corresponding statistics. Several theoretical anisotropy profiles are suggested and their corresponding delay power spectra and statistics are shown. The multipath spread parameter for each spectra is calculated. The effect of the anisotropy on the irreducible BER due to intermodulation distortion is studied utilizing Bello's intermodulation theory. Chapter V concludes this study and contains suggestions for further work.

II. REVIEW OF TROPOSPHERIC BEYOND-THE-HORIZON PROPAGATION AND THE RAKE SYSTEM

A. Introduction.

Extensive studies of beyond-the-horizon tropospheric propagation, both theoretically and experimentally, have been reported since the late forties. Numerous papers on the theory of beyond-the-horizon propagation have been reported in the literature, among them is the paper of Booker and Gordon in 1950 [2] that laid the foundations for scattering by atmospheric turbulence. However, the mathematical models of the turbulence were arbitrary and different assumptions were made. Another theory of beyond-the-horizon propagation was developed by Friis et al. [1]. It was based on the assumption that beyond-the-horizon propagation is due to reflections from a large number of randomly disposed layers located in the common volume. Both theories have found experimental verification. It seems evident that both scattering and reflection contribute to the phenomenon of propagation beyond-the-horizon.

The RAKE system has been found to be of use in overcoming some of the multipathing problems encountered in beyond-the-horizon propagation. This system is capable of splitting the common volume into time delay shells, thus providing spatial information about the received signal. It has been found of great use in characterizing the atmospheric conditions [8].

In this chapter, a review of the propagation theories for beyond-the-horizon communication links is presented and the main characteristics of this model of propagation are shown. Also, the RAKE coordinate system

and its relevant parameters are presented.

B. Scattering Theory

According to this theory, signals arriving at the receiver are the result of scattering by a homogeneous random continuum of scatters of differing dielectric constant. The scattered fields from different elementary volumes are assumed to be uncorrelated, therefore, the scattered power is given by [9]

$$P_r = P_t \int \frac{\lambda^2 G_t(\hat{i}) G_r(\hat{o})}{(4\pi)^2 R_1^2 R_2^2} \sigma(\hat{o}, \hat{i}) dv \quad (2.1)$$

where P_t = the transmitted power,

$G_t(\hat{i})$, $G_r(\hat{o})$ = the transmitter and receiver antenna patterns, respectively,

R_1 , R_2 = the distances from the transmitter and receiver to the scattering point, and

$\sigma(\hat{o}, \hat{i})$ = the scattering cross section per unit volume of the random medium. It is defined to be the fraction of incident power scattered per unit volume of the scatterers.

Figure 2.1 shows the geometry of scattering path and the corresponding parameters mentioned in Equation 2.1.

The whole problem of scattering lies in determining the scattering cross section σ . An expression for σ is given by [9]

$$\sigma(\hat{o}, \hat{i}) = \frac{k^4 \sin^2 \chi}{(4\pi)^2} \int_{\delta v} \int_{\delta v} \langle \epsilon_1(\vec{r}_1) \epsilon_2(\vec{r}_2) \rangle \exp i \vec{k}_s \cdot (\vec{r}_1 - \vec{r}_2) dv_1 dv_2 \quad (2.2)$$

\hat{i} unit vector of incident signal
 \hat{o} unit vector of scattered signal
 θ_s scattering angle
 θ_0 half power beam width
 γ_t, γ_r take off angles at the trans. and the rec., respectively

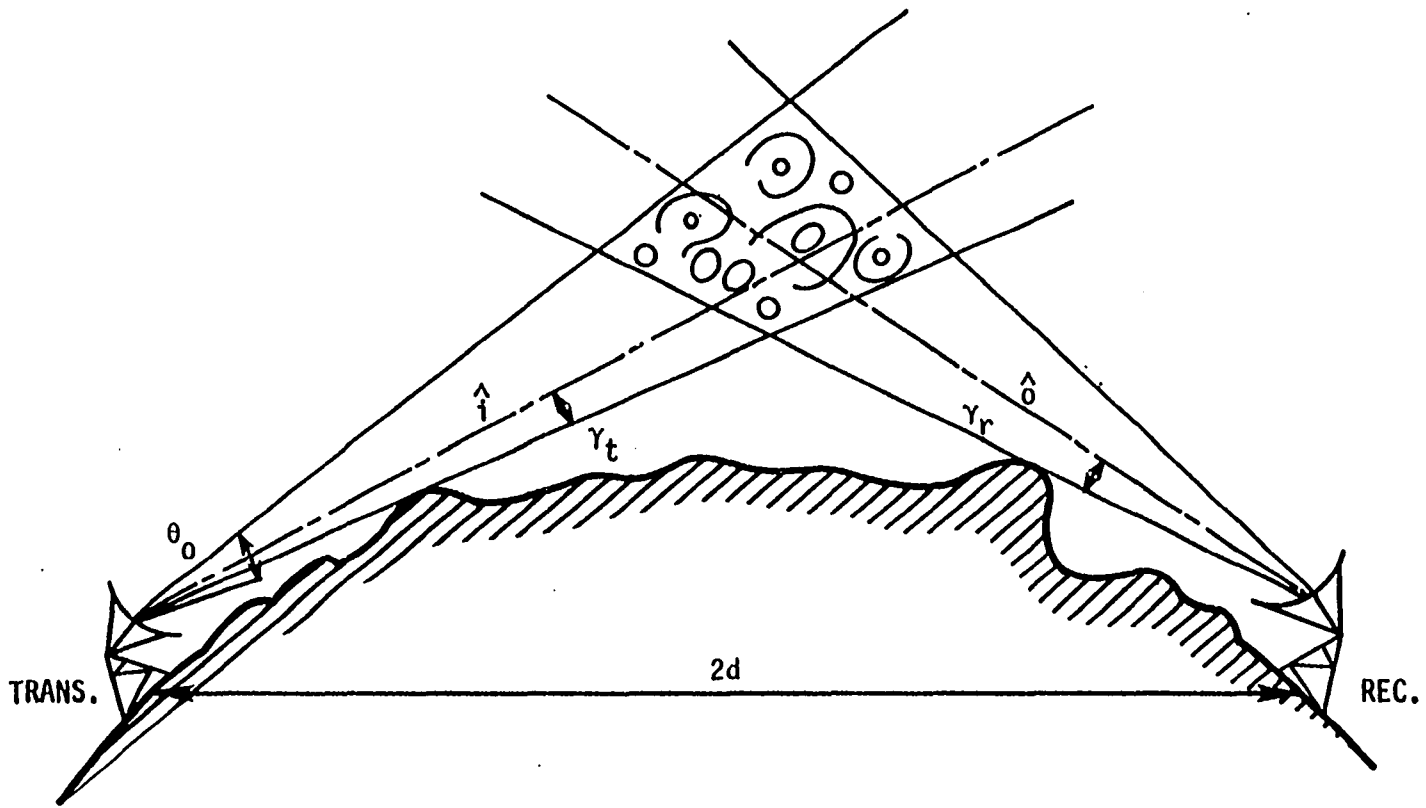


Figure 2.1. General troposcatter geometry

where dv_1' and dv_2' are the volume elements at r_1' and r_2' , respectively. At this point, it is necessary to talk briefly about the descriptions of random fields and random processes.

A random field could be a vector field like the wind velocity in a turbulent atmosphere or it could be a scalar field like temperature, humidity, or dielectric constant. Random fields, as well as random processes, are described by different methods. One method makes use of multidimensional probability distributions which are complex and lengthy; another method uses averages and moments of representative samples, where different moments represent different characteristics. The use of functions indicating the degree of independence between samples of the random variable is common. The most common functions used are: the correlation function, the structure function, and the spectral density function. These functions will be discussed briefly since they will be used in describing the randomness of the dielectric constant of the atmosphere.

1. The correlation function

The correlation function is used to indicate the degree of dependence between two different random variables at the same instant or the same variable at different instants of time. Both time and spatial separation are considered as follows:

$$B_f(t_1, t_2) = \frac{[f(t_1) - \overline{f(t_1)}][f^*(t_2) - \overline{f^*(t_2)}]}{\overline{[f(t_1) - \overline{f(t_1)}][f^*(t_2) - \overline{f^*(t_2)}]}} \quad (2.3)$$

$$B_f(r_1, r_2) = \frac{[f(\vec{r}_1) - \overline{f(\vec{r}_1)}][f^*(\vec{r}_2) - \overline{f^*(\vec{r}_2)}]}{\overline{[f(\vec{r}_1) - \overline{f(\vec{r}_1)}][f^*(\vec{r}_2) - \overline{f^*(\vec{r}_2)}]}} \quad (2.4)$$

where B_f denotes the correlation function, $f(t_1)$ and $f(t_2)$ are samples of the random variable at instants t_1 , and t_2 , $f(\vec{r}_1)$ and $f(\vec{r}_2)$ are the corresponding functions at \vec{r}_1 and \vec{r}_2 at a certain instant. The asterisks mean conjugate value, and the overbar means average value.

2. The structure function

The use of such functions is recommended when the mean value of a certain random variable is not constant. The structure function D_f is used to take such variations into account by considering only changes after a period τ_0 or distance r_0 , which are very small. It is defined as follows,

$$D_f(t_1, t_2) = \overline{[f(t_1) - f(t_2)]^2} \quad (2.5)$$

$$D_f(\vec{r}_1, \vec{r}_2) = \overline{[f(\vec{r}_1) - f(\vec{r}_2)]^2} \quad (2.6)$$

Although the structure functions are usually used to describe variables with varying averages, they may also be used to describe stationary variables.

3. The spectral density function

The Fourier Transform of the correlation function is the spectral density which is defined such that

$$B_f(t_1, t_2) = \int_{-\infty}^{\infty} W_f(w) \exp(iw(t_2 - t_1)) dw \quad (2.7)$$

$$B_f(\vec{r}_1, \vec{r}_2) = \int_{-\infty}^{\infty} \phi_f(\vec{K}) \exp(i\vec{K} \cdot (\vec{r}_2 - \vec{r}_1)) d\vec{K} \quad (2.8)$$

where $W_f(w)$ is the spectral density function of the random process, $\phi_f(\vec{K})$ is the three-dimensional spectral density function, and $L \propto 1/K$ is a geometric measure of the size of the eddies. The importance of the three-dimensional spectral density function is to indicate the energy content of the amplitude of turbulence at different geometric lengths.

Random fields are generally classified as stationary or with a varying mean, as homogeneous and isotropic or locally homogeneous and isotropic, or inhomogeneous and anisotropic. Of these field categories, the first type is usually considered and experimentally confirmed. A homogeneous field is called isotropic if $B_f(\vec{r})$ depends only on $r = |\vec{r}|$. For isotropic fields, $D_f(\vec{r}) = D_f(r)$, $\phi_f(\vec{K}) = \phi_f(K)$. A homogeneous field is not necessarily isotropic. For example, consider the field with the following correlation function,

$$B_f(\vec{r}_1 - \vec{r}_2) = B_f [a(x_1 - x_2) + b(y_1 - y_2) + c(z_1 - z_2)] .$$

The latter field is the one which we are concerned with in this thesis.

The randomness of the dielectric constant is the main cause of scattering in the troposphere. Following the above procedure in describing the random fields, the permittivity $\epsilon(\vec{r}, t)$ is usually considered time invariant, homogeneous and isotropic, $\epsilon_1(\vec{r}, t)$ is the fluctuating part with zero average. Under these conditions,

$$\langle \epsilon_1(\vec{r}_1) \epsilon_1(\vec{r}_2) \rangle = B_\epsilon(|\vec{r}_2 - \vec{r}_1|) = B_\epsilon(r_d) \quad (2.9)$$

where $B_\epsilon(r_d)$ is the correlation function of the dielectric constant.

In terms of the refractive index fluctuations, we can write [9],

$$B_{\epsilon}(r_d) = 4B_n(r_d) . \quad (2.10)$$

Following Ishimaru [9], Equation 2.2 can be written as

$$\sigma(\hat{o}, \hat{i}) = 2\pi K^4 \sin^2 \chi \phi_n(\vec{K}_S) \quad (2.11)$$

where $\phi_n(\vec{K}_S)$ is the three-dimensional spectral density evaluated at $\vec{K} = \vec{K}_S$; it is given by

$$\phi_n(\vec{K}_S) = \frac{1}{(2\pi)^3} \int B_n(\vec{r}_d) \exp(i\vec{K}_S \cdot \vec{r}_d) dv_d . \quad (2.12)$$

Different correlation functions have been used by different authors. Examples of these are given below, together with their corresponding three-dimensional spectral densities,

$$\text{Booker-Gordon} \quad B_n(r_d) = \langle n_l^2 \rangle e^{-r_d/l} \quad (2.13)$$

$$\text{Gaussian} \quad B_n(r_d) = \langle n_l^2 \rangle e^{-(r_d/l)^2} \quad (2.14)$$

$$\text{Bessel} \quad B_n(r_d) = \langle n_l^2 \rangle \left(\frac{2^{1-\nu}}{\Gamma(\nu)} \right) \left(\frac{r_d}{l} \right)^2 K_{\nu}(r_d/l) \quad (2.15)$$

where $r_d = (x_l^2 + y_l^2 + z_l^2)^{1/2}$,

Γ = the Gamma function,

K_{ν} = the modified Bessel function of the second kind, and

l = the correlation distance.

For the isotropic case, the loci of constant correlations are concentric spheres. The above three equations can be used to describe the anisotropic version of scattering by properly defining r_d . The loci of

constant correlation become concentric ellipsoids. In this case, r_d is written as

$$r_d = 1 \left[\left(\frac{x_1}{l_x} \right)^2 + \left(\frac{y_1}{l_y} \right)^2 + \left(\frac{z_1}{l_z} \right)^2 \right]^{1/2} \quad (2.16)$$

where l_x , l_y , and l_z are the correlation distances in x, y, and z directions.

The corresponding three-dimensional spectral densities for the isotropic versions are found by using Equation 2.12, the results are

$$\phi_n(k_s) = \langle n_1^2 \rangle l^3 \frac{1}{\pi} (1 + (k_s l)^2)^{-2} \quad (2.17)$$

$$\phi_n(k_s) = \langle n_1^2 \rangle \frac{l^3}{8\pi \sqrt{\pi}} \exp(-(k_s l/2)^2) \quad (2.18)$$

$$\phi_n(k_s) = \langle n_1^2 \rangle \frac{l^3}{\pi \sqrt{\pi}} \frac{\Gamma(\nu+1.5)}{\Gamma(\nu)} (1+(k_s l)^2)^{-\nu-1.5} \quad (2.19)$$

where $\nu > 0$.

For the anisotropic version of the correlation functions, the three-dimensional spectral densities will be presented after the coordinate system is considered. The exponential model used by Booker-Gordon and the Gaussian model are not able to explain the detailed characteristics of the scattering process. Complete knowledge of the scattering phenomenon depends upon the full knowledge of turbulence. Many authors have studied the atmospheric turbulence, the leading among them are Kolmogorov and Obukov. The Kolmogorov spectrum, which is based on the physics of turbulence is the most accepted one used in describing the characteristics of scattering. A detailed description of the Kolmogorov spectrum, as shown in Figure 2.2, is found in many texts [9-11],

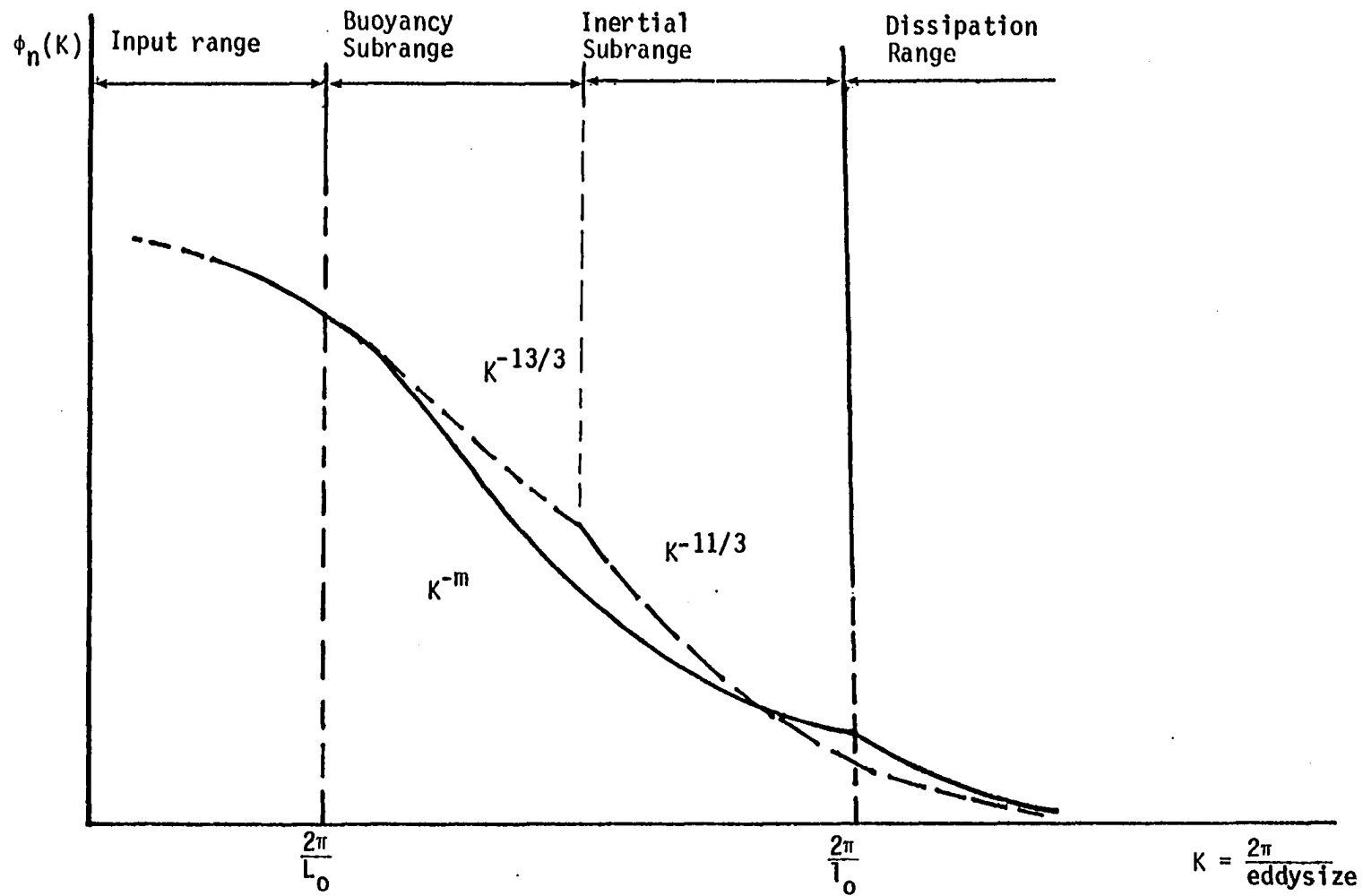


Figure 2.2. Kolmogorov spectrum for the three-dimensional spectral density of the refractive index [10]

and is presented briefly here for completeness.

According to Kolmogorov theory, the turbulence eddies are characterized by two sizes: the outer scale of turbulence L_0 , and the inner scale of turbulence l_0 . The spectrum is mainly divided into three regions.

a. The input range This is the range of the largest eddies (i.e. L_0) which are generally homogeneous but not isotropic. No specific form for the spectral density exists in this range.

b. The inertial range In this range, neither production nor dissipation of energy takes place. The only possible means of energy change is by inertial transfer to smaller eddies. Such a range of eddies is called the inertial range. It is generally divided into two subranges, the buoyant subrange in which the breaking of eddies is mainly due to buoyant forces, and the inertial subrange in which the breakup of eddies is mainly affected by wind forces. Within the inertial subrange, the spectral density is given by

$$\phi_n(K) = .033 C_n^2 K^{-11/3} \frac{2\pi}{L_0} < K < \frac{2\pi}{l_0} \quad (2.20)$$

$\phi_n(K) \propto K^{-13/3}$ for the buoyant subrange and C_n^2 is the structure constant of the refractive index fluctuations. The turbulence in this range is essentially isotropic.

c. The dissipation range In this range, dissipation of energy is dominant, the spectra are completely isotropic, and their magnitudes are very small. Usually,

$$\phi_n(K) = 0 \quad K > \frac{2\pi}{l_0} .$$

The three regions are often combined to give

$$\phi_n(K) = 0.033 C_n^2 \left(K^2 + \frac{1}{L_0^2} \right)^{-11/6} \exp(-K^2/Km^2)$$

which is usually called the Karman spectrum, where $Km = \frac{5.92}{l_0}$.

C. Reflection Theory

In the range of frequencies used in beyond-the-horizon propagation (100 MHz to 10 GHz), the reflection theory of Friis et al. [1] has been found to be relatively useful since it depends primarily on the wave length, the distance, and the size of the antennas. It serves as a guide for estimating the roles of the various parameters involved in beyond-the-horizon propagation.

According to this theory, uncorrelated signals are received due to reflections from random layers of different sizes that exist in common volume. Large, intermediate, and small layers are considered by Friis, however, case 2 (intermediate layers) is considered to be the most prevalent. The expression for the received power for this case is given by:

$$P_r = P_t \frac{A_T A_R N b^2}{3\lambda^3 a^3} \int_v \Delta^2 q^2 dv \quad (2.21)$$

where P_t, P_r = the same as in Equation 2.1,

A_T, A_R = the effective areas of the transmitting and receiving antennas,

$2a$ = the path length,

Δ = the grazing angle at the layer,

b = the along-the-path dimension of the reflecting layer, and intermediate layer size is given by

$$\sqrt{2a\lambda} < b < \sqrt{2a\lambda} / \Delta,$$

N = the number of layers in the common volume, and

q = the amplitude reflection coefficient of the dielectric constant at the layer boundaries. For smooth boundaries, it is given by

$$q = \frac{K\lambda}{16\pi\Delta^3} \frac{\sin(\pi n/2)}{(\pi n/2)} \text{ where } n \text{ integer positive.}$$

Following Friis, Equation 2.21 can be written, after performing the integration in terms of the geometries of the antennas and the path, as follows:

$$P_r = P_t \left[\frac{\lambda^2}{4a^2\alpha^4} \right] \left[\frac{4M\lambda}{3\theta^4} \right] \left[\frac{(\alpha/\theta)f(\alpha/\theta)}{2+\alpha/\theta} \right] \quad (2.22)$$

where

α = the half power beam width of the antennas,

θ = the grazing angle of the lower edge of the beam with respect to the chord,

$M \approx 2000 b^2 K_1^2 N$ = the change in gradient of the dielectric constant at the lower edge of the common volume,

$$f(\alpha/\theta) = 1 + \frac{1}{(1+\alpha/\theta)^4} - \frac{1}{8} \left(\frac{2+\alpha/\theta}{1+\alpha/\theta} \right)^4$$

It should be noted from the previous paragraphs that the reflection theory is not related in any way to the turbulent state of the atmosphere as is the more physical scattering theory. However, layers formed by relatively sharp gradients of the refractive index have been confirmed

experimentally and the reflection theory for such cases exhibits good agreement with experimental data obtained. This is due to the complicated nature of this mode of propagation. The interest in a better model to explain these anomalies led Cianos in 1978 to look for a model that combines both the scattering and the reflection parts. Taking into account that part of the signal due to reflection, Cianos [12] was able to deduce exponents of the scattering angle which agree well with the theory of scattering based on physical arguments. As will be shown later, reflection by layers results in large zero Doppler amplitudes of the received signals. Also, layering is considered to contribute very much to the anisotropy of the atmosphere.

D. The RAKE System

In 1958, R. Price and P. E. Green [13], using the principles of statistical communication theory, developed the RAKE Communication system to combat multipath effects; namely, selective fading and intersymbol interference. D. R. Bitzer et al. [14], in 1966, adapted the RAKE system to tropospheric scatter communication links. He collected data on a path of 250 Km to describe a number of propagation phenomena. These included selective fading, envelope fluctuation, diurnal variations, correlation bandwidth of the medium, fading rates, diversity combining, and others.

The RAKE system utilizes a wide-band signal code, having pseudo-random character, to biphase modulate the carrier frequency. At the receiver, an identical delayed replica of the pseudorandom code is correlated with the received signal to yield that portion of the signal

corresponding to the specific delay. By varying the delay or using a bank of correlators, the total received power as a function of delay can be resolved. Figure 2.3 shows a coordinate system for the forward scatter radar utilizing a RAKE receiver. Constant time delays correspond to confocal prolate spheroids with foci at the transmitter and receiver, the x coordinate is along the path, y is the cross path direction and z is the vertical. The origin of this coordinate system is usually taken at midpath. Any scattering point could be identified either by its x, y, z components or by its azimuth, elevation, and range.

Usually, the signals received with the RAKE system are in the form of instantaneous values of the impulse response $h(\tau, t)$ for each time delay tap. This gives insight into the time variations or fading of the medium. Another useful representation of the signal is the "scattering function", which is the Fourier transform of the correlation function of $h(\tau, t)$, $R_h(\tau, t)$, and is given by

$$V(\tau, f_d) = \int_{-\infty}^{\infty} R_h(\tau, t) \exp(i2\pi f_d t) dt \quad (2.23)$$

where

$$R_h(\tau, t) = \langle h(\tau, r) h^*(\tau, r+t) \rangle .$$

The shape of $V(\tau, f_d)$ in the frequency variable f_d can be physically interpreted as a Doppler broadening with f_d as the Doppler frequency. In the present thesis, we will depend on the shape of the scattering function as related to the anisotropic nature of the atmosphere. References [8, 15] present a good analysis of the RAKE tropospheric scattering

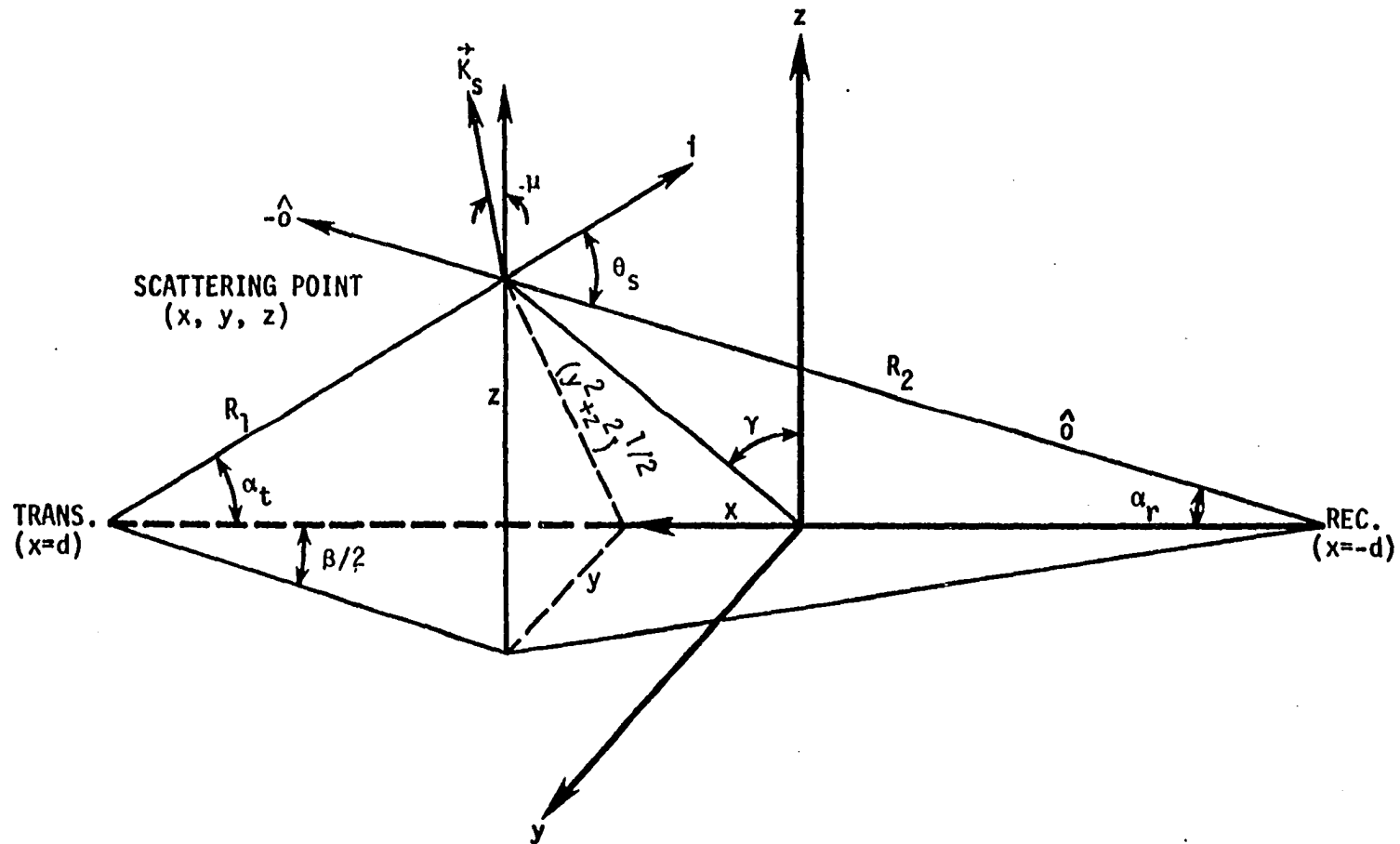


Figure 2.3. The RAKE coordinate system

techniques to be utilized in indirect atmospheric measurements. The system equations for determining the constant time delay contours and the Doppler frequency for a RAKE sounding system are given here [8].

$$\begin{aligned} L &= \text{length of propagation path} \\ &= [(d-x)^2 + y^2 + z^2]^{1/2} + [(d+x)^2 + y^2 + z^2]^{1/2} \end{aligned} \quad (2.24)$$

$$\xi = \text{signal time delay} = L/C \quad (2.25)$$

$$\begin{aligned} f_d &= \text{Doppler frequency} \\ &= -\frac{4}{\lambda L} \frac{ux(1-(2d/L)^2) + vy + wz}{1-16(xd/L^2)^2} \end{aligned} \quad (2.26)$$

In the above equations, C is the wave velocity; λ is the wavelength of the Rf signal; and u, v, w are the longitudinal, crosspath, and vertical components of the wind, respectively.

The Doppler frequency expression in Equation 2.26 can be simplified by observing that the term $1-(2d/L)^2$ is typically very small, as is the term $(xd/L^2)^2$. Also, it can be assumed that the vertical wind, w , is much less than the crosspath wind, v . Under these conditions, Equation 2.26 reduces to

$$f_d = -\frac{4vy}{\lambda L} \quad (2.27)$$

Since $L \approx 2d$, Equation 2.27 can be rewritten as

$$f_d = -\frac{2v}{\lambda} \left(\frac{2y}{L}\right) = -\frac{2v}{\lambda} \sin \alpha = -\frac{2v\alpha}{\lambda} \quad (2.28)$$

where α is the azimuthal angle of the scatterer.

In the present thesis, data taken from the troposcatter radar system with RAKE receiver operating as a cooperative project between Iowa State University (ISU) and the University of Wisconsin (UW) will be utilized in characterizing the anisotropy of the atmosphere. The important parameters of this system are shown in Appendix A, the system operates between Moingona, IA and Arlington, WI. Cross sections of the time delay shells in the y-z plane near midpath, for a 5 MHz modulation rate (0.2 μ sec. resolution), are shown in Appendix A.

E. Anisotropic Spectral Densities

The anisotropic versions of the correlation functions were presented in Section 2.1. In order to write the anisotropic version of the spectral density, the components of the scattering wave number vector should be expressed in terms of the x, y, z axes. Referring to Figure 2.3, the scattering angle, θ_s , is given by

$$\theta_s = \alpha_r + \alpha_t \quad (2.29)$$

where

$$\alpha_t = \arctan [(y^2 + z^2)^{1/2}/(d-x)] \quad (2.30)$$

$$\alpha_r = \arctan [(y^2 + z^2)^{1/2}/d+x] . \quad (2.31)$$

The direction of the vector \vec{k}_s can be expressed in terms of two angles. One angle, γ , is between the x-z plane and the plane containing the x axis, the incident ray and the scattered ray (r-x) plane, is given by

$$\gamma = \arctan (y/z) . \quad (2.32)$$

The other angle, μ , is between the vector \vec{K}_S and y-z plane. It is given by

$$\mu = (\alpha_t - \alpha_r)/2 \quad (2.33)$$

\vec{K}_S can now be written as

$$\vec{K}_S = K_x \vec{a}_x + K_y \vec{a}_y + K_z \vec{a}_z \quad (2.34)$$

where

$$K_x = |\vec{K}_S| \sin \mu$$

$$K_y = |\vec{K}_S| \cos \mu \sin \gamma$$

$$K_z = |\vec{K}_S| \cos \mu \cos \gamma$$

$$|\vec{K}_S| = \frac{4\pi}{\lambda} \sin \theta_s/2 .$$

The anisotropic versions of the spectral densities corresponding to Equations 2.13, 2.14, and 2.15 utilizing Equation 2.12, are listed below as Equations 2.35, 2.36, and 2.37.

$$\phi_n(\vec{K}_S) = \langle n_1^2 \rangle l_x l_y l_z 8\pi (1 + |\vec{q}|^2)^{-2} \quad (2.35)$$

$$\phi_n(\vec{K}_S) = \langle n_1^2 \rangle l_x l_y l_z \frac{1}{\sqrt{\pi}} [\exp -(|\vec{q}|/2)^2] \quad (2.36)$$

$$\phi_n(\vec{K}_S) = \langle n_1^2 \rangle l_x l_y l_z \frac{8}{\pi\sqrt{\pi}} [(\nu+1.5)/ (\nu)] (1+|\vec{q}|^2)^{-\nu-1.5} \quad (2.37)$$

where

$$q^2 = K_S^2 \{ (l_z^2 \cos^2 \gamma + l_y^2 \sin^2 \gamma) \cos^2 \mu + l_x^2 \sin^2 \mu \} . \quad (2.38)$$

Near the midpath ($x=0$ plane), $\mu = 0$ and Equation 2.38 reduces to

$$q = K_S (l_z^2 \cos^2 \gamma + l_y^2 \sin^2 \gamma) . \quad (2.39)$$

The anisotropic version corresponding to Equation 2.38 will be utilized in Chapter III since it approximates the Kolmogorov spectrum when $\nu = 1/3$.

III. A SIMPLIFIED MODEL FOR EXTRACTING THE ANISOTROPY COEFFICIENT FROM THE DOPPLER SPECTRUM

A. Introduction

Records of the Doppler frequency of signals received by a RAKE Forward Scatter Radar Sounding system exhibit a great deal of variability in the shape of the Doppler spectra. Much of this variability is due to winds in the scattering volume. However, even after the effect of the wind has been taken into account, the half power width of the Doppler spectrum can fluctuate a great deal.

This effect has been explained by use of an anisotropic scattering model developed by Birkemeier et al. [8]. The anisotropy in the scattering model accounts for the differences in the correlation length along the different axes. In Birkemeier's model, the ratio of the horizontal correlation distance to the vertical correlation distance is defined as the anisotropy coefficient A . This coefficient is considered to be a basic parameter characterizing the state of the atmosphere. Gage et al. [16] suggest that there is a relationship between the degree of anisotropy and the dynamic stability of the atmosphere. Birkemeier [4] has pointed out that the degree of the anisotropy affects the multipath spread of the forward scattered signals.

No direct measurements of atmospheric anisotropy have been tried due to difficulties in measuring small scale refractivity temporally and spatially. Birkemeier's model extracts the anisotropy from the Doppler frequency data. However, this model is not amenable to the inversion process due to the fact that received power versus Doppler frequency or

versus crosspath position must be fit to a family of theoretical curves using the same variables, but with A as a parameter.

This chapter presents an approximate anisotropic scattering model which is easily inverted and permits evaluation of the anisotropy coefficient in a direct and simple manner. In Section B, the development of the model is given and Section C presents the experimental verification of the model.

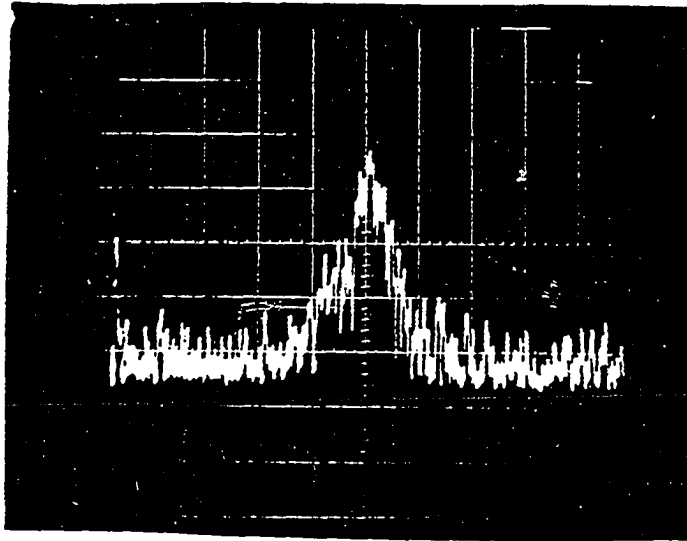
B. Development of the Simplified Model [17]

Figure 3.1 shows the kind of variations in the half power width of the Doppler spectra experimentally obtained at different periods of time. Broader width, as shown in Figure 3.1a, indicates strong crosspath winds, while smaller width, shown in Figure 3.1b, indicates signals coming from layered atmospheric structure.

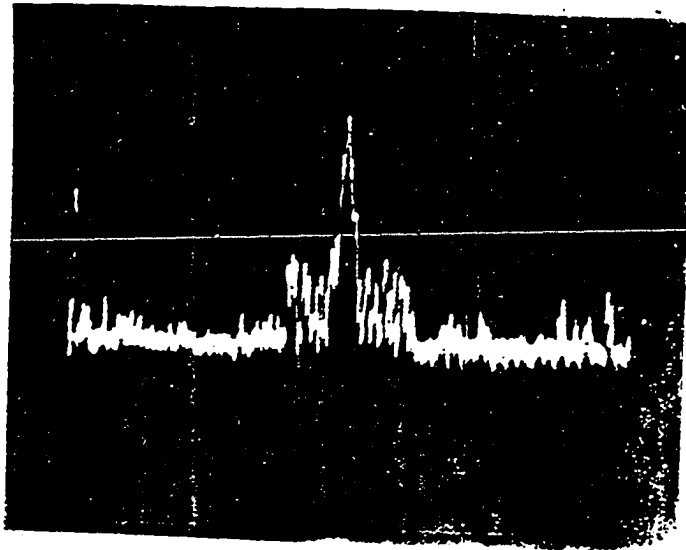
The simplified model developed here combines the transhorizon fading model developed by Crawford, Hogg and Kummer [18] and the anisotropic scattering model proposed by Birkemeier et al. [8]. The two models will be discussed first, followed by a development of the simplified model.

1. Crawford model

In this model, Gaussian-shaped characteristics for the antenna patterns and the power reflection coefficient are assumed. The argument of these Gaussian characteristics is the azimuthal width β , which is related to the crosspath wind velocity, v , and the Doppler frequency, f_d , of the received signal by Equation 2.28. After putting $\beta = 2\alpha$, the result is



(a)



(b)

Figure 3.1. Variation of half power Doppler width

$$\beta = \frac{\lambda f_d}{v} = \frac{2y}{d} \quad (3.1)$$

where the different parameters are defined in Figure 2.3. Figure 3.2 shows the effect of the azimuthal width on the Doppler frequency. The antenna patterns can be expressed as

$$G_t(\beta) = \exp(-\beta^2/2(0.85\beta_t)^2) \quad (\text{transmitting antenna}) \quad (3.2)$$

$$G_r(\beta) = \exp(-\beta^2/2(0.85\beta_r)^2) \quad (\text{receiving antenna}) \quad (3.3)$$

where β_t and β_r are the half power beamwidths of the transmitting and receiving antennas, respectively.

The formulation of Crawford et al. [18] accounts for the scattering in the atmosphere by introducing a reflection coefficient function $Q(\beta)$, which is also assumed to be a Gaussian function of β . That is,

$$Q(\beta) = \exp(-\beta^2/2(0.85\beta_e)^2) \quad (3.4)$$

where β_e is the half power azimuthal width of the reflection coefficient function. The received power is proportional to the product of three Gaussian shaped functions of β as follows:

$$P_r = \text{Const. } G_r(\beta)G_t(\beta)Q(\beta)$$

which can be written in terms of β_r , β_t , and β_e as follows:

$$P_r = \text{Const. } \exp \left\{ - \left(\frac{1}{\beta_r^2} + \frac{1}{\beta_t^2} + \frac{1}{\beta_e^2} \right) \frac{\beta^2}{2(0.85)^2} \right\} . \quad (3.5)$$

Since β is related to the Doppler frequency by Equation 3.1, the Doppler spectrum of the received signal can be written as

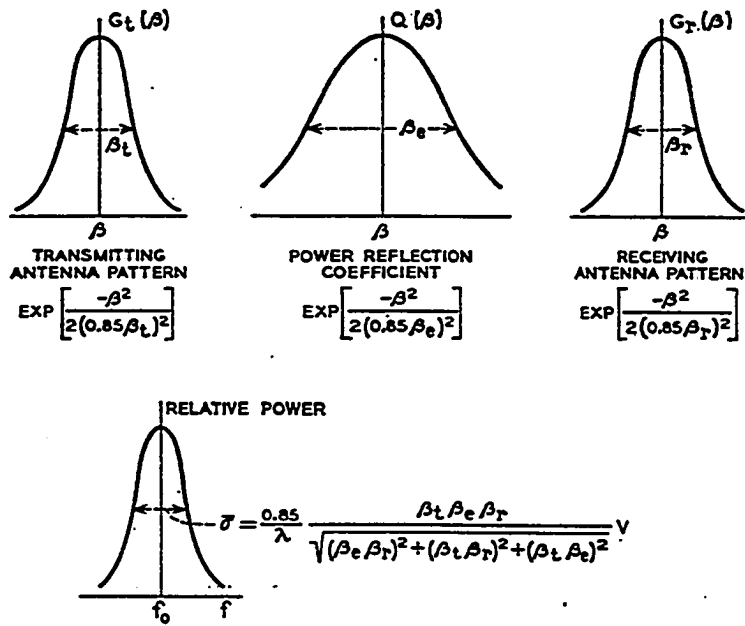


Figure 3.2. Factors affecting the frequency distribution of the received signal [18]

$$P_r(f_d) = \text{Const.} \exp(-f_d^2/2\bar{\sigma}^2) \quad (3.6)$$

where $\bar{\sigma}^2$ is the standard deviation of $P_r(f_d)$ and is given by

$$\frac{1}{\bar{\sigma}^2} = \frac{\lambda^2}{(0.85V)^2} \left(\frac{1}{\beta_t^2} + \frac{1}{\beta_r^2} + \frac{1}{\beta_e^2} \right) = \frac{\lambda^2}{(0.85V)^2} \frac{1}{\bar{\beta}^2} .$$

Since the half power width of the composite Doppler spectrum, $\bar{\beta}^2$, can be inferred from the received signal data, and since $\bar{\beta}^2$ includes β_e^2 , the half power width of the reflection function, $Q(\beta)$, $\bar{\beta}_e^2$ contains significant information about the state of the atmosphere.

2. Birkemeier's anisotropic model

The Crawford model is based on a theory of "reflection from layers" presented in Chapter II. This theory does not have the direct connection to the turbulent state of the atmosphere that characterizes the scattering theories developed by Tatarski [3] and others [2] presented in Section II.B. In an effort to resolve discrepancies between theory and observation, an anisotropic version of the turbulence theory of scattering was developed by Birkemeier et al. [8]. The distinctive feature of this model is the introduction of different correlation distances to characterize the structure of turbulence along different axes. The different forms of the anisotropic correlation functions and their corresponding spectra are presented in Chapter II. The formula used by Birkemeier is the one given by Equation 2.37, corresponding to the Bessel correlation function. Under the condition, $l_i K \gg 1$ ($i=x,y,z$), the resulting spectral density of position function has the form of a

power law as follows:

$$\phi(K_S) \sim l_x l_y l_z \langle n^2 \rangle q^{-p} \quad (3.7)$$

where p is taken to be $11/3$, and q^2 is given by Equation 2.38. Near midpath q^2 is given by Equation 2.39, which is repeated here for convenience:

$$q = K_S [l_z^2 \cos^2 \gamma + l_y^2 \sin^2 \gamma]^{1/2}.$$

Defining $A = l_y/l_z$ as the "coefficient" of anisotropy and substituting by the value of $K_S = (\frac{4\pi}{\lambda}) \sin(\theta_S/2)$ in Equation 3.7, we get

$$\phi(K_S) \sim A^2 l_0^{2/3} \langle n^2 \rangle (\frac{4\pi}{\lambda} \sin \theta_S/2)^{-11/3} (\cos^2 \gamma + A^2 \sin^2 \gamma)^{-11/6} \quad (3.8)$$

where the horizontal correlation distances are assumed equal and the vertical correlation distance remains equal to the isotropic value l_0 . Equation 3.8 can be written as

$$\phi(K_S) = \text{const. } A^2 (\frac{4\pi}{\lambda} \sin \theta_S/2)^{-11/3} (1 + (A^2 - 1) \sin^2 \gamma)^{-11/6}. \quad (3.9)$$

Since we are considering data taken from a time delay shell by means of a RAKE receiver system, the quantities $z_T = (z^2 + y^2)^{1/2}$, $\theta_S/2$ are approximately constant for a given time delay tap. Substituting by $\sin \gamma = y/z_T$, Equation 3.9 can be written as

$$\phi(K_S) = \text{Const. } A^2 [1 + (A^2 - 1) \frac{y^2}{z_T^2}]^{-11/6}. \quad (3.10)$$

This function can be expressed in terms of the azimuthal width, since $\sin \beta/2 \approx \beta/2 = y/d$. Equation 3.10 can be written as

$$\phi(K_S) = \text{const. } A^2 [1+(A^2-1) \frac{d^2 \beta^2}{4z_T^2}]^{-11/6} . \quad (3.11)$$

3. Developing the simplified model

In order to exploit the utility of the Gaussian model developed by Crawford, yet incorporate the scattering model based on the theory of anisotropic turbulence, the anisotropic scattering model is fit to an equivalent Gaussian curve. This process matches the two curves given by Equations 3.4 and 3.11 at the maximum value, $\beta = 0$ and at the half power point where $\beta = \beta_e$ in the Gaussian model. In developing this equivalence, it is necessary that

$$\beta_e^2 = \frac{1.838 z_T^2}{(A^2-1)d^2} . \quad (3.12)$$

The resultant form of Equation 3.11 becomes

$$\phi(\beta) = \text{Const. } A^2 [1+0.4595(\beta/\beta_e)^2]^{-11/6} . \quad (3.13)$$

The resulting expression describing the equivalent Gaussian approximation to $\phi(\vec{K}_S)$ as a function of y is

$$\phi(K_S) = \text{Const. } A^2 \exp \left[- \frac{1.506(A^2-1)y^2}{z_T^2} \right] \quad (3.14)$$

when $A = 1$, $\phi(K_S) = \text{Const.}$ and the shape of the Doppler spectrum of the received signal is controlled by the antenna patterns, the volume of the time delay shell, and the scattering angle. This is the isotropic turbulence scattering situation. A comparison of the anisotropic scattering model with the equivalent Gaussian curve is shown in

Figure 3.3. Note that the two curves coincide at $\beta/\beta_e = 0$ and $\beta/\beta_e = 1$; also the disagreement between the two curves is less than three percent for values of β/β_e less than 1.1.

In order to extract the anisotropy coefficient A from Doppler distribution of the power received by a RAKE system, it is necessary to consider the effect of the different variables such as antenna patterns, scattering angle and volume for each time delay shell. In this process, it is most helpful to know the fraction of the received power emanating from a differential width in the cross path direction for each time delay shell for isotropic scattering. These calculations are performed by a computer program developed for this purpose. The program utilizes the radar equation, assuming Gaussian antenna patterns of 2.6° beam width and isotropic scattering in the inertial subrange of Kolmogorov spectrum. The computer program is shown in Appendix B.

The normalized differential power versus y curve is approximately Gaussian in character and can be represented by an equation of the form

$$P_j(y) = C_{Ij} \exp(-a_{Ij}y^2) \quad (3.15)$$

where the index j indicates the tap number corresponding to the jth time delay shell and the index I means isotropic scattering. This expression is combined with the equivalent anisotropic scattering function given by Equation 3.14. The result is

$$P_j(y) = A_j^2 C_{Ij} \exp \left[- \left\{ a_{Ij} + \frac{1.506}{z_T^2} (A_j^2 - 1) \right\} y^2 \right] . \quad (3.16)$$

Equation 3.16 can be expressed in terms of the Doppler frequency, f_d ,

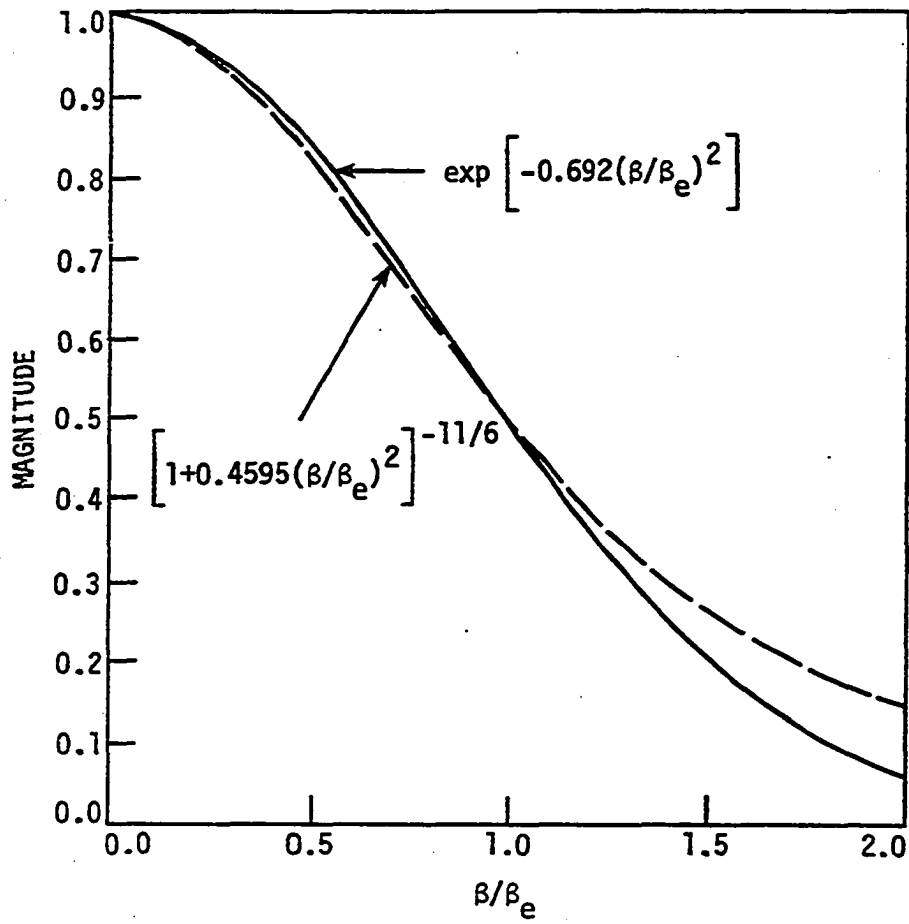


Figure 3.3. Comparison of the anisotropic scattering model with the equivalent Gaussian model

instead of y by using the relationship given in Equation 2.27, written in the following form,

$$y = -\frac{\lambda d}{2v} f_d .$$

The result is

$$P_j(f_d) = A_j^2 C_{Ij} \exp \left[\frac{\lambda^2 d^2}{4v_j^2} \left\{ a_{Ij} + \frac{1.506}{z_T} (A_j^2 - 1) \right\} f_d^2 \right] . \quad (3.17)$$

In the case of ISU-UW Radar system, Equation 3.17 can be written as,

$$P_j(f_d) = A_j^2 C_{Ij} \exp \left[-\frac{1049}{v_j^2} \left\{ a_{Ij} + \frac{1.506}{z_T} (A_j^2 - 1) \right\} f_d^2 \right] \quad (3.18)$$

where v is the crosspath wind in m/sec.

The received signal from a given tap can be processed through a Fast Fourier Transform routine to determine its Doppler spectrum. This data is then fit to an equivalent Gaussian curve of the form

$$P_j(f_d) = C_{2j} \exp [-B_j f_d^2] . \quad (3.19)$$

If the crosspath wind, v , is known or can be estimated, one can determine the anisotropy coefficient A by equating the argument of the exponential term of Equation 3.18 to the exponential term of Equation 3.19. That is,

$$\frac{1049}{v_j^2} \left[a_{Ij} + \frac{1.506}{z_T} (A_j^2 - 1) \right] = B_j \quad (3.20)$$

from which

$$A_j = \left[\left(\frac{B_j v_j^2}{1049} - a_{Ij} \right) \frac{z_T^2}{1.506} + 1 \right]^{1/2} . \quad (3.21)$$

The parameters a_{Ij} , v_j and B_j are assumed to be known, so the remaining unknown is the anisotropy coefficient A_j , which can be readily determined. Next, the calculations and experimental data required to extract the value of A are presented.

C. Experimental Verification of the Simplified Model

The different parameters encountered in Equation 3.21 will be presented and discussed.

1. The isotropic component of the argument a_{Ij}

The normalized differential scattered power emanating from a differential crosspath distance is calculated from the radar equation where the power scattered from a scatterer at x, y, z can be written as

$$P_r(x,y,z) \sim P_t \frac{G_t(x,y,z)}{4\pi R_1^2} \cdot \frac{G_r(x,y,z)}{4\pi R_2^2} \sigma(\hat{i}, \hat{o}) dx dy dz . \quad (3.22)$$

The parameters in the above equation can be written in terms of x, y, z coordinates for the RAKE system as follows:

$$R_1^2 = (d-x)^2 + z^2 + y^2$$

is the distance from the transmitter to the scattering point.

$$R_2^2 = (d+x)^2 + z^2 + y^2$$

is the distance from the receiver to the scattering point.

The antenna patterns are assumed to be Gaussian in shape. This is an often used assumption which is simple and quite accurate. In terms of the azimuth and elevation angles of the scattering point, measured

from the beam axis, the patterns can be written as follows:

$$G_t = G_{t0} \exp \left\{ -(\ln 2) \left[\left(\frac{2\theta_t}{\theta_1} \right)^2 + \left(\frac{2\phi_t}{\phi_1} \right)^2 \right] \right\} \quad (3.23)$$

$$G_r = G_{r0} \exp \left\{ -(\ln 2) \left[\left(\frac{2\theta_r}{\theta_2} \right)^2 + \left(\frac{2\phi_r}{\phi_2} \right)^2 \right] \right\} \quad (3.24)$$

where θ_1 and ϕ_1 are the half power beamwidths of the transmitting antenna in the vertical and the horizontal, respectively; and θ_2 and ϕ_2 are the half power beamwidths of the receiving antenna in the vertical and horizontal, respectively. $\sigma(\hat{o}, \hat{i})$ is the scattering cross section given by Equation 2.11, which for isotropic scattering following the Kolmogorov spectrum, is given in terms of θ_s as

$$\sigma(\theta_s) = 0.03 C_n^2 \lambda^{-1/3} \sin^2 x \sin^{-11/3}(\theta_s/2) . \quad (3.25)$$

The details of these calculations and the computer program developed for this purpose are given in Appendix B. Here, representative samples of these calculations together with their corresponding plots for the different conditions of elevation and delay resolution are presented. A Gaussian fit for these curves is also done. Figures 3.4 and 3.5 show the calculations for unsymmetrical elevation conditions in which the elevation of the receiver beam is 0.5° and that of the transmitter is 1.1° . These elevations result in sufficient received power for the experiments. Two different resolutions of 0.1 and 0.2 microseconds are used corresponding to modulation frequencies of 10 and 5 MHz.

Figures 3.6 and 3.7 show the calculations for symmetrical elevations of 2.4° for both the transmitter and the receiver. The plots are given for

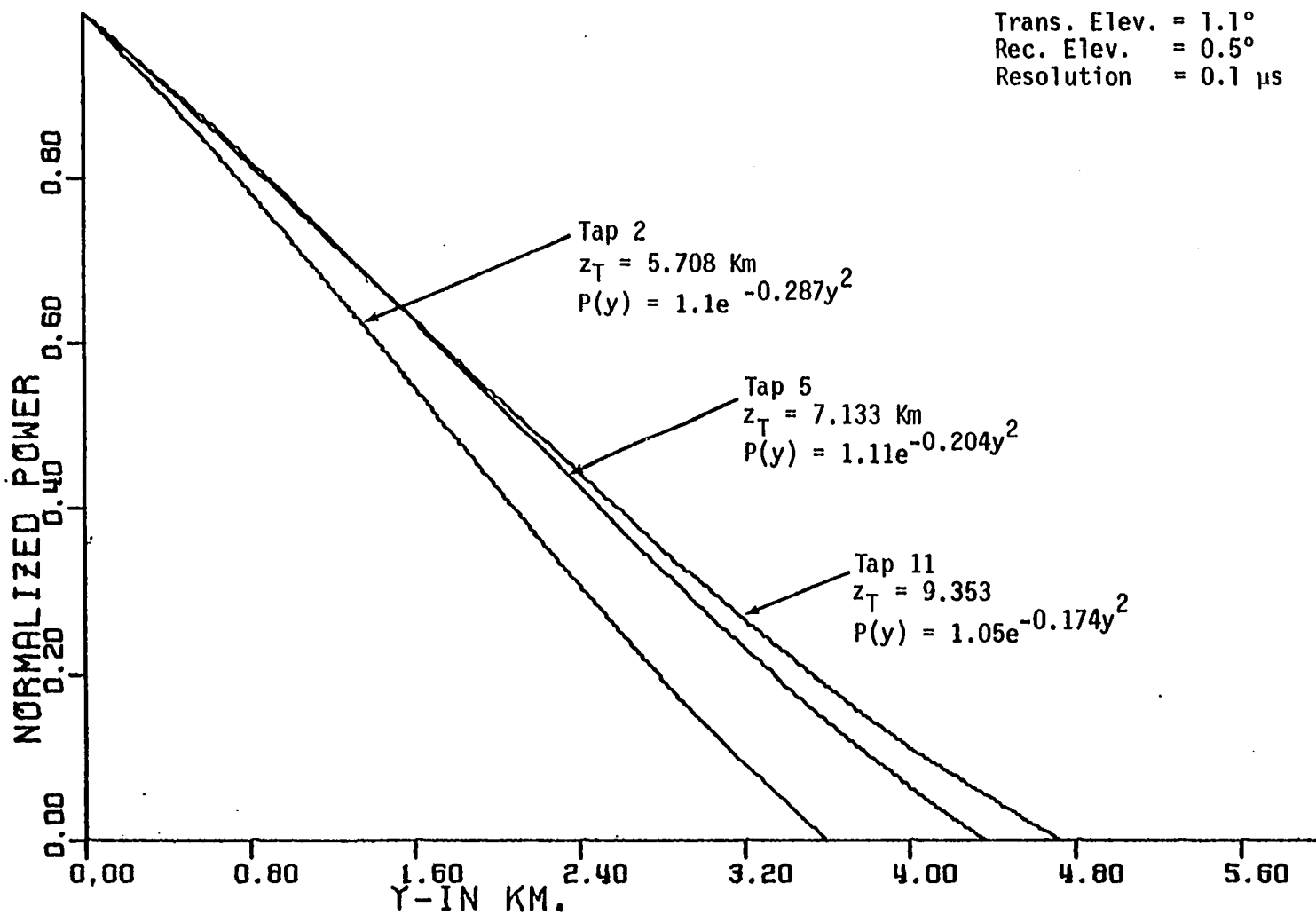


Figure 3.4. Isotropic normalized received power vs crosspath position for taps 2, 5 and 11

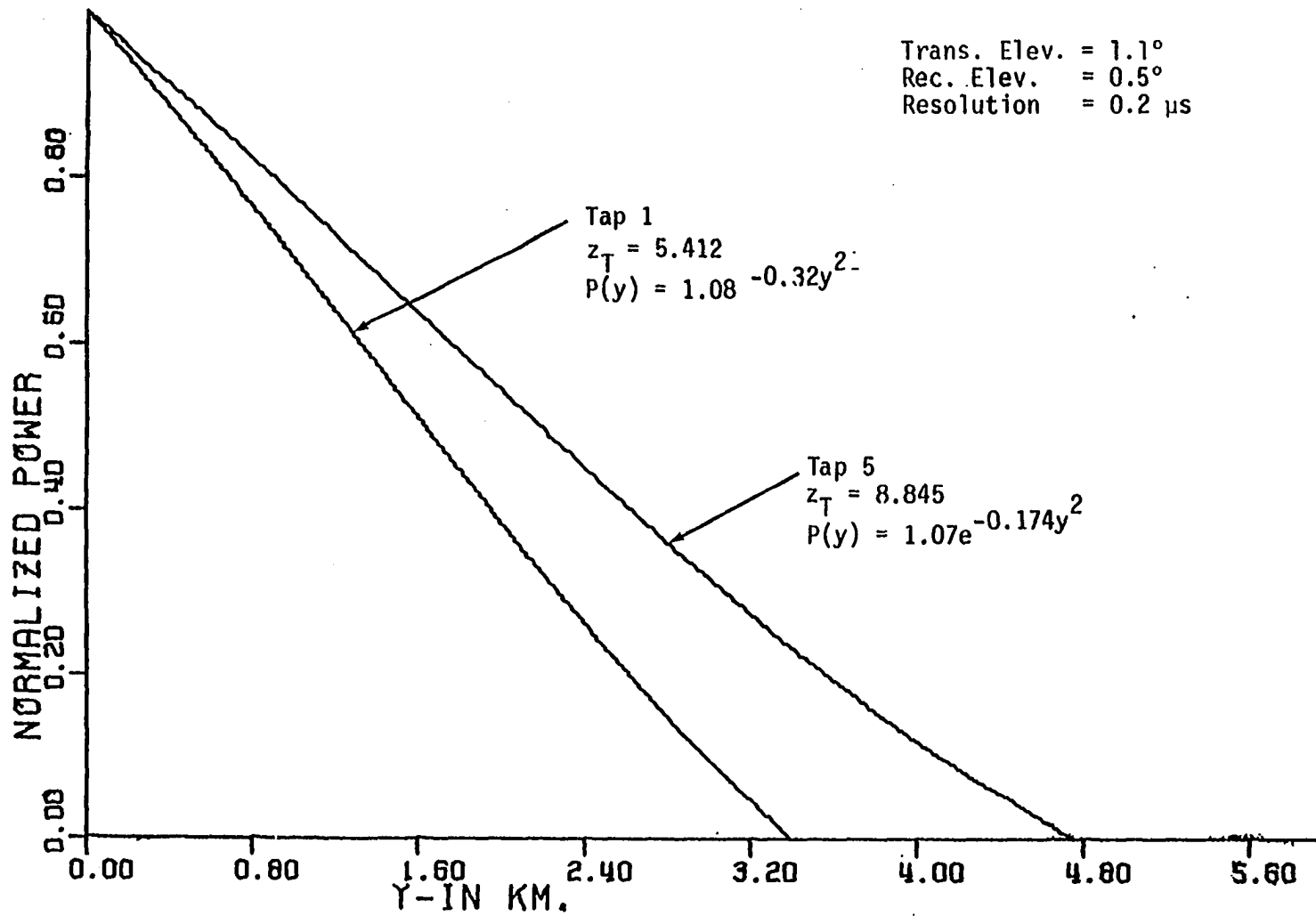


Figure 3.5. Isotropic normalized received power vs crosspath position for taps 1 and 5

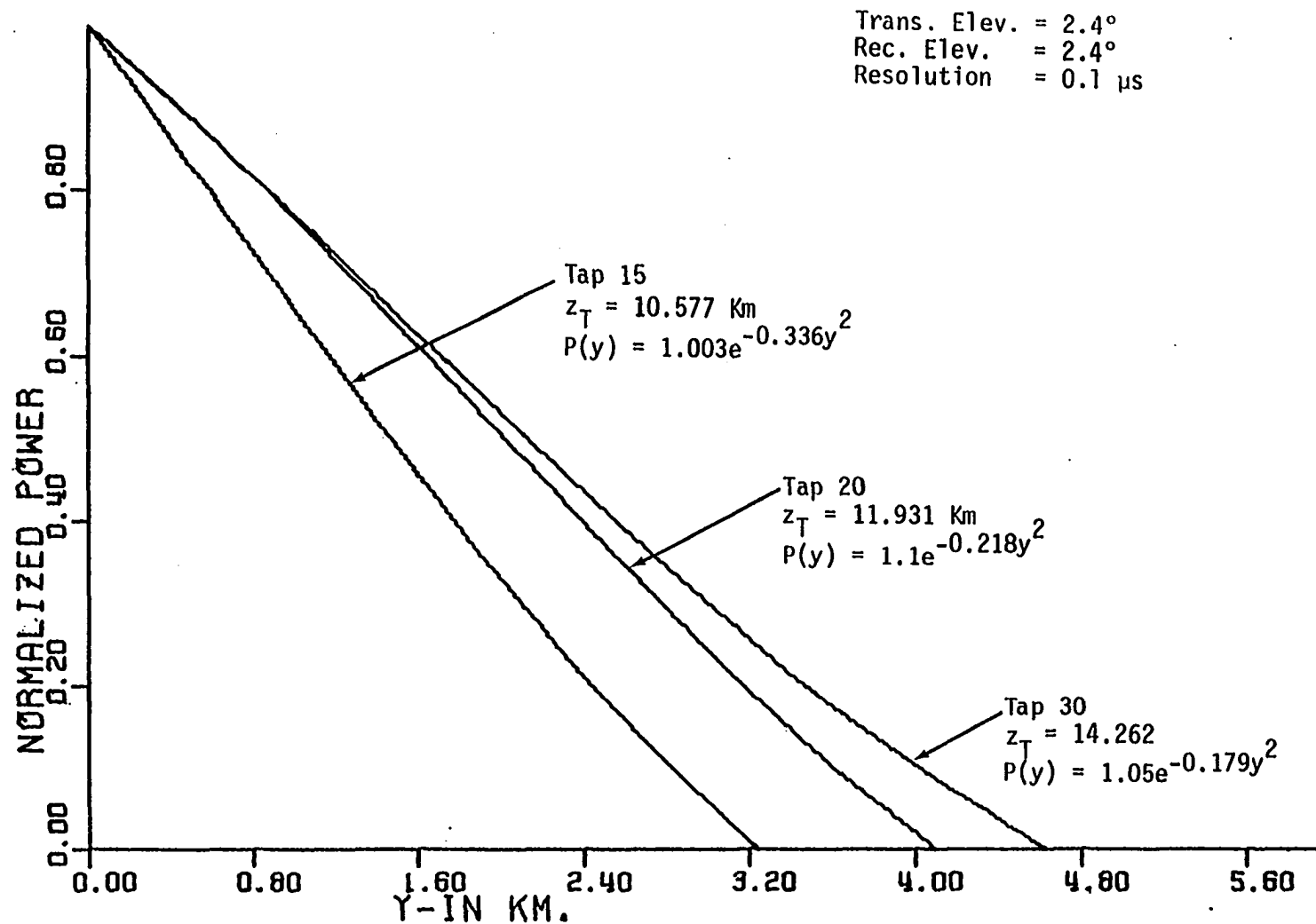


Figure 3.6. Isotropic normalized received power vs crosspath position for taps 15, 20 and 30

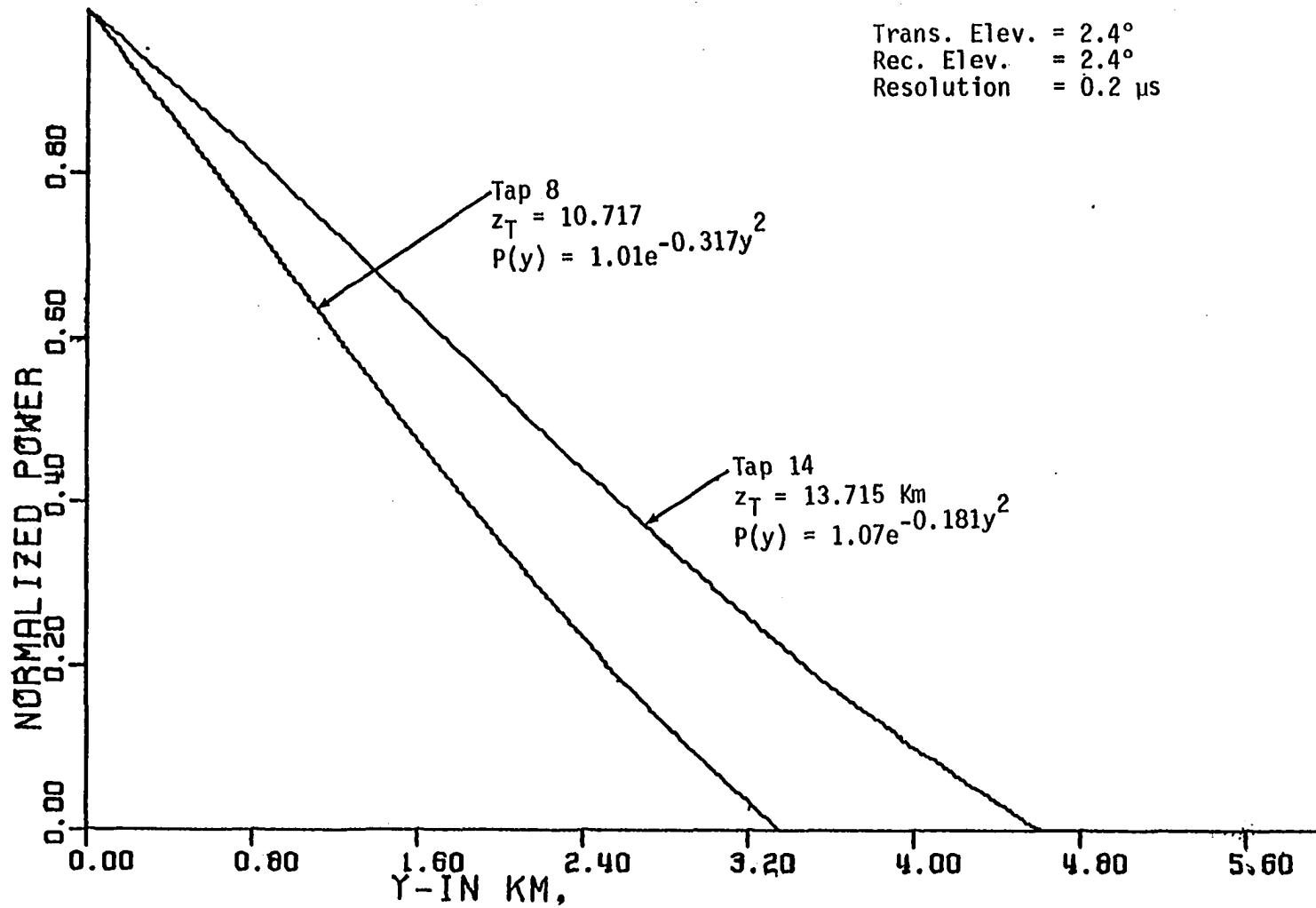


Figure 3.7. Isotropic normalized received power vs crosspath position for taps 8 and 14

the same modulation frequencies of 10 and 5 MHz. Other similar plots are generated for the whole common volume.

In order to extract the parameter a_{Ij} in Equation 3.20, a Gaussian least square fit for the curves is performed for all the taps included in the common volume. For the samples presented, the Gaussian fit is shown on the corresponding curve beside its tap height. It should be noticed that the parameter a_{Ij} for a given elevation and resolution tends to decrease as the tap height increases, and reaches a minimum before it increases again.

2. The crosspath wind speed

The crosspath wind plays an important role in determining the Doppler frequency, as shown in Chapter II, Equation 2.27. The wind data used in our analysis is a forecasted wind aloft from the nearest meteorological station to the common volume. This station is at Dubuque, Iowa, which is about 50 km from the line joining the transmitter at the Fick Observatory, Ames, Iowa and the receiver at Arlington, Wisconsin. This line is 70° East of North. Table 3.1 shows a sample of the forecasted wind at Dubuque, Iowa on April 2, 1981.

It should be emphasized here that the wind data used in our analysis is a forecasted wind near the common volume. This is all we have at the present time, while actual crosspath wind at the common volume should be used in Equation 3.21. This problem arises whenever one attempts to use Doppler frequency information to determine the anisotropy coefficient and it is independent of the scattering model employed in the process. Birkemeier et al. [19] have shown that the

Table 3.1. Wind aloft at Dubuque on April 2, 1981

Height in meters	Wind speed in m/s	Direction from North in degrees
3658	16.923	260
5486	25.641	270
7315	30.769	270
9144	37.436	280
10363	42.564	280
11887	45.641	280

RAKE system is capable of measuring the cross path wind. To do so requires that a characteristic wind "signature" be recognized in the scattering function plot. Because this method requires the analysis of the spectra of several time delay taps at a given instant of time, it will not be used in our analysis.

3. The coefficient B_j

The data coming from the RAKE receiver are in the form of voltages, both the inphase "I" and the Quadrature "Q" components are obtained. A microprocessor based data acquisition and analysis system developed especially for the troposcatter project at ISU is used in calculating the Doppler spectra of the received signal. This system has two parts; one at the receiver site in Arlington, WI that sequentially samples both the I and Q components of the signal for each tap at a rate of 28.41 samples/sec. The sampled data are digitized and recorded on a tape

cassette for further processing. Information such as date, time, tap given, and tap gain are also recorded at the beginning of each tap record. The second part of the data acquisition system is in Ames, Iowa. This part processes the recorded data, calculates the Fast Fourier Transform and plots the Doppler spectrum for each tap. Samples of the form of the output plots are shown in Figures 3.8 through 3.10. These samples correspond to data taken on November 20, 1981. The antenna elevations were 1.1° and 0.5° for the transmitter and receiver, respectively. The modulation frequency was 5 MHz. The samples show the nature of the variations in the half power width of the Doppler spectra. In tap 14, the width is comparably smaller with respect to tap 1 which is a typical representative. Tap 3 shows a broadening of the Doppler spectrum.

The coefficient B_j in Equation 3.21 is found by a Gaussian least square fit in the form of Equation 3.19 for the Doppler spectrum for each tap. Equation 3.19 can be put in a convenient form for linear regression as follows:

$$10 \log_{10} P(f_d) = 10 \log_{10} C_{2j} - (10B_j \log_{10} e) f_d^2. \quad (3.26)$$

Thus, a regression between the received power in dB, $10 \log P(f_d)$, and the Doppler frequency squared f_d^2 will give the first term and the factor between parentheses in Equation 3.26, which includes B_j . The data are fitted to points from around the zero Doppler out to those points for which the power is well below the 3dB level, since we are interested only in the half power width of the Doppler spectrum. It is

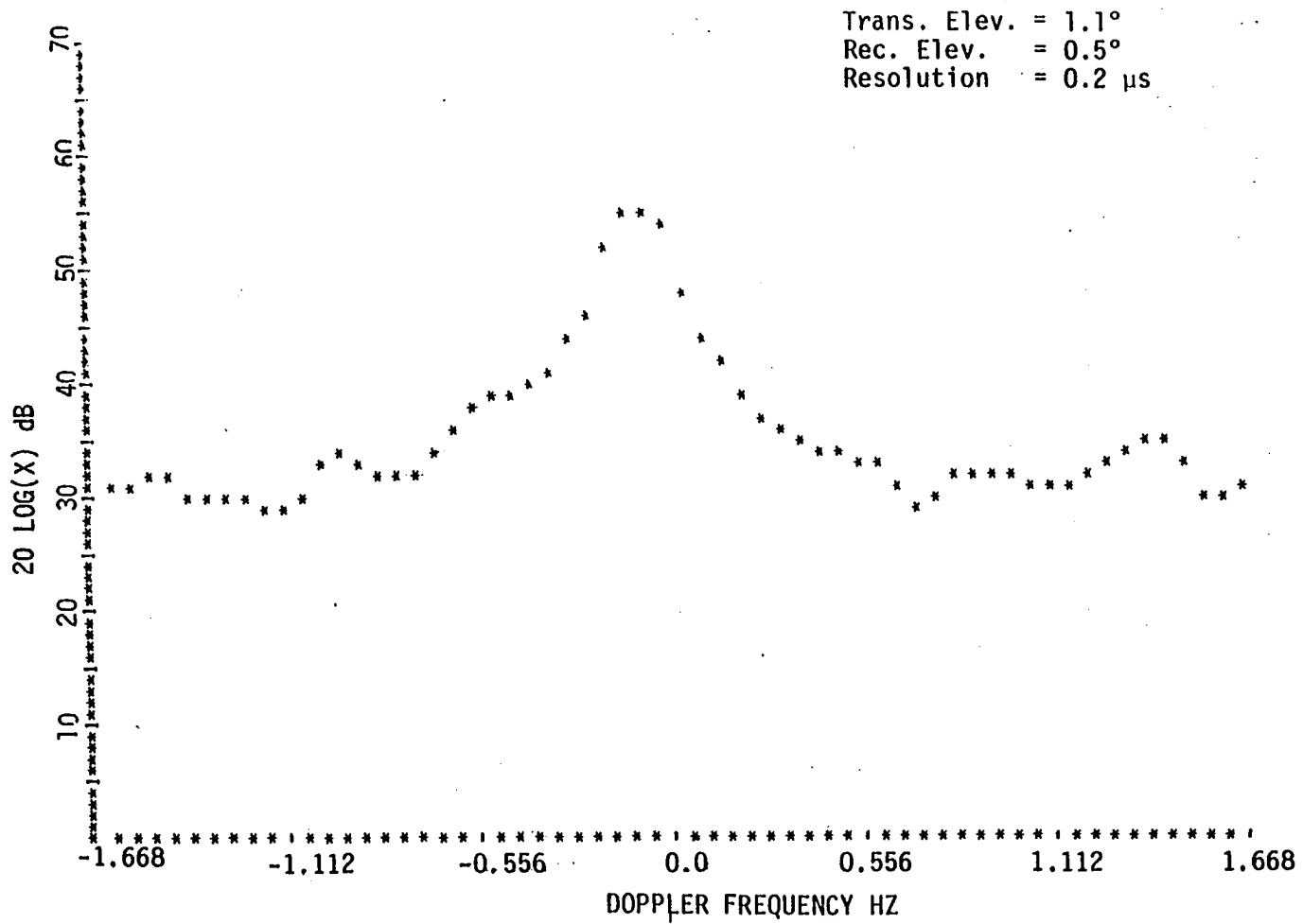


Figure 3.8. Doppler spectra for tap 14, November 20, 1981

Trans. Elev. = 1.1°
Rec. Elev. = 0.5°
Resolution = 0.2 μs

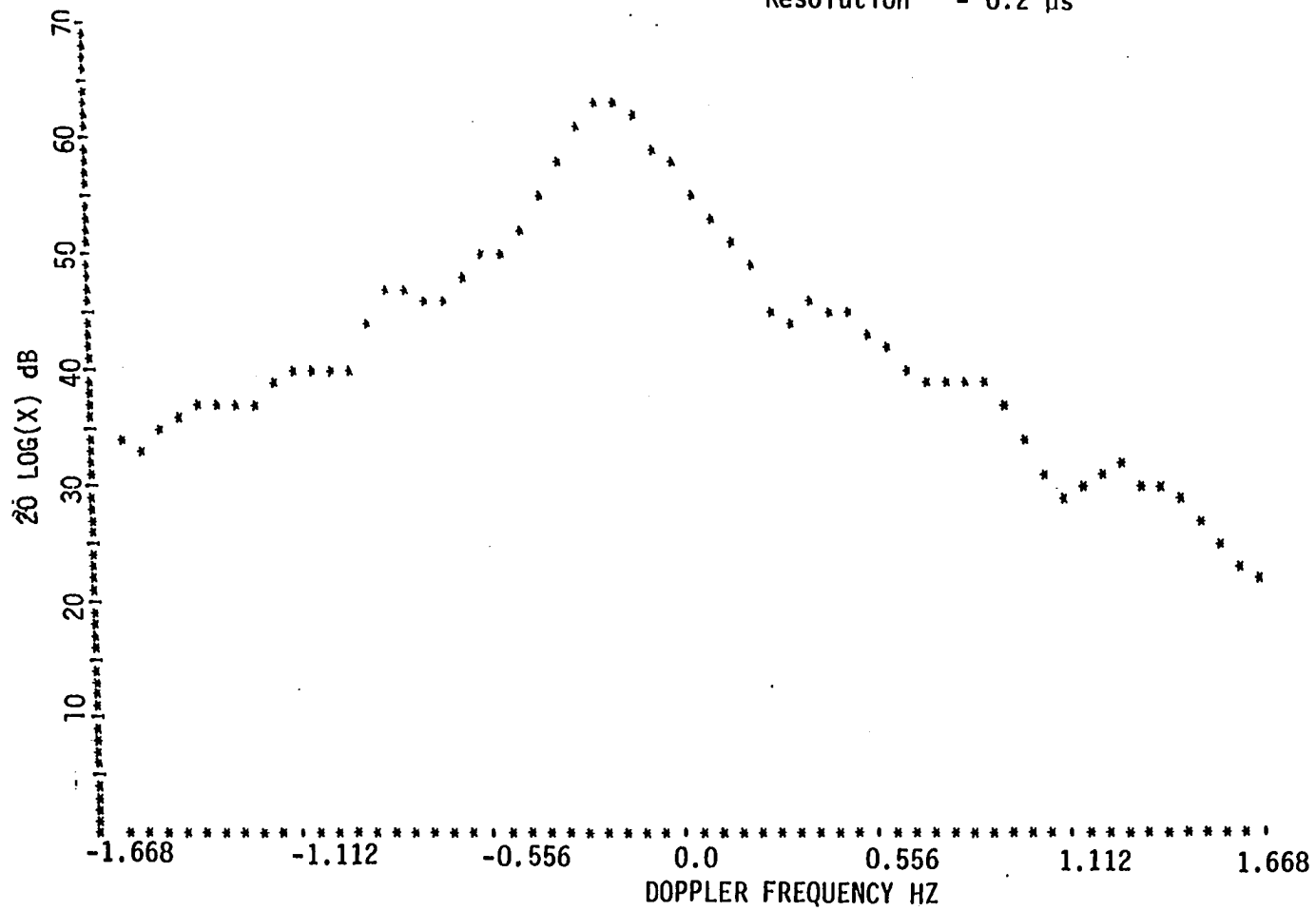


Figure 3.9. Doppler spectra of tap 1, November 20, 1981

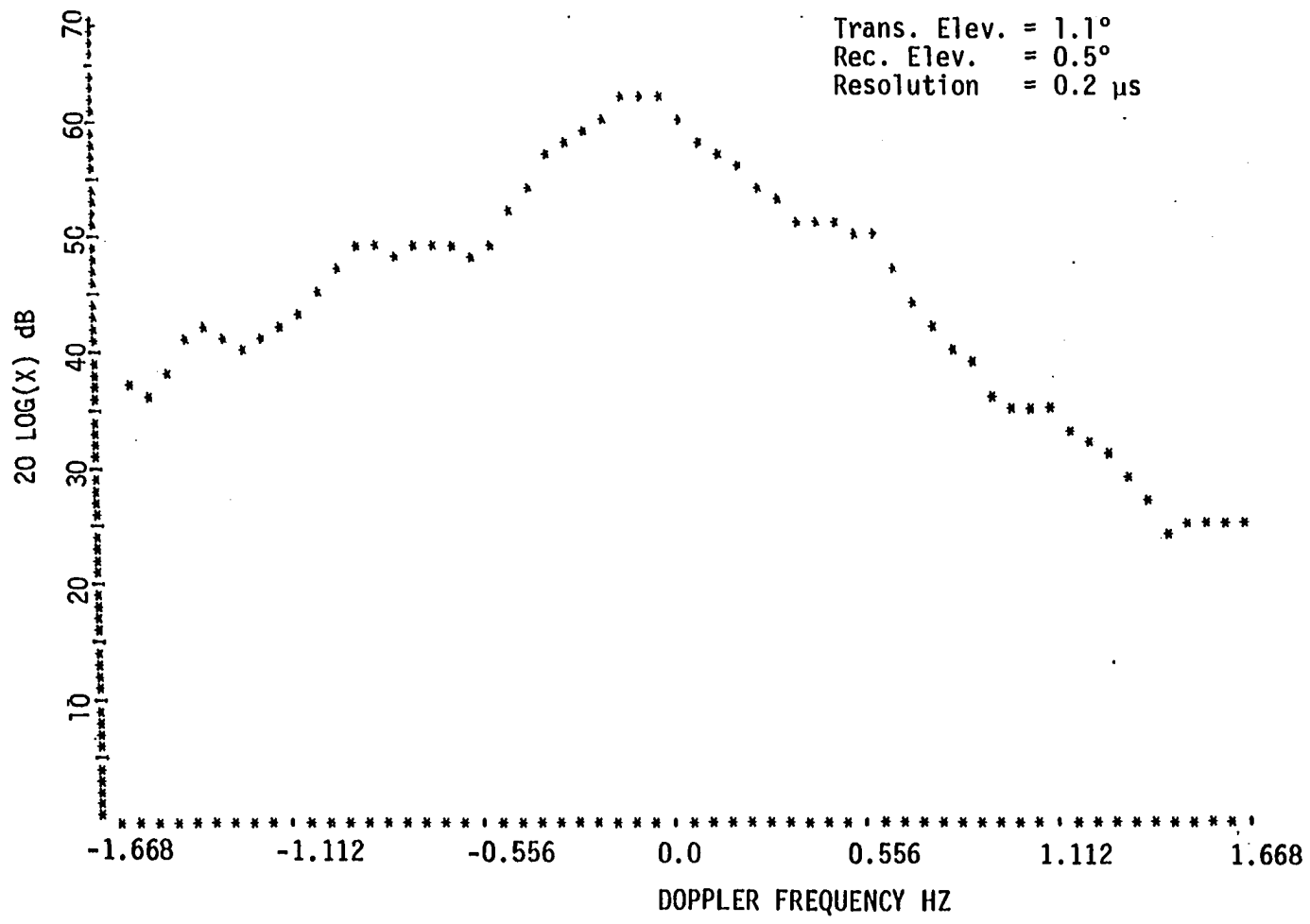


Figure 3.10. Doppler spectra of tap 3, November 20, 1981

found that 10 data points above and below the zero Doppler, besides the zero Doppler point, together with intermediate cross path wind speed give the most satisfactory anisotropy coefficient. A short program is written to calculate the parameter B_j and C_{2j} for each tap based on the data points for that tap.

4. Illustrative examples

All the parameters needed for the inversion process to get the anisotropy coefficient A from Equation 3.21 have been discussed in the preceding section. Since we do not have the facilities for radio sounding at midpath to get more accurate meteorological information, no concentrated runs over several consecutive days were performed. Instead, runs every two or three weeks were carried out through 1981 and 1982. Forecasted wind information aloft, which is provided by the National Weather Service Office in Des Moines, was used.

Among the data available, the analysis for data of April 2, November 20, 1981 and March 11, April 6, 1982 are presented. The results are shown in the form of variation of the anisotropy coefficient A with tap number (height, or delay) in Figures 3.11 through 3.14 for the mentioned dates. Tables 3.2 through 3.9 summarize the necessary calculations. Two runs are usually shown for each date to show the stationarity of the atmosphere and to get some kind of average value of A . In all the figures, the two runs for each day show nearly the same type of variation of A with tap numbers which indicate that the atmosphere is stationary during the course of the measurements. It should be noticed that due to some difficulties in the data taking or reading the

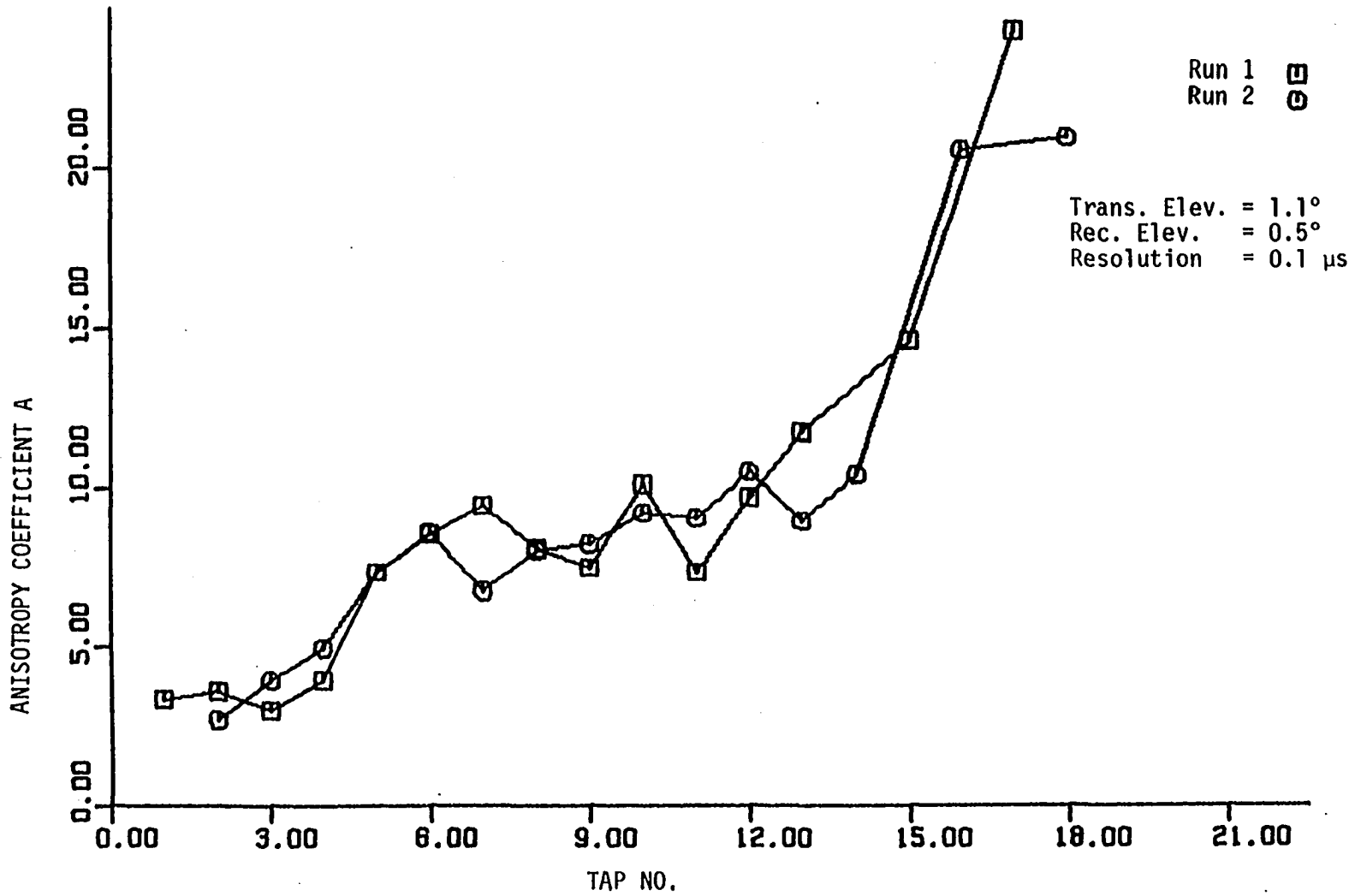


Figure 3.11. Anisotropy variation with height, April 2, 1981

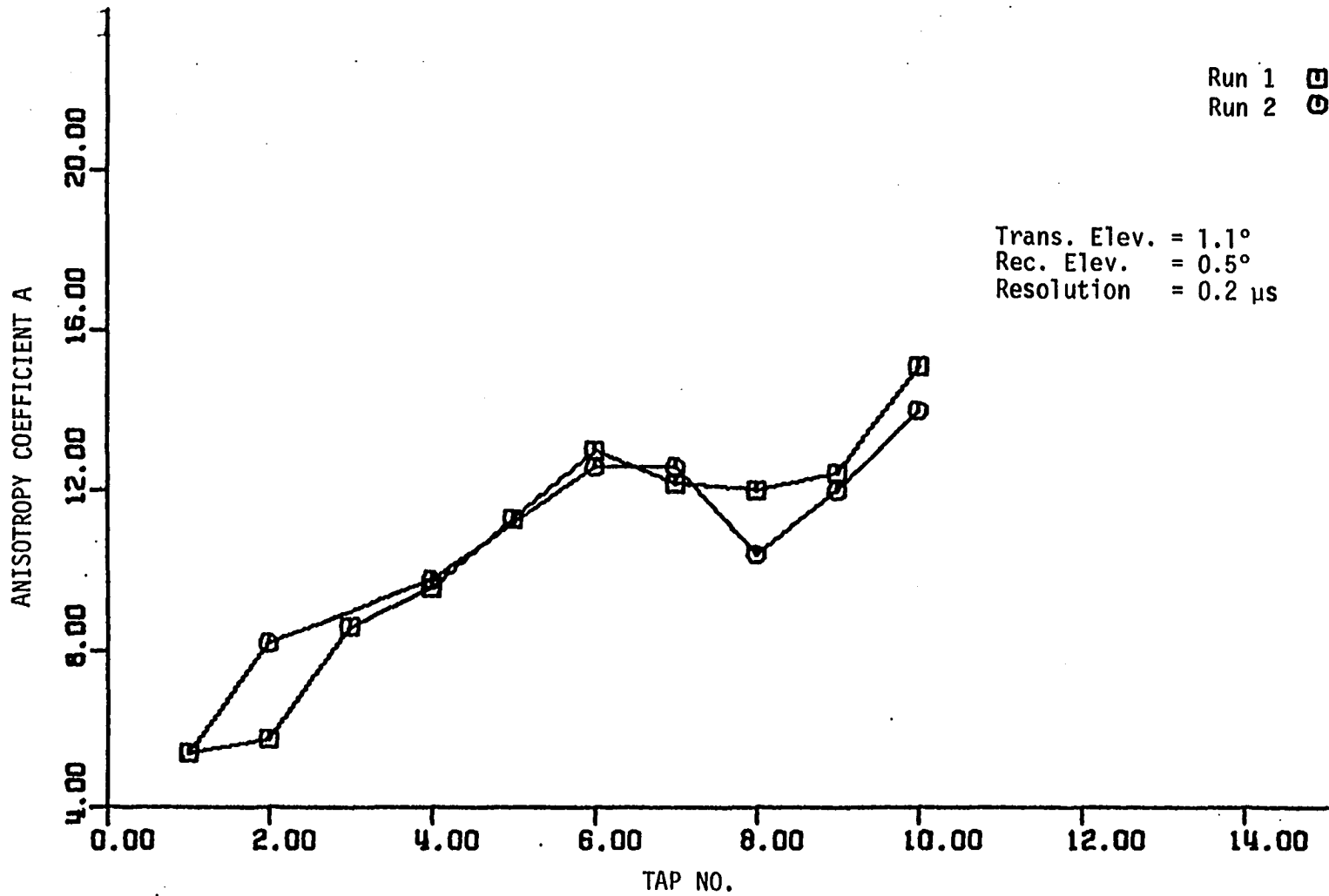


Figure 3.12. Anisotropy variation with height, November 20, 1981

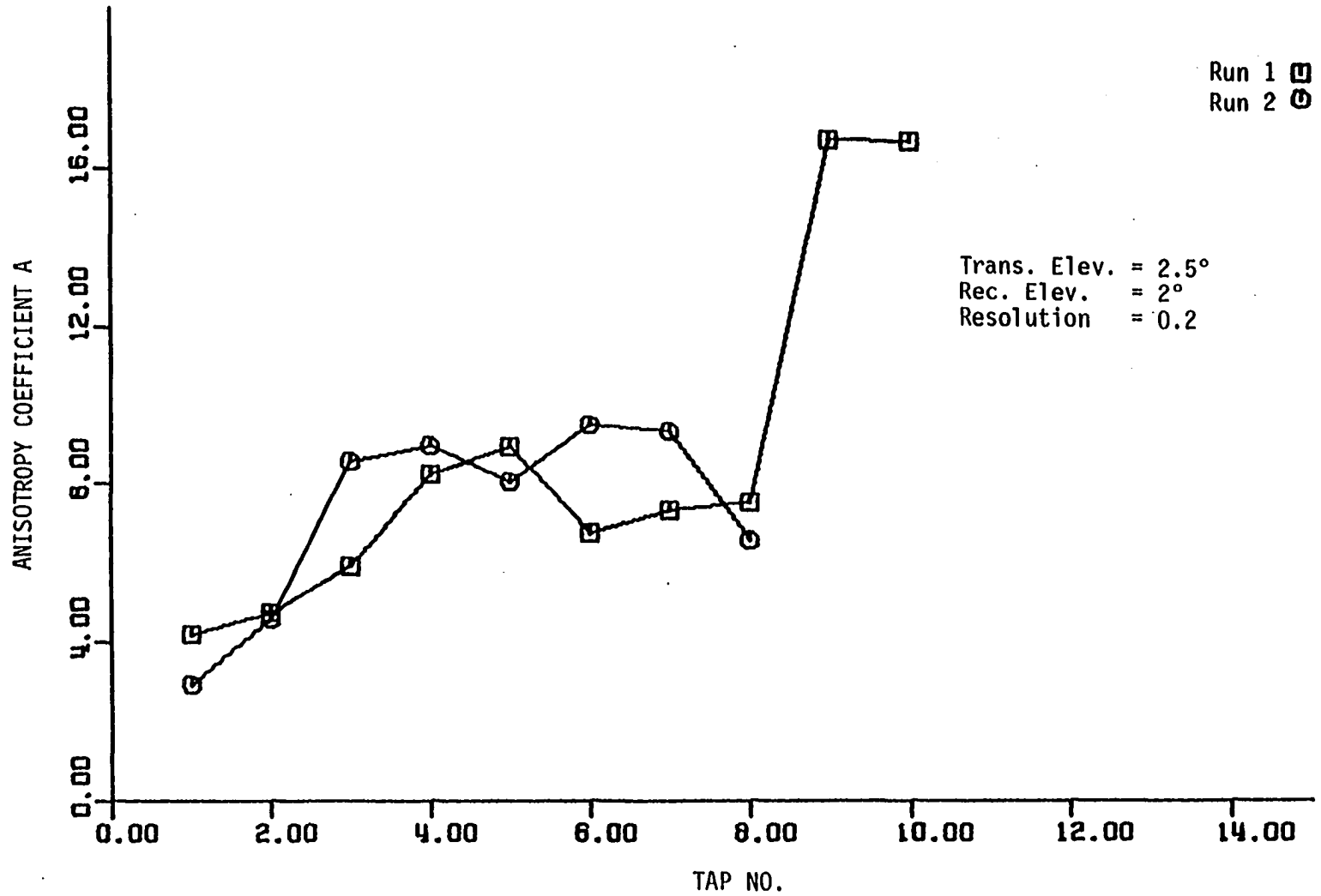


Figure 3.13. Anisotropy variation with height, March 11, 1982

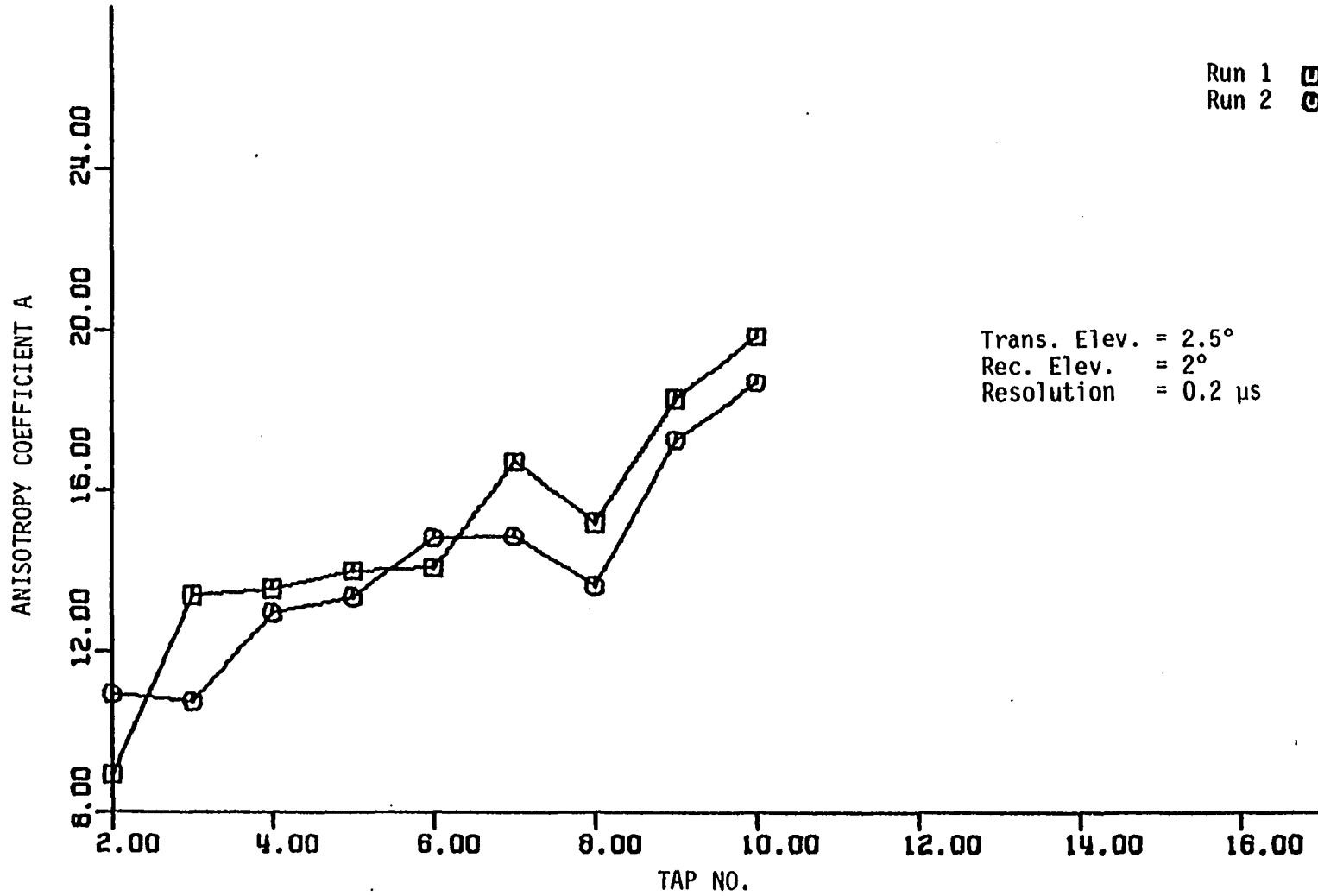


Figure 3.14. Anisotropy variation with height, April 6, 1982

Table 3.2. Data of April 2, 1981, Run 1; Trans. Elevation = 1.1°, Rec. Elevation = 0.5°; Resolution = 0.1 microseconds

Tap #	z_T (Km)	V(m/s)	Ln P(f_d)	10 log P(f_d)	B_j	A_j
1	5.145	8.46	0.073-0.354 y^2	50.28-59.26 f_d^2	13.65	3.34
2	5.708	8.46	0.093-0.287 y^2	51.29-53.47 f_d^2	12.31	3.6
3	6.22	8.46	0.115-0.245 y^2	49.57-35.36 f_d^2	8.14	3.0
4	6.692	8.46	0.112-0.221 y^2	49.95-45.38 f_d^2	10.45	3.95
5	7.134	12.82	0.106-0.204 y^2	53.16-48.41 f_d^2	11.38	7.37
6	7.549	12.82	0.100-0.192 y^2	46.46-57.98 f_d^2	13.35	8.54
7	7.942	12.82	0.092-0.184 y^2	53.38-63.56 f_d^2	14.64	9.45
8	8.317	12.82	0.083-0.178 y^2	52.20-43.82 f_d^2	10.09	8.09
9	8.676	12.82	0.0725-0.175 y^2	50.44-35.43 f_d^2	8.16	7.49
10	9.021	15.38	0.062-0.173 y^2	48.92-39.31 f_d^2	9.05	10.1
11	9.353	15.38	0.050-0.174 y^2	46.66-20.99 f_d^2	4.833	7.36
12	9.673	15.38	0.039-0.176 y^2	42.78-32.18 f_d^2	7.41	9.69
13	9.983	15.38	0.027-0.182 y^2	41.22-43.19 f_d^2	9.94	11.72
15	10.577	15.38	0.004-0.203 y^2	38.24-58.88 f_d^2	13.56	14.6
17	11.138	24.06	-0.017-0.250 y^2	38.22-58.32 f_d^2	13.43	24.31

Table 3.3. Data of April 2, 1981, Run 2; Trans. Elevation = 1.1°, Rec. Elevation = 0.5°; Resolution = 0.1 microseconds

Tap #	z_T (Km)	V(m/s)	$\ln P(f_d)$	$10 \log P(f_d)$	B_j	A_j
2	5.708	8.46	$0.093-0.287 y^2$	$50.42-36.94 f_d^2$	8.51	2.71
3	6.22	8.46	$0.115-0.245 y^2$	$54.66-51.68 f_d^2$	11.94	3.94
4	6.692	8.46	$0.112-0.221 y^2$	$50.96-64.49 f_d^2$	14.85	4.96
5	7.134	12.82	$0.106-0.204 y^2$	$56.71-49.21 f_d^2$	11.33	7.36
6	7.549	12.82	$0.100-0.192 y^2$	$56.23-40.74 f_d^2$	9.38	8.59
7	7.942	12.82	$0.092-0.184 y^2$	$60.84-34.79 f_d^2$	8.01	6.77
8	8.317	12.82	$0.083-0.178 y^2$	$57.33-43.33 f_d^2$	9.98	8.04
9	8.676	12.82	$0.073-0.175 y^2$	$56.88-41.86 f_d^2$	9.64	8.23
10	9.021	15.38	$0.062-0.173 y^2$	$58.18-33.16 f_d^2$	7.63	9.2
11	9.353	15.38	$0.050-0.174 y^2$	$55.73-30.05 f_d^2$	6.923	9.03
12	9.673	15.38	$0.039-0.176 y^2$	$55.88-37.24 f_d^2$	8.57	10.5
13	9.983	15.38	$0.027-0.182 y^2$	$54.09-26.49 f_d^2$	6.14	8.94
14	10.284	15.38	$0.015-0.19 y^2$	$51.68-32.95 f_d^2$	7.59	10.38
16	10.861	24.06	$-0.007-0.221 y^2$	$51.32-44.06 f_d^2$	10.14	20.55
18	11.409	24.06	$-0.026-0.297 y^2$	$46.16-42.21 f_d^2$	9.72	20.95

Table 3.4. Data of Nov. 20, 1981, Run 1; Trans. Elevation = 1.1°, Rec. Elevation = 0.5°; Resolution = 0.2 microseconds

Tap #	z_T (Km)	V(m/s)	$\text{Ln } P(f_d)$	$10 \log P(f_d)$	B_j	A_j
1	5.412	14.36	0.079-0.32 y^2	52.83-38.89 f_d^2	8.95	5.39
2	6.447	14.36	0.112-0.233 y^2	55.78-30.86 f_d^2	7.11	5.75
3	7.335	15.96	0.103-0.198 y^2	60.98-40.27 f_d^2	9.27	8.59
4	8.126	15.92	0.087-0.181 y^2	52.05-40.44 f_d^2	9.31	9.56
5	8.845	15.92	0.067-0.174 y^2	56.69-46.89 f_d^2	10.88	11.27
6	9.51	18.46	0.045-0.175 y^2	49.77-39.66 f_d^2	9.13	12.99
7	10.131	18.46	0.021-0.185 y^2	44.77-31.32 f_d^2	7.21	12.17
8	10.717	18.46	-0.002-0.211 y^2	52.64-27.96 f_d^2	6.44	12.02
9	11.272	16.41	-0.022-0.27 y^2	54.87-35.47 f_d^2	8.17	12.45
10	11.801	16.41	-0.038-0.463 y^2	54.13-49.57 f_d^2	11.41	15.15

Table 3.5. Data of Nov. 20, 1981, Run 2; Trans. Elevation - 1.1°, Rec. Elevation = 0.5°; Resolution = 0.2 microseconds

Tap #	z_T (Km)	V(m/s)	Ln P(f_d)	10 log P(f_d)	B_j	A_j
1	5.412	14.36	0.079-0.32 y^2	57.17-39.34 f_d^2	9.06	5.42
2	6.447	14.36	0.112-0.233 y^2	59.01-58.15 f_d^2	13.39	8.2
4	8.126	15.9	0.087-0.181 y^2	52.23-42.04 f_d^2	9.68	9.76
6	9.51	18.46	0.045-0.175 y^2	54.29-37.45 f_d^2	8.62	12.6
7	10.131	18.46	0.021-0.185 y^2	53.30-33.38 f_d^2	7.69	12.59
8	10.717	18.46	-0.002-0.211 y^2	46.69-21.65 f_d^2	4.98	10.41
9	11.272	16.41	-0.022-0.027 y^2	52.67-33.26 f_d^2	7.66	12.0
10	11.801	16.41	-0.038-0.463 y^2	51.60-43.567 f_d^2	10.03	14.01

Table 3.6. Data of March 11, 1982, Run 1; Trans. Elevation = 2.5°, Rec. Elevation = 1°; Resolution = 0.2 microseconds

Tap #	z_T (Km)	V (m/s)	$\text{Ln } P(f_d)$	$10 \log P(f_d)$	B_j	A_j
1	5.412	12.18	0.053-0.97 y^2	51.01-56.04 f_d^2	12.9	4.2
2	6.447	12.18	0.070-0.421 y^2	55.77-23.15 f_d^2	8.55	4.77
3	7.335	16.43	0.075-0.293 y^2	57.47-20.96 f_d^2	4.83	5.91
4	8.126	16.43	0.077-0.235 y^2	60.4-29.694 f_d^2	6.84	8.24
5	8.845	16.43	0.086-0.201 y^2	56.99-28.96 f_d^2	6.67	8.93
6	9.51	18.65	0.101-0.179 y^2	55.4-12.085 f_d^2	2.78	6.75
7	10.131	18.65	0.122-0.163 y^2	56.95-12.20 f_d^2	2.81	7.31
8	10.717	18.65	0.131-0.153 y^2	49-97-11.50 f_d^2	2.66	7.53
9	11.272	23.17	0.122-0.149 y^2	53.46-29.33 f_d^2	6.75	16.73
10	11.801	23.17	0.108-0.147 y^2	53.45-26.66 f_d^2	6.14	16.67

Table 3.7. Data of March 11, 1982, Run 2; Trans. Elevation = 2.5°, Rec. Elevation = 1°; Resolution = 0.2 microseconds

Tap #	z_T (Km)	V(m/s)	Ln P(f_d)	$10 \log P(f_d)$	B_j	A_j
1	5.412	12.18	0.053-0.97 y^2	49.02-41.83 f_d^2	9.63	2.94
2	6.447	12.18	0.07-0.421 y^2	55.47-35.28 f_d^2	8.12	4.59
3	7.335	16.43	0.075-0.293 y^2	60.33-39.06 f_d^2	8.99	8.56
4	8.126	16.43	0.077-0.235 y^2	57.24-34.54 f_d^2	7.94	8.96
5	8.845	16.43	0.086-0.201 y^2	58.4-24.126 f_d^2	5.55	8.05
6	9.51	18.65	0.101-0.179 y^2	60.08-21.76 f_d^2	5.01	9.49
7	10.131	18.65	0.122-0.163 y^2	57.97-18.64 f_d^2	4.29	9.32
8	10.717	18.65	0.131-0.153 y^2	56.43-9.280 f_d^2	2.14	6.59

Table 3.8. Data of April 6, 1982, Run 1; Trans. Elevation = 2.5°, Rec. Elevation = 2.0°; Resolution = 0.2 microseconds

Tap #	z_T (Km)	V(m/s)	$\text{Ln } P(f_d)$	$10 \log P(f_d)$	B_j	A_j
2	6.447	18.68	$0.045-0.648 y^2$	$44.63-45.93 f_d^2$	10.58	8.96
3	7.335	20.87	$0.008-0.355 y^2$	$45.34-56.04 f_d^2$	12.99	13.41
4	8.126	20.87	$0.045-0.256 y^2$	$56.34-46.34 f_d^2$	10.67	13.57
5	8.845	20.87	$0.112-0.208 y^2$	$58.97-41.44 f_d^2$	9.54	14.0
6	9.51	24.42	$0.143-0.178 y^2$	$58.43-26.57 f_d^2$	6.11	14.1
7	10.131	24.42	$0.162-0.158 y^2$	$57.98-32.25 f_d^2$	7.43	16.67
8	10.717	24.42	$0.165-0.145 y^2$	$62.68-24.11 f_d^2$	5.55	15.19
9	11.272	24.75	$0.165-0.135 y^2$	$57.44-30.4 f_d^2$	7.0	18.29
10	11.801	24.75	$0.163-0.1275y^2$	$58.45-32.59 f_d^2$	7.5	19.86

Table 3.9. Data of April 6, 1982, Run 2; Trans. Elevation = 2.5°, Rec. Elevation = 2.0°; Resolution = 0.2 microseconds

Tap #	z_T (Km)	V(m/s)	Ln $P(f_d)$	10 log $P(f_d)$	B_j	A_j
2	6.447	18.68	0.045-0.648 y^2	53.14-4.77 f_d^2	14.91	10.95
3	7.335	20.87	0.008-0.355 y^2	58.56-37.39 f_d^2	8.61	10.77
4	8.126	20.87	0.045-0.256 y^2	60.41-42.72 f_d^2	9.84	12.99
5	8.845	20.87	0.112-0.208 y^2	59.33-37.86 f_d^2	8.72	13.35
6	9.51	24.42	0.143-0.178 y^2	60.6-29.297 f_d^2	6.74	14.85
7	10.131	24.42	0.162-0.158 y^2	58.69-25.88 f_d^2	5.96	14.87
8	10.717	24.42	0.165-0.145 y^2	55.79-19.61 f_d^2	4.51	13.63
9	11.272	24.75	0.165-0.135 y^2	52.74-27.16 f_d^2	6.25	17.25
10	11.801	24.75	0.163-0.1275 y^2	60.61-28.97 f_d^2	6.67	18.69

taps, some of the data corresponding to certain tap are missed.

Examining these figures, one notices that data of April 2, November 20, 1981 and March 11, 1982 exhibit a larger variability than that of April 6, 1982. A general feature of the data is an increase of the anisotropy with height (tap number), leveling off at intermediate heights before it starts to increase again at large altitudes.

Figure 3.11 starts with a small value of A near the grazing height (taps 1, 2) and then levels off from tap 6 to tap 13 before it starts to increase more rapidly at tap 14. In Figure 3.12, the anisotropy increases more rapidly until tap 6 before it levels off. Figure 3.13 exhibits an increase to tap 3 and then levels off. Figure 3.14 is characterized by high value of anisotropy and less oscillations.

At this point, it is instructive to see the general variation of the anisotropy with height obtained by other experimentors. The only information available is that of Birkemeier in his report of 1974 to the Rome Air Development Center [4]. Figure 3.15 summarizes his results on the anisotropy variation. He found the values of A from both layer tracks and the zero Doppler signal enhancement over that predicted by balloon measurements of the refractive index fluctuation (ΔC_n^2). The results show the general trend of increase of A with height starting with a nearly isotropic, $A = 1$, near grazing and increasing to about $A = 6$ before it levels off with increasing height. It should be noticed that the values of A shown in Figure 3.15a are average values for each tap. Values of A up to 30 in each tap were reported. This feature of variation of A exists in our data, which indicates that our model gives

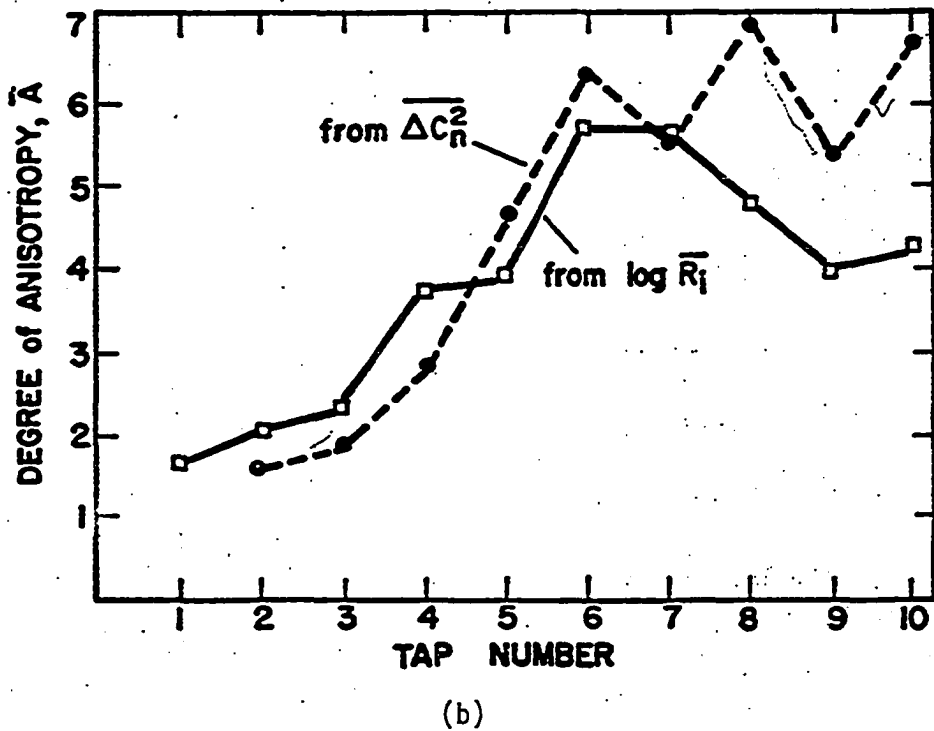
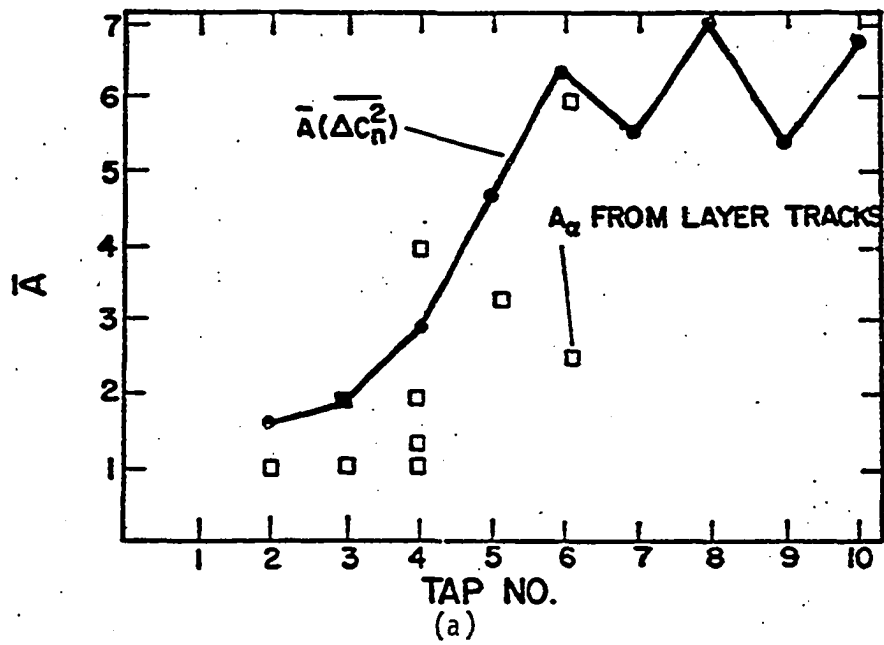


Figure 3.15. Comparison of \bar{A} values for C_n^2 and both layer track and $\log \bar{R}_i$ [4]

a reasonable estimate of A.

Another aspect that gives a clue about the variation of the anisotropy with height is its relation to atmospheric stability. A suggested relation between the anisotropy and the stability measured by Birkemeier [4] is $A \approx \log_{10} R_i$, where R_i is Richardson's number for determining atmospheric stability. Values of $R_i < 0$ indicate turbulence and the scattering is considered to be isotropic, i.e. $A = 1$. $R_i \geq 0.25$ indicates high stability. A general feature of atmospheric stability is its increase with height and a corresponding increase of A will follow the same trend. This is clear in Figure 3.15b.

Our data are supported by the above-mentioned literature, except for the sudden increase in the anisotropy coefficient at higher altitude. This is believed to correspond to the tropopause height at which a high degree of stability will result in higher values of the anisotropy coefficient.

IV. THE EFFECT OF ANISOTROPY ON THE DELAY POWER SPECTRA AND MULTIPATH SPREAD OF TROPOSCATTER SIGNALS

A. Introduction

The shape of the delay power spectra of signals received on scatter communication links plays a very important role in the performance of these links. Bello and Ehrman [7] have shown that the multipath spread (Δ) is a basic parameter that affects the irreducible BER produced by frequency selective fading. However, Bello's model is based on average isotropic atmospheric conditions. Several studies [20, 21] to improve the ability of Bello's model to accurately predict the delay power spectrum of troposcatter links of different characteristics have been reported. It is believed that the delay power spectra could not only vary from one link to another depending on the path geometry and the antenna beam width, but also could vary on the same link depending on the state of the atmosphere.

In this chapter, the more realistic description of scattering in terms of the anisotropic model presented in the previous chapter is utilized in the calculations of the delay power spectra. Several profiles of the anisotropy coefficient are used and their corresponding spectra are shown. The main effect of the delay spectra on received signals appears in the form of intermodulation distortion. Several studies on this phenomenon have been reported [6, 22, 23], among which we utilize the one reported by Bello and Nelin [6] because it is more general and more complete. Intermodulation distortion results in an irreducible error in digital troposcatter transmission [7].

Section B describes the calculations used to find the delay power spectra based on an anisotropic scattering model. Section C shows several theoretical anisotropy profiles which are used to demonstrate the effect of anisotropy on the delay power spectra. The probability density function of the intermodulation distortion and its sensitivity to the anisotropy profiles together with the irreducible error probabilities are also shown in Section C. Section D presents the experimental results for the measurements of the multipath spread and compares them with calculations based on the anisotropic model.

B. The Description and Calculations of Delay Power Spectra Based on an Anisotropic Model

In 1969, Bello introduced a more physical characterization of the troposcatter channel in the time domain and presented the concept of the delay power spectrum which represents the average path gain as a function of multipath delay. On a short time basis, the troposcatter channel is regarded as a continuum of statistically stationary, independently fading paths, each providing complex Gaussian signal fluctuations. The resulting envelope of the received carrier has a Rayleigh fading characteristic.

The troposcatter channel suffers what is known as frequency selective fading which means that at any time instant, the amplitude and phase of the transfer function vary in a random fashion along the frequency axis. An approximately constant amplitude and linear phase can only be observed over a sufficiently small frequency interval. The fading is highly correlated in this case, whereas for sufficiently

separated frequencies, the fading is highly uncorrelated. This frequency selective behavior is usually described by the frequency correlation function, which is the cross correlation between two received carriers as a function of their frequency separation.

While the frequency selective behavior could be described by the frequency correlation function, the delay power spectra gives a more physical characterization. In order to gain insight into the delay power spectra and its relation to the input and output processes, a brief description of the delay power spectra, following Bello and Nelin [6] will be in order. Their treatment is based on the following assumptions:

1. The amounts of frequency selective fading is small.
2. The scattering channel is wide sense stationary uncorrelated (WSSUS) with Gaussian statistics.
3. Additive noise effects can be ignored in computing intermodulation distortion noise.

The relation between the output and the input is given by

$$W(t) = \int Z(t - \xi) g(t, \xi) d\xi \quad (4.1)$$

where $g(t, \xi) =$ a time varying impulse response,

$g(t, \xi)d\xi =$ the gain associated with path delays in the interval $(\xi, \xi + d\xi)$, and

$Z(t), W(t) =$ the complex envelopes of the input and output, respectively; the actual input and output are $R_e\{Z(t) \exp(i2\pi f_c t)\}$ and $R_e\{W(t) \exp(i2\pi f_c t)\}$ where f_c is the carrier frequency.

The uncorrelated scattering assumption (2) implies

$$\overline{g^*(t, \xi) g(t + \tau, \eta)} = Q(\tau, \xi) \delta(\eta - \xi) \quad (4.2)$$

where $\delta(\eta - \xi)$ is a unit impulse, and $Q(\tau, \xi)$ is the autocorrelation function of the gain fluctuations for path delays in the interval $(\xi, \xi + d\xi)$. It is called the path gain autocorrelation function. Under the slow fading conditions, $g(t, \xi)$ is practically constant over the duration of several pulses, and Equations 4.1 and 4.2 could be written as

$$W(t) = \int Z(t, \xi) g(\xi) d\xi \quad (4.3)$$

$$\overline{g^*(\xi) g(\eta)} = Q(\xi) \delta(\eta - \xi) \quad (4.4)$$

where $g(\xi)$ is the channel impulse response at the time the series of pulses are transmitted. $Q(\xi)$ is proportional to the strength of the gain fluctuations for path delays in the interval $(\xi, \xi + d\xi)$. The function $Q(\xi)$ is called the delay power density spectrum. The frequency correlation function $q(\Omega)$ and $Q(\xi)$ are Fourier transform pairs [24], i.e.

$$Q(\xi) = \int q(\Omega) \exp(i2\pi\Omega\xi) d\Omega \quad (4.5)$$

$$q(\Omega) = \int Q(\xi) \exp(i2\pi\Omega\xi) d\xi \quad (4.6)$$

The shape of the function $Q(\xi)$ plays an important role in the study of intermodulation distortion and the bit error rate for digital troposcatter transmission.

1. Bello's model for calculating the delay power spectra

Bello [5] introduced a single integral troposcatter channel model to calculate the received power as a function of the path delay. As

mentioned in Chapter II, paths of constant time delay correspond to prolate spheroids with foci at the transmitter and receiver. Starting from Equation 2.1 in its differential form, which is repeated here for convenience,

$$dP_r = Q(\xi)d\xi \sim \frac{G_t G_r}{R_1^2 R_2^2} \sigma(\theta) dV \quad (4.7)$$

and using the Booker-Gordon blob scattering theory for which the three-dimensional spectral density of the refractive index fluctuation of Equation 2.16, $\sigma(\theta)$ is written as

$$\sigma(\theta) \approx \frac{1}{h\theta^m} \quad (4.8)$$

where m is the scattering angle exponent and h is the height of the scattering blob above the chord joining the transmitter and the receiver, Bello developed the following general integral for $Q(\xi)$:

$$Q(\xi) = \frac{1}{\delta^{(1+m/2)}} \int_{\psi_0/\sqrt{2\delta}}^{\sqrt{2\delta}/\phi_0} \frac{G_t(x\sqrt{2\delta}-\psi_0)G_r(\frac{\sqrt{2\delta}}{x}-\phi_0)}{x(x+\frac{1}{x})^{m-2}} dx \quad (4.9)$$

Where ψ_0 and ϕ_0 = the elevation angles of the horizon at the transmitter and the receiver, respectively,

$\delta = \frac{C}{D} \xi - 1$ = a normalized delay parameter, C is the velocity of light and D is the straight line distance between the transmitter and the receiver, and

$G_t()$ and $G_r()$ = the vertical antenna patterns of the transmitter and the receiver (refer to Figure 2.1).

It should be noted that in the integral of Equation 4.9, the antenna elevations are adjusted to have maximum gain at ψ_0 and ϕ_0 , which is not necessarily the general situation. Sometimes it is advantageous to clear the total half power beam width above the horizon, in which case ψ_0 and ϕ_0 in the integration limit are understood to be the horizon elevations and ψ_0 and ϕ_0 in the gain formulas are understood to be the elevations of the center beams.

Bello used a value of $m=5$, which did not accurately predict the delay power spectra for short troposcatter paths. His model was later modified by Daniel and Reinman [20], and by Pusone and Hoag [21] who developed a delay power model based on the physics of the gases in the troposphere together with mean meteorological measurements.

2. Delay power spectra based on an anisotropic model

The model presented in the previous section for calculating the delay power spectra represents the power actually received at zero Doppler frequency in the Doppler delay plane of the scattering function representation of the forward scatter power. The difference between the zero Doppler power and the total power for a specific delay was shown by Birkemeier [4] to be very slight. Thus, the zero Doppler power as a function of the delay represents a very good estimate for the delay power spectrum. In addition, it is relatively easy to measure experimentally using a RAKE receiver. It was shown in the previous chapter that the received Doppler power for a delay tap j is given by Equation 3.18. The equation is repeated here for convenience as Equation 4.10.

$$P_j(f_d) = A_j^2 C_{Ij} \exp \left\{ -\frac{1049}{v_j^2} (a_{Ij} + \frac{1.506}{z_T} (A_j^2 - 1) f_d^2) \right\} . \quad (4.10)$$

For zero Doppler conditions, Equation 4.10 reduces to

$$P_j(0) = A_j^2 C_{Ij} . \quad (4.11)$$

The index j refers to the delay tap and C_{Ij} represents the received zero Doppler power under isotropic conditions.

Two important facts can be deduced from Equation 4.11. First, the zero Doppler power increases above that predicted under isotropic conditions as the square of the anisotropy coefficient. Second, the delay power spectra is seen to be a function of the variation of the anisotropy with the multipath delay; or in other words, with the anisotropy profile.

Incorporating Equation 4.11 into Bello's integral for the delay power spectra given by Equation 4.9 and using the well-accepted $-11/3$ spectrum of the refractive index fluctuations for average isotropic scattering conditions, the anisotropic version of the delay power spectrum becomes:

$$Q(\xi) = \frac{A^2(\xi)}{\delta^{14/3}} \int_{\Psi_0/\sqrt{2\delta}}^{\sqrt{2\delta}/\phi_0} \frac{G_t(x\sqrt{2\delta} - \Psi_0) G_r(\frac{\sqrt{2\delta}}{x} - \phi_0)}{x(x + \frac{1}{x})^{5/3}} dx \quad (4.12)$$

where the anisotropy coefficient A is written in terms of the delay.

A computer program shown in Appendix C has been developed to numerically evaluate the integral in Equation 4.12 as a function of the delay. The program has as its inputs, the anisotropy profile, the path

length, and the antenna half power beam width. Gaussian antenna patterns are assumed. The program was verified by recalculating the delay power spectra of previously calculated examples from the literature [5]. This program is also used to process the ISU-UW link data.

C. Anisotropy Profiles and Their Effect on the Delay Power Spectrum

The general behavior of the anisotropy profiles is discussed in Chapter III. It is shown that the general trend of the profile of the average anisotropy coefficient A with height (or delay) is an increase starting with a value of nearly 1 near the grazing ray height and leveling off at higher elevations. Thus, a profile that is a smoothly varying function of height will be used in showing the order of magnitude of the corresponding variation in the delay power spectra. The profiles used are: 1) a linear increase of A with delay; 2) an exponential increase of A with delay; 3) a one path model to represent elevated layers; and 4) a two-path model. Before presenting these results, some measures of the shapes of the delay power spectra which are useful for comparison purposes and which are important parameters in the study of intermodulation distortion will be considered. It is convenient to normalize $Q(\xi)$ so that

$$\int Q(\xi)d\xi = 1 . \quad (4.13)$$

With this normalization, $Q(\xi)$ has all the attributes of a probability density function [6].

The mean path delay, ξ_0 , and the multipath spread, Δ , are then defined as follows:

$$\xi_0 = \int \xi Q(\xi) d\xi \quad (4.14)$$

$$\Delta = \left[\int \xi^2 Q(\xi + \xi_0) d\xi \right]^{1/2} . \quad (4.15)$$

Sometimes a double-sided definition of Δ which is twice the value given by Equation 4.15 is used [25, 21]. In our study, the single-sided definition given by Equation 4.15 will be utilized. Two other moments are usually defined as:

$$\mu_3 = \int \xi^3 Q(\xi + \xi_0) d\xi \quad (4.16)$$

and

$$\mu_4 = \int \xi^4 Q(\xi + \xi_0) d\xi . \quad (4.17)$$

The ratio $\beta_3 = \mu_3/\Delta^3$ and $\beta_4 = \mu_4/\Delta^4$ are used in statistics as a measure of "asymmetry" and "flatness of peak" and are called the Skewness and the Excess, respectively.

1. Linear increase of anisotropy with delay

Starting with a simple case, the linear dependence of A on the delay takes the following form:

$$A(\xi) = 1 + S\xi \quad (4.18)$$

where S is the slope and has dimension of sec^{-1} . It should be noted that zero delay is chosen to correspond to the grazing ray at which

point the scattering is assumed to be isotropic ($A = 1$). Based on Birkemeier's data [4], S could range from 0 to 32 sec^{-1} .

2. Exponential increase of anisotropy with delay

An anisotropy coefficient model that has the property of leveling off at higher delays, yet maintains the increasing behavior with delay, is the following exponential:

$$A(\xi) = 1 + a(1 - \exp(-b\xi)) \quad (4.19)$$

where a and b are constants to be determined. In our case, the constant a is chosen to represent typical estimated values of anisotropy. Values of a of 7, 16, and 25 are used to represent typical, high, and very high values of the anisotropy. The determination of the constant b is based on a least square estimate for the experimentally obtained values of the anisotropy shown in Chapter III. Values of b of 1 and 0.5 are used.

3. One elevated layer

This situation is of practical importance since very often signals received via tropospheric scattering are dominated by a constant component plus a randomly scattered component. This situation is an indication of a layer [26], that reflects signals instead of scattering them. In the case of a layer, the correlation distance of the refractive index in the horizontal direction is much larger than the vertical correlation distance; and it is nearly constant. Thus, a layer could be represented by an anisotropic scattering model having a constant value

of the anisotropy coefficient A ($A = 1_x/1_z$). The effect of a layer on the delay power spectra is represented by the following equation:

$$A(\xi) = 1 + C[U(\xi - (\xi_0 - \Delta/2)) - U(\xi - (\xi_0 + \Delta/2))] \quad (4.20)$$

where C is a constant and $U(\)$ is the unit step function. The layer is chosen to be at a height corresponding to the mean delay and of width equal to the multipath spread Δ .

4. Two-layer model

Situations in propagation exist in which the atmosphere has one elevated layer and another near the surface. It also represents two-path propagation found in experimental results [27]. Thus, this situation can be considered from the anisotropic model point of view. The anisotropy coefficient is taken to vary with delay in the following form:

$$A(\xi) = \begin{cases} C & \xi_0 - \frac{3\Delta}{4} < \xi < \xi_0 - \frac{\Delta}{4} \\ C & \xi_0 + \frac{\Delta}{4} < \xi < \xi_0 + \frac{3\Delta}{4} \\ 1 & \text{otherwise} \end{cases} \quad (4.21)$$

where the two layers are assumed to have equal anisotropy coefficient C .

The delay power spectra of the previously mentioned anisotropic situations have been calculated and the results are shown in Figures 4.1, 4.2, and 4.3. Table 4.1 summarizes the different characteristics of each spectrum. The isotropic spectrum is graphed on each figure to

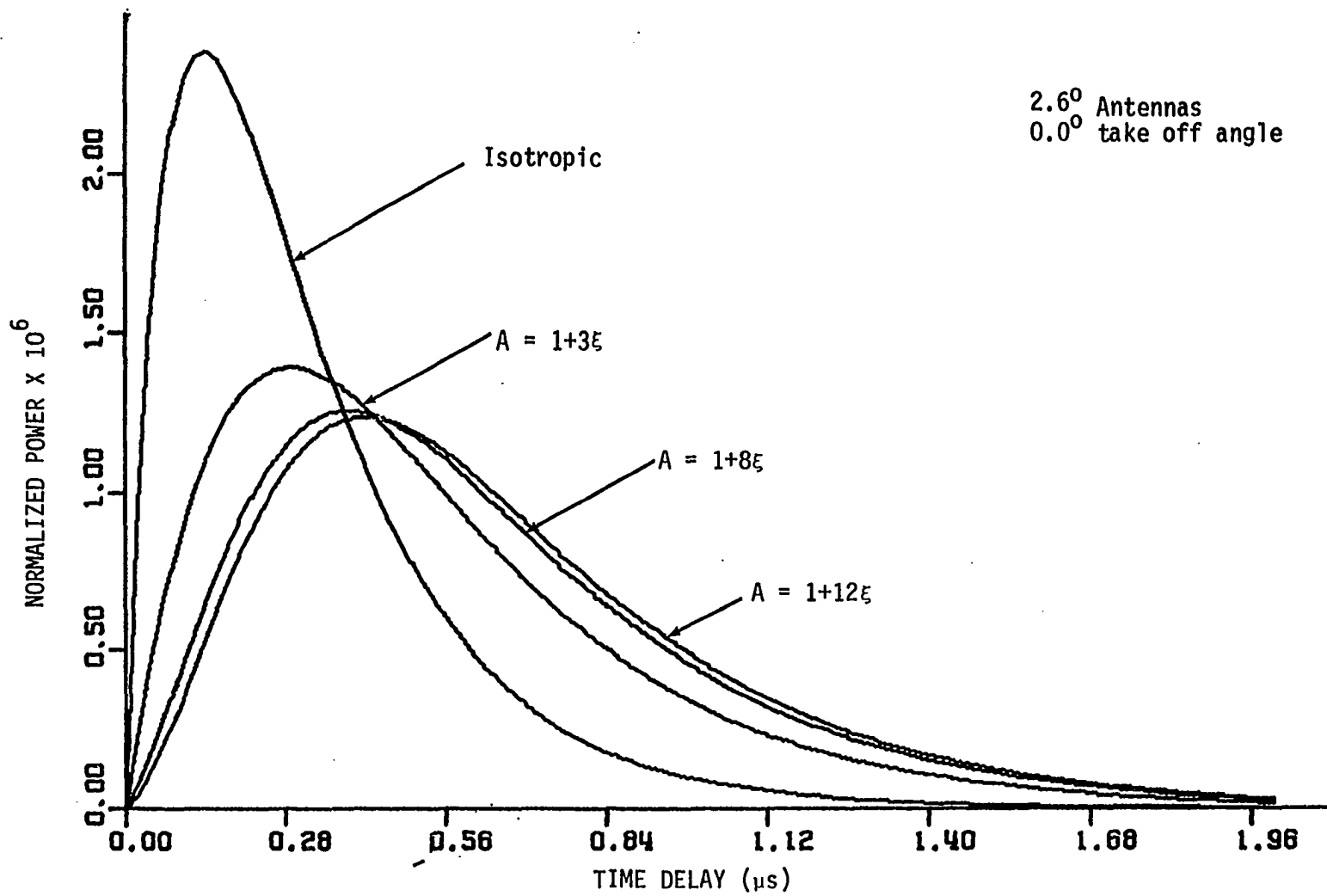


Figure 4.1. The effect of a linear anisotropy variation on the delay power spectra

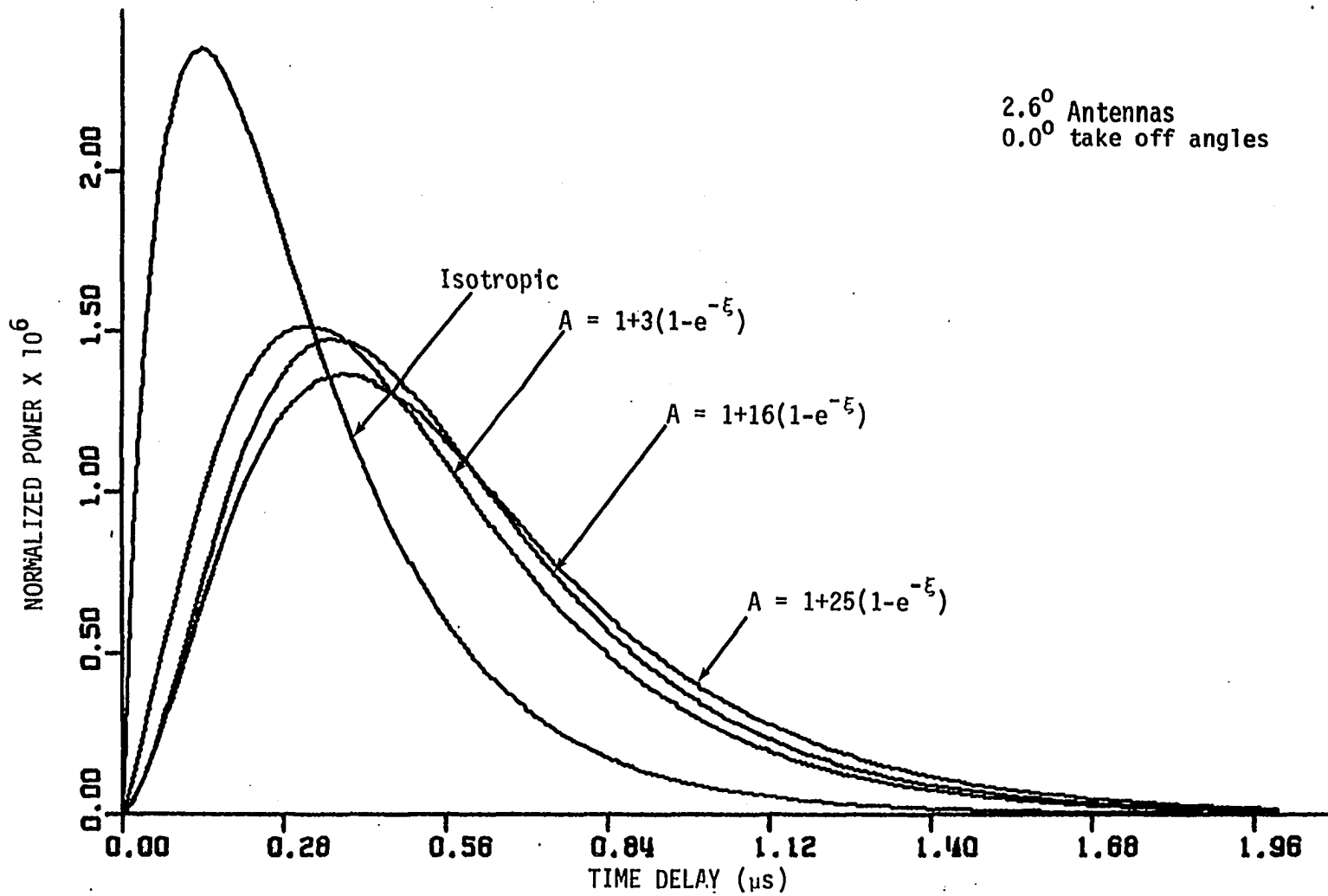


Figure 4.2. The effect of an exponential anisotropy variation on the delay power spectra

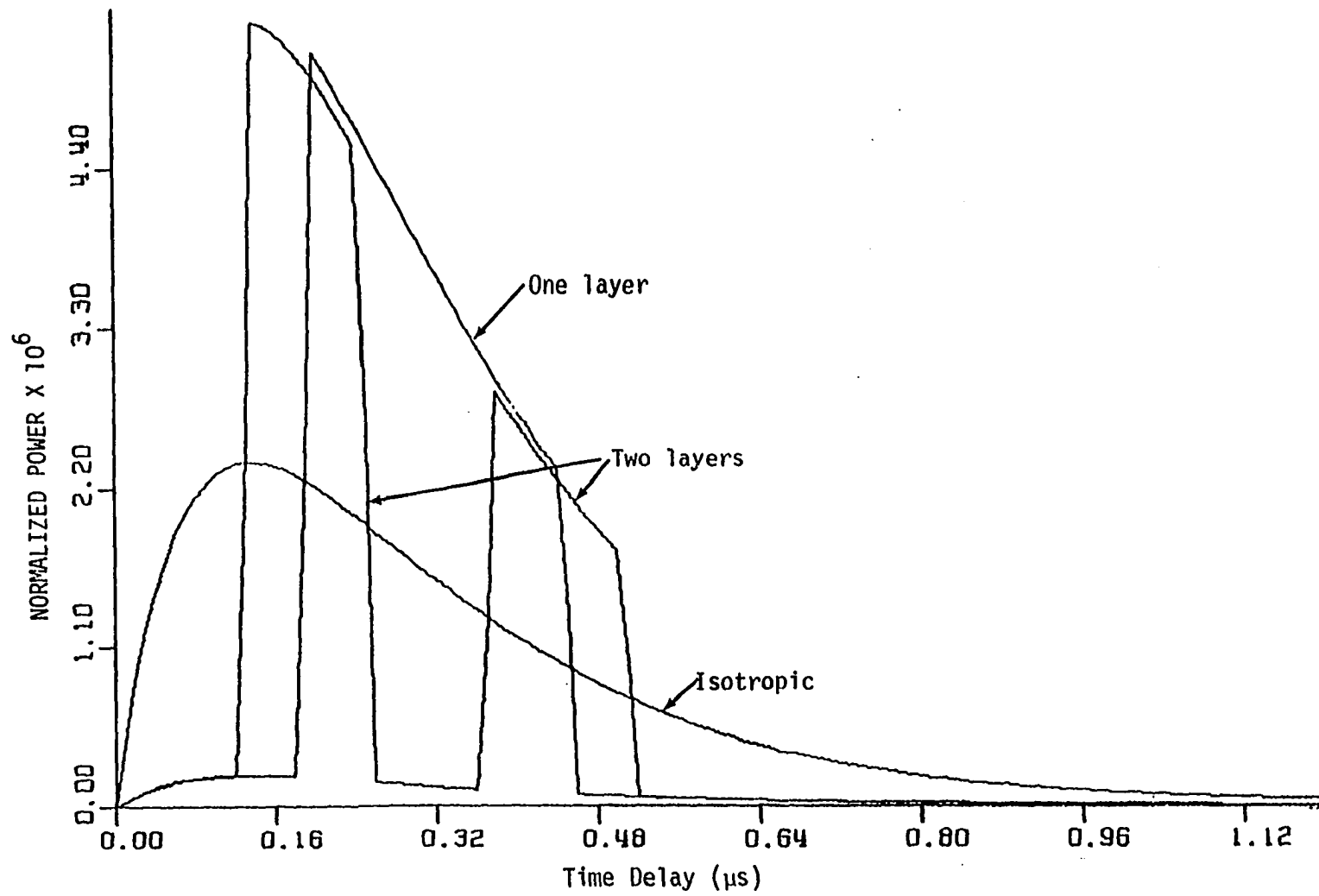


Figure 4.3. The effect of layering on the delay power spectra

Table 4.1. Summary of the delay power characteristics for the presented anisotropy profiles

Anisotropy variation	Form	Mean delay in μs	Multipath spread μs	Skew	Excess
Isotropic	$A = 1$	0.317	0.247	1.756	7.836
Linear	$A = 1+3\xi$	0.536	0.370	1.324	5.22
	$A = 1+8\xi$	0.631	0.391	1.168	4.616
	$A = 1+12\xi$	0.657	0.395	1.137	4.5
Exponential	$A = 1+7(1-\exp(-\xi))$	0.516	0.327	1.293	5.37
	$A = 1+16(1-\exp(-\xi))$	0.560	0.334	1.244	5.17
	$A = 1+25(1-\exp(-0.5\xi))$	0.595	0.358	1.203	4.9
One layer	$A = \begin{cases} 5\xi_0 - \frac{\Delta}{2} < \xi < \xi_0 + \frac{\Delta}{2} \\ 1 \text{ otherwise} \end{cases}$	0.304	0.101	2.666	27.475
Two layers	$A = \begin{cases} 5, \xi_0 - \frac{3\Delta}{4} < \xi < \xi_0 - \frac{\Delta}{4} \\ 5, \xi_0 + \frac{\Delta}{4} < \xi < \xi_0 + \frac{3\Delta}{4} \\ 1 \text{ otherwise} \end{cases}$	0.277	0.140	1.417	8.836

serve as a reference. These spectra are calculated using the parameters of the ISU-UW troposcatter link.

The main features of the spectra of the linear variation of anisotropy are shown in Figure 3.1, where it is seen that the multipath spread increases significantly with anisotropy. A slight ($S=3$) linear increase in anisotropy will bring about a 50% increase in multipath spread parameter, larger increases ($s=8$ to $s=12$) in anisotropy will bring up to a 60% increase in multipath spread. It should be noted that any further increase will not produce a significant change in spread. This is clear from Figure 4.1. The exponential variation of anisotropy produces an increase in multipath spread, which is less than the linear case. A 32% up to a 45% increase in multipath spread could result from changing a smaller ($a=7$, $b=1$) exponential increase in anisotropy to larger one ($a=25$, $b=0.5$). The situation is different for the single layer where the multipath spread decreases by 59%. The two-layer case results in 43% decrease in multipath spread. The result for the one-layer case is intuitively plausible since received energy is no longer spread over the whole delay range, rather it is concentrated in one delay interval.

The mean delay is also greatly affected by the anisotropy change. For the use of a linear increase of anisotropy, the mean delay increases from about 69% for a smaller increase in anisotropy to 99% and up to 107% for a larger increase. For the exponential anisotropy variation, the increase in the mean delay is smaller, ranging from about 63% to 77% and up to 88% for smaller, medium and large increases of

anisotropy. The situation is different for the one-layer case where the mean delay is reduced very slightly by about 3%. For the two-layer case, a decrease by about 13% could occur. It is clear that the linear anisotropy increase has the most impact on the mean delay and on the multipath spread; however, the mean delay will actually depend on the height of the layer. It should be emphasized here that the numbers obtained are based on the profiles presented which could vary from one link to another.

D. The Effect of Anisotropy on Intermodulation Distortion and Error Probability of Binary Communication Systems

In communication systems, when the signal level is small due to severe fading, thermal noise becomes a limiting factor in the performance of the system. On the other hand, when the signal level is high, the nonlinear noise (or intermodulation noise) becomes the limiting factor. In the frequency modulation systems widely used in tropospheric scatter links, the main causes of the intermodulation are: 1) transmitter nonlinearity; 2) multipathing in the medium; and 3) receiver nonlinearity. A great deal of effort has been devoted to the study of this phenomena [7, 21, 27, 28]. This study is concerned with the impact of the transmission medium (the troposphere) on the received signals. As shown in the previous section, the atmospheric anisotropy has a significant effect on the multipath spread and consequently, will have the same effect on intermodulation distortion.

1. Intermodulation distortion

The intermodulation theory developed by Bello et al. [6, 7] will be utilized here since it is more general and more complete. Although it is limited to cases exhibiting small frequency selective fading, this restriction does not limit its applicability to troposcatter systems since large amounts of frequency selectivity are unacceptable.

Intermodulation is usually characterized by its power in a narrow band located at a certain baseband frequency f and is given by [6]:

$$I(f, t) = \Delta^4 P_{xx} \cdot (f) \gamma(t) \quad (4.22)$$

where $x(t)$ is the modulating signal, $x'(t)$ its time derivative, $P_{xx} \cdot (f)$ is the power spectrum of the product $x(t)x'(t)$, and $\gamma(t)$ is called the normalized intermodulation distortion power. A quantity of importance in practical applications is the ratio of the intermodulation distortion power to signal power in a narrow band at a specified baseband frequency. This can be expressed as follows [7]:

$$\eta(f, t) = \frac{I(f, t)}{P_x(f)} = \frac{P_{xx} \cdot (f)}{P_x(f)} \Delta^4 (t) . \quad (4.23)$$

If $x(t)$ is a Gaussian process with a flat power spectrum extending from aW to W and zero elsewhere, the value of $\eta(f, t)$ at the top of the baseband ($f=W$) is given by [6]:

$$\eta(W, t) = \gamma(t) (2\pi\Delta)^4 \frac{\sigma^2 W^2}{4} \left(\frac{1-2a}{1-a} \right) \quad (4.24)$$

where σ is the rms value of $x(t)$.

The time dependent part of $\gamma(t)$ in Equation 4.23 is described in terms of its probability density functions of all orders. Considering the case of no diversity, a first order probability density function for γ , $W(\gamma)$ could be written as [6]:

$$W(\gamma) = \frac{1}{2\pi\sqrt{\gamma}} \int_{-\infty}^{\infty} \frac{dR}{\sqrt{f(R)} \left(1 + R^2 + \frac{\gamma}{4f(R)}\right)^2} \quad (4.25)$$

where

$$f(R) = R^2 + \frac{\mu_3}{\Delta^3} + \frac{1}{4} \left(\frac{\mu_4}{\Delta^4} - 1 \right) \quad (4.26)$$

and Δ , μ_3 and μ_4 are defined by Equations 4.15, 4.16, and 4.17.

Equation 4.25 is a function of the delay power spectrum parameters which are highly dependent on the atmospheric anisotropy profiles. No exact closed form for $W(\gamma)$ has been found, so a numerical integration is usually used for these calculations. Practical values of γ are large, i.e. > 10 , and for a 10 dB signal-to-noise ratio, the value of γ is 10^4 . Thus, an approximate formula for $W(\gamma)$ can be used. For the nondiversity case, the following formula from reference 7 can be used.

$$W(\gamma) = \frac{1}{\pi\gamma^2} \quad \gamma > 10 \quad (4.27)$$

$$W(\gamma) = \frac{0.11}{\sqrt{\gamma}} \quad \gamma \ll 1 \quad (4.28)$$

A computer program to numerically evaluate $W(\gamma)$ in Equation 4.25 for the ISU-UW link has been written for the delay power spectra presented in Table 4.1. The probability density functions and the

cumulative distribution functions are shown in Figures 4.4 and 4.5 for the isotropic linear and exponential anisotropy profiles. It is clear from the figures that the probability density function of the normalized intermodulation is practically unaffected by the different anisotropy profiles. The general shape of $W(\gamma)$ is characterized by a steep increase for $\gamma < 1$ while for $\gamma > 1$, it decreases more rapidly.

2. Effect of anisotropy on the error rate of a binary communication system

In a binary communication system, one of two signals, $s_0(t)$ or $s_1(t)$, is received in the time interval ($0 \leq t \leq T$). The received signal is corrupted by both the medium through which it propagates and the unavoidable noise at the receiver. The medium manifests itself by producing intermodulation, while the noise will result in an uncertainty of the received signal. Both will result in errors in deciding whether the received signal is $s_0(t)$ or $s_1(t)$. The performance of digital communication systems is usually expressed by curves representing the probability of error versus a characteristic parameter of the receiver; for example, signal-to-noise ratio. The noise is usually assumed to be Gaussian with zero mean. The error performance due to the receiver noise can be found in many texts. This study will use the development in reference [29] where the error probability is given by:

$$P_e = \int_0^{\infty} \frac{1}{\sqrt{2\pi}} \exp(-z^2/2) dz = \frac{1}{2} \operatorname{Erfc} \left[\frac{(1-\rho)E}{2N_0} \right]^{1/2} \quad (4.29)$$

$((1-\rho) \frac{E}{N_0})^{1/2}$

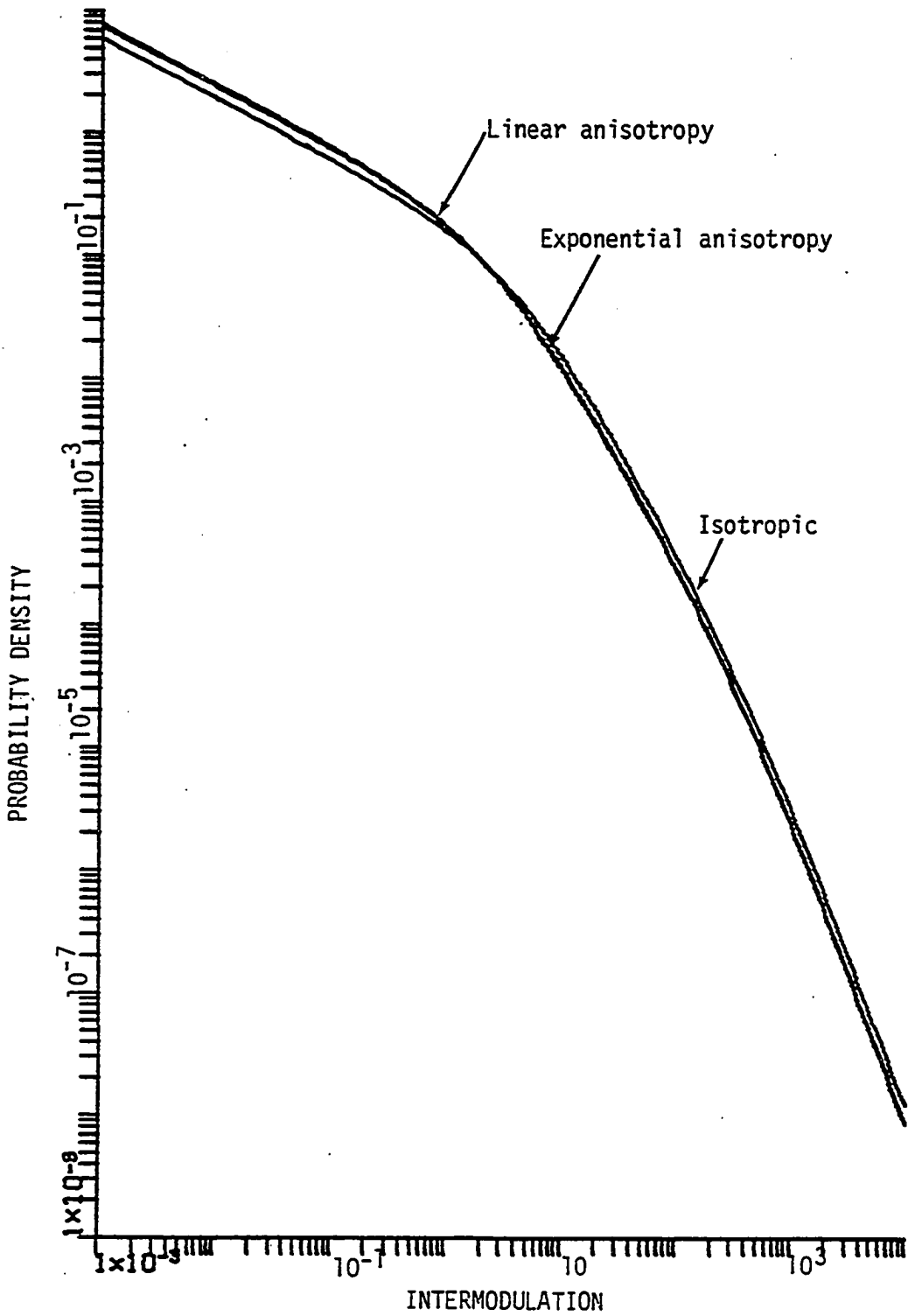


Figure 4.4. The probability density function of normalized intermodulation

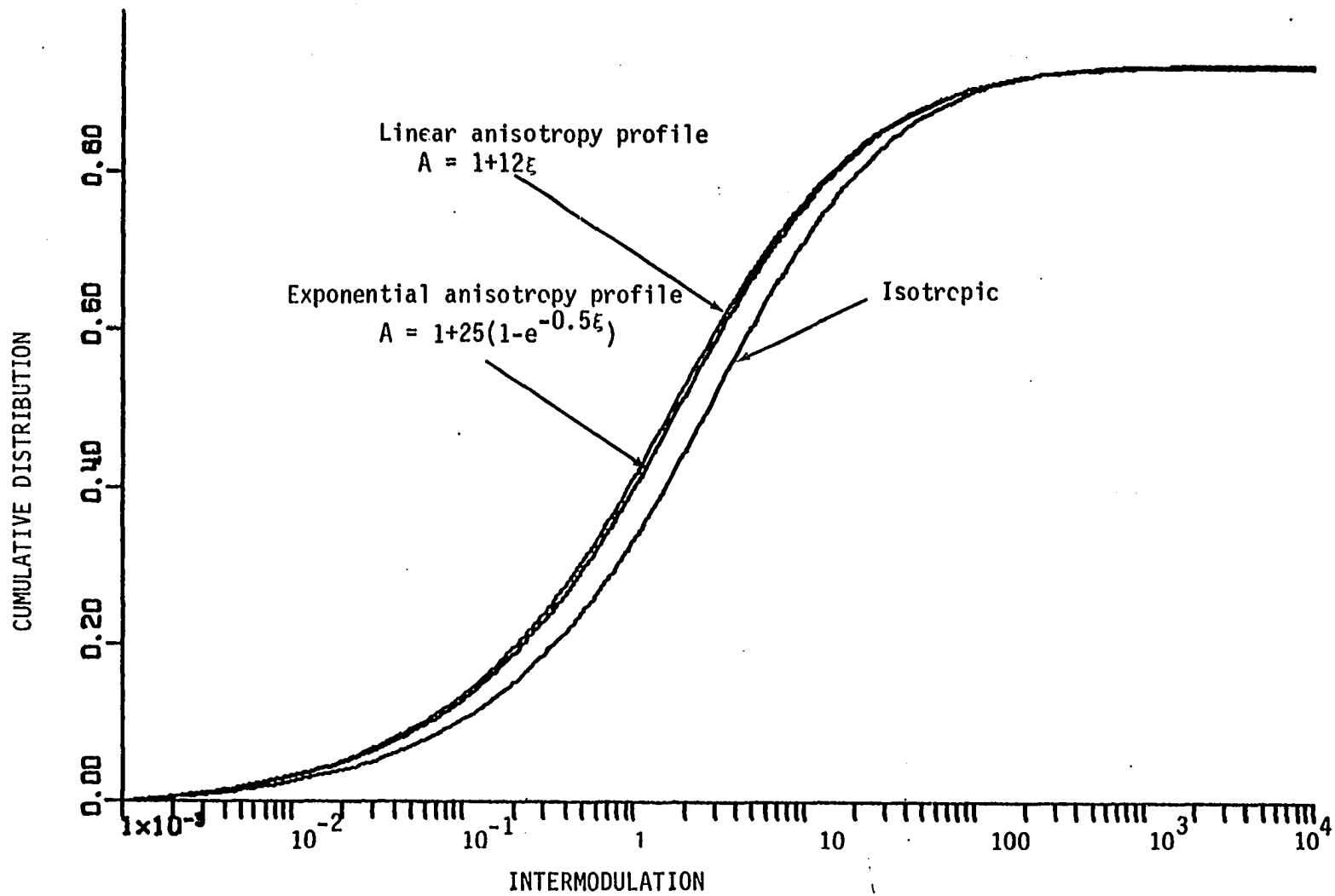


Figure 4.5. The cumulative distribution function of the normalized intermodulation

where E is the average energy and is given by

$$E = \frac{1}{2} \int_0^T [s_0^2(t) + s_1^2(t)] dt .$$

ρ is the correlation coefficient between $s_0(t)$ and $s_1(t)$;

$$\rho = \frac{1}{E} \int_0^T s_0(t) s_1(t) dt, \text{ and } N_0/2 \text{ is the two-sided noise spectral density.}$$

E/N_0 is the signal-to-noise ratio.

The error probability decreases as $(1-\rho)E/N_0$ increases and for fixed E/N_0 , the optimum system is that for which $\rho = -1$. Figure 4.6 shows the error performance of three binary communication systems of practical use. The curve corresponding to $\rho = -1$ is for coherent phase shift keying (CPSK), which is the optimum binary system. The curve corresponding to $\rho = 0$ is for coherent frequency shift keying (CFSK) and ON-OFF carrier keying. For a given error probability, a 3-db increase in signal-to-noise ratio results when using CPSK instead of CFSK or ON-OFF carrier.

The error resulting from intermodulation distortion can be estimated for the binary communication systems by using Equation 4.29 and the proper definition of the signal-to-noise ratio, E/N_0 . Averaging this error probability over the probability density function of the intermodulation distortion given by Equation 4.25, results in an expression for the error performance of PSK systems.

$$P_e(s) = \frac{1}{2} \operatorname{Erfc}(s)^{1/2} \quad (4.30)$$

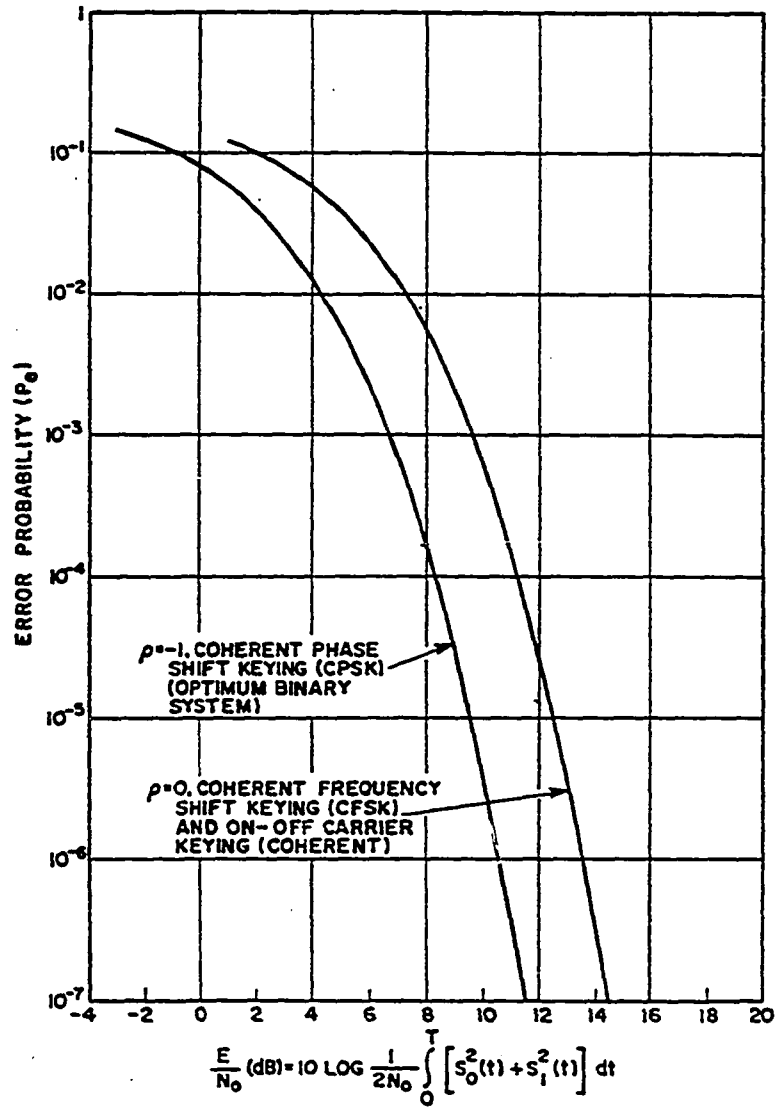


Figure 4.6. Error performance for binary communication systems [29]

and for FSK

$$P_e(s) = \frac{1}{2} \operatorname{Erfc} \left(\frac{s}{2} \right)^{1/2} \quad (4.31)$$

where $s = E/N_0$, the signal-to-noise ratio.

For the intermodulation distortion, the signal-to-noise ratio, s , is equal to $1/\eta(f)$ in Equation 4.23 where $\eta(f)$ denotes the ratio of the intermodulation distortion power to signal power in a narrow frequency band located at some specified baseband frequency. The average error probability is given by:

$$P_e = \int_0^{\infty} \frac{1}{2} \operatorname{Erfc} \sqrt{1/2\eta} W(\gamma) d\gamma . \quad (4.32)$$

As shown in the previous section, $W(\gamma)$ is essentially independent of the anisotropy profiles, thus, the only parameter that affects the error rate is the multipath spread parameter implied through η . A normalized parameter is often used instead of η and is given by [7]:

$$\eta = g\gamma \quad (4.33)$$

$$\text{where } g = \Delta^4 \frac{P_{XX}(f)}{P_X(f)} .$$

Thus, on a given troposcatter link, anisotropy will result in a change in the multipath spread parameter, Δ . Equation 4.32 is numerically evaluated by means of computer program written for this purpose for the anisotropy conditions shown in Table 4.1. The approximate form of Equation 4.27 is used in these calculations since the practical range of Δ is >10 . Figure 4.7 shows the effect of the anisotropy change on

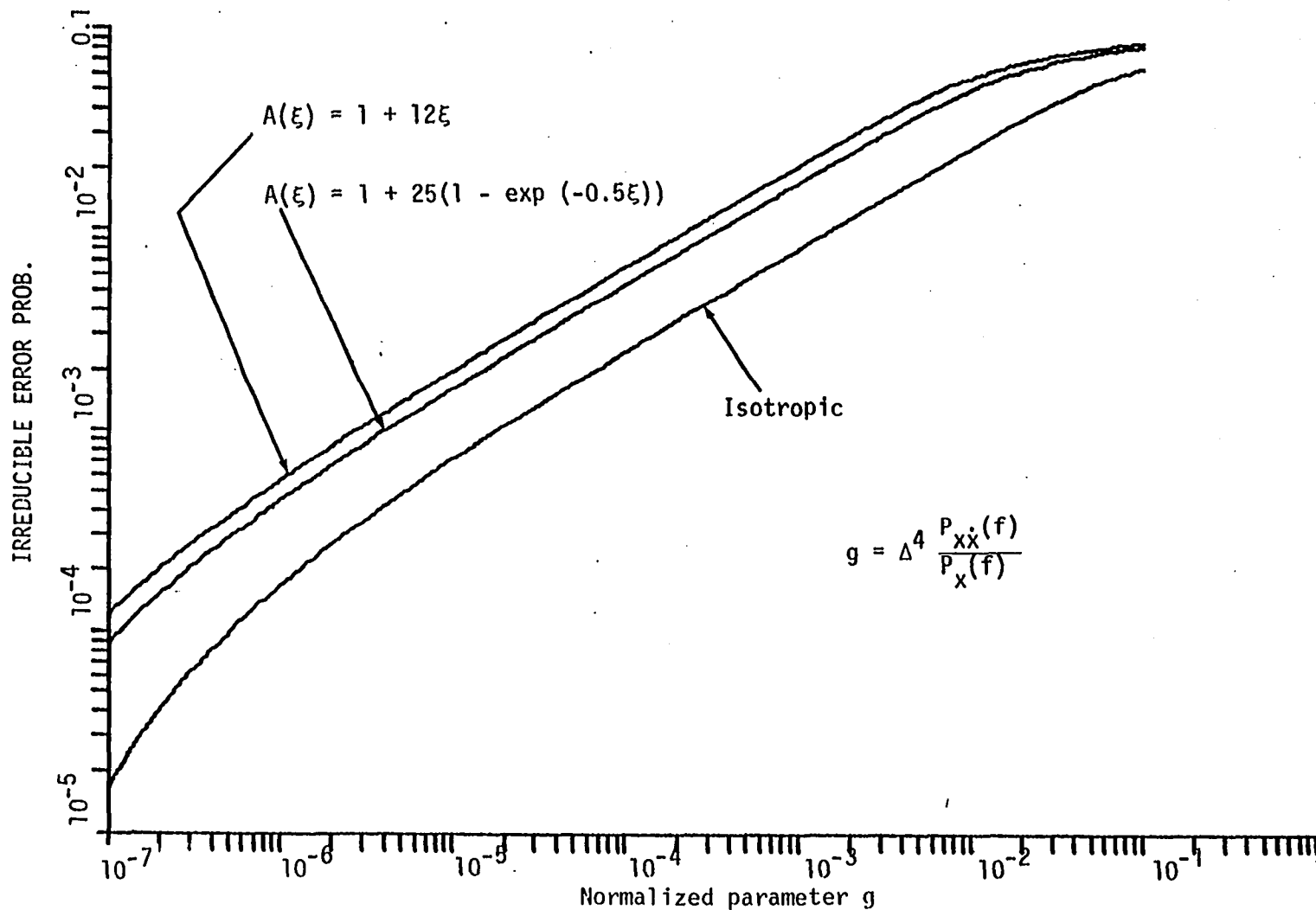


Figure 4.7. The effect of the anisotropy on the irreducible error probability

the irreducible error probability for isotropic, linear, and exponential anisotropy profiles. It is found that anisotropy will tend to increase the error probability by an order of magnitude or more. For a given error probability, about a 6dB increase in intermodulation distortion due to a linear increase ($s=12$) in anisotropy will result. The error probability of intermodulation distortion is found by estimating the multipath spread parameter Δ for the isotropic case from Figure 4.7, then the anisotropy profile is determined, the change in g value is found, and the new value of the error probability is found. The total error probability of a binary communication system is approximated by the sum of the probabilities due to the Gaussian noise and the intermodulation distortion.

E. Measurements of the Multipath Characteristics

In addition to its sounding capability, the RAKE system is also useful in measuring the multipath characteristics since delay tap spectra can be processed to find the total power for each delay. It was mentioned earlier that there is little difference between the zero Doppler power and the total power; so the zero Doppler power is a very good estimate of the total power for a given delay. The delay power spectra taken from the ISU-UW link for April 2, November 20, 1981, March 11, April 6, 1982 are shown in Figures 4.8 through 4.11, respectively. These are presented to demonstrate the nature of variations of the multipath characteristics that can exist on a troposcatter link. The multipath characteristics for the above-mentioned dates are theoretically calculated based on isotropic scattering

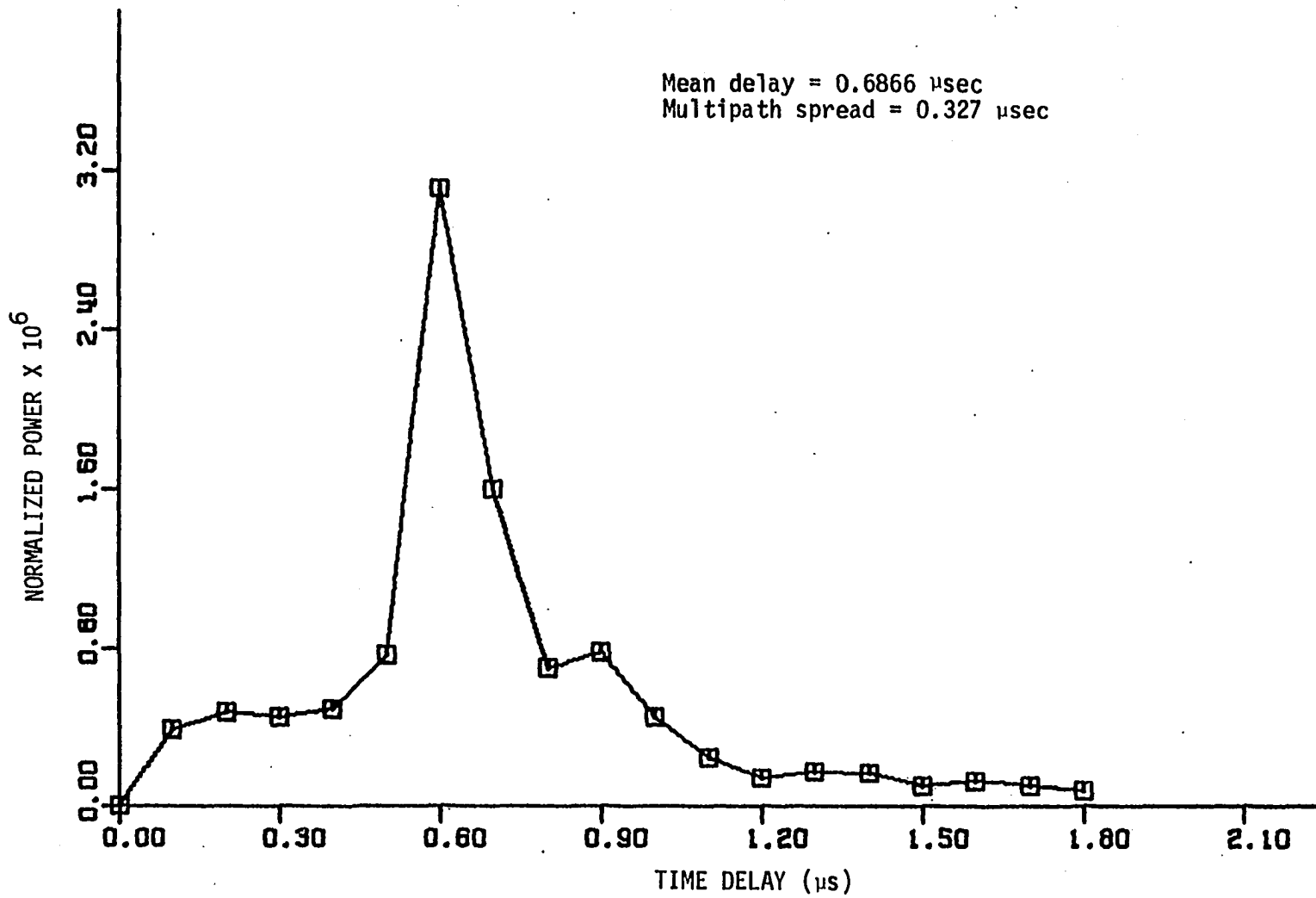


Figure 4.8. Measured delay power spectra of April 2, 1981

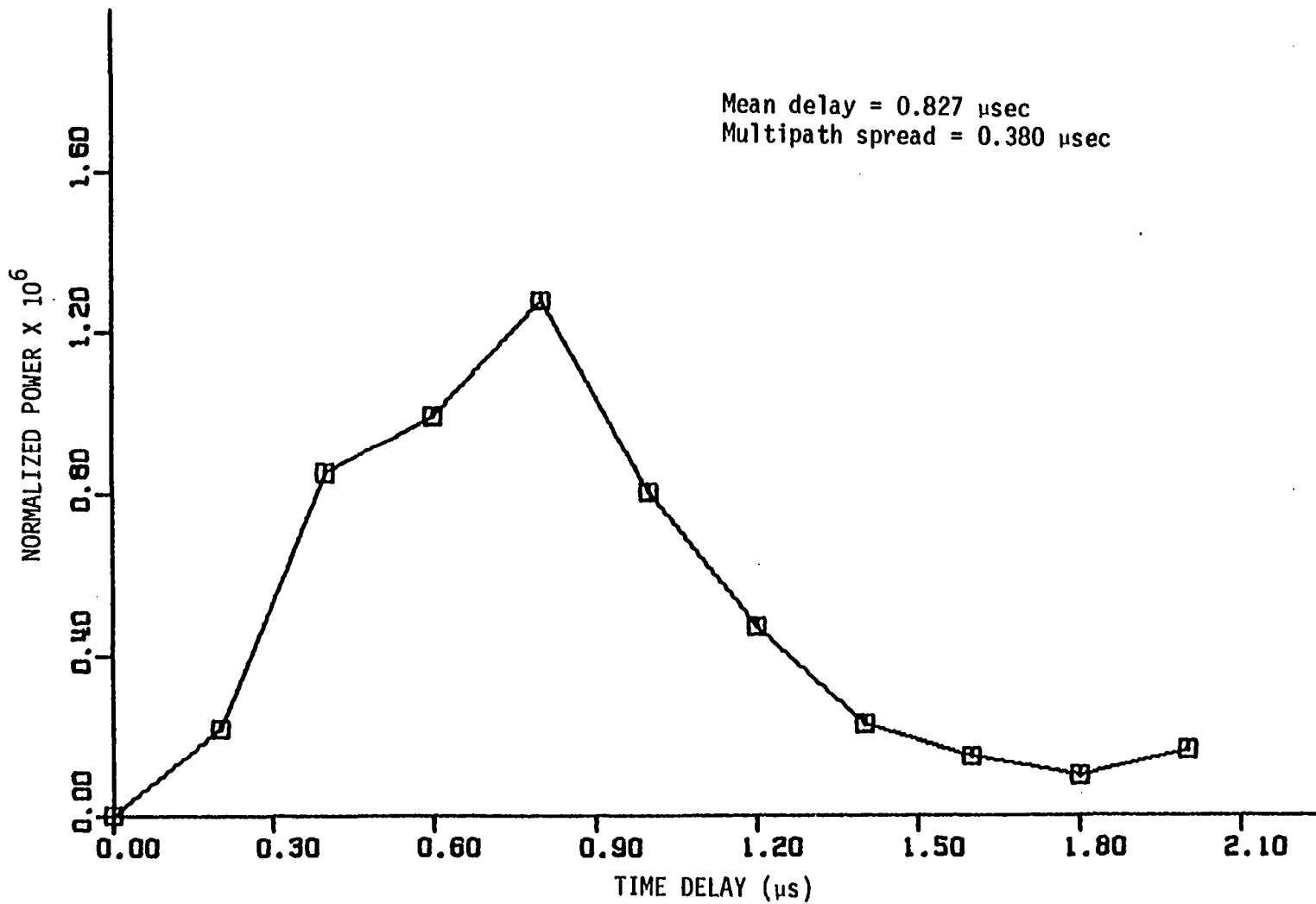


Figure 4.9. Measured delay power spectra of March 11, 1982

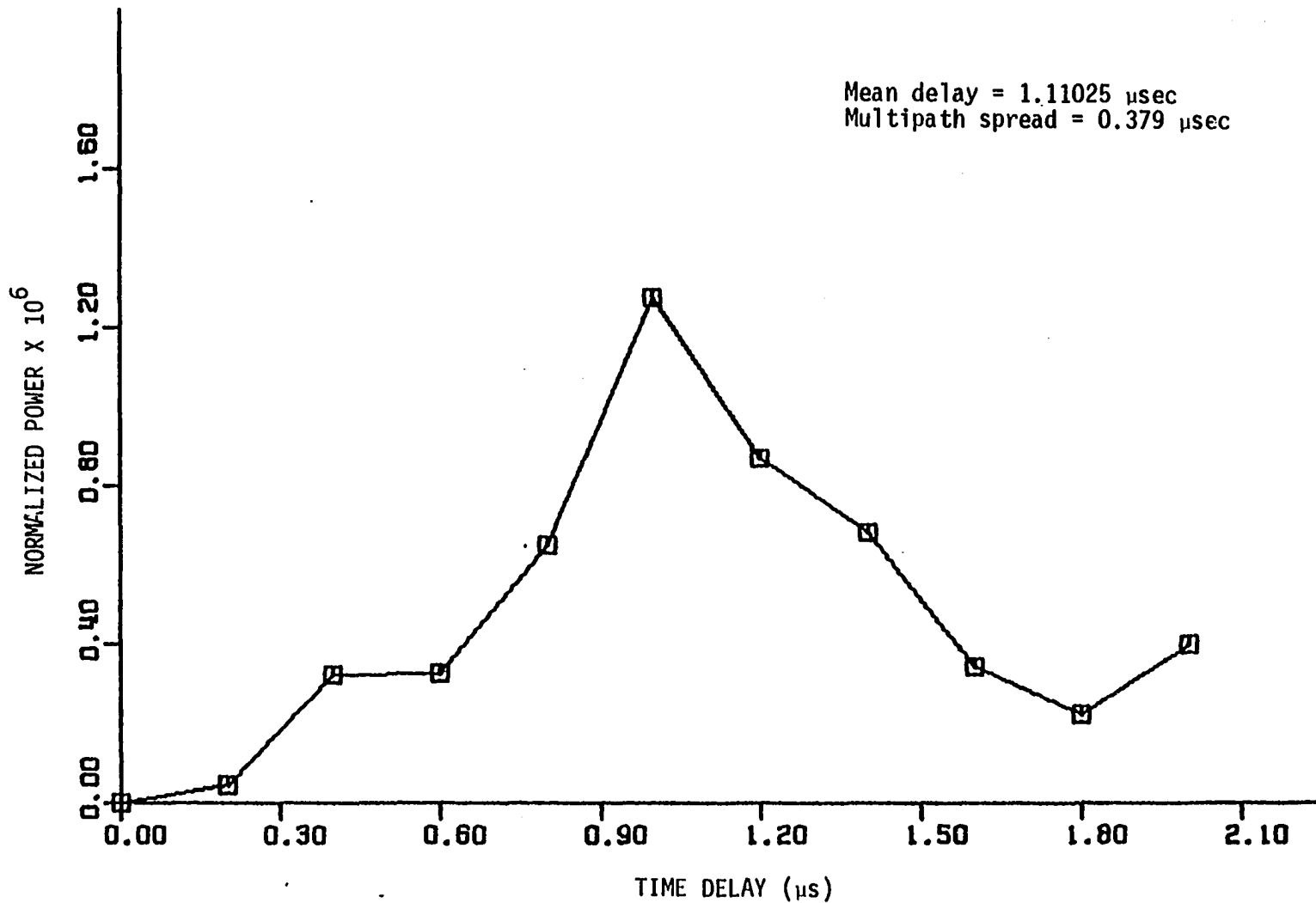


Figure 4.10. Measured delay power spectra of April 6, 1982

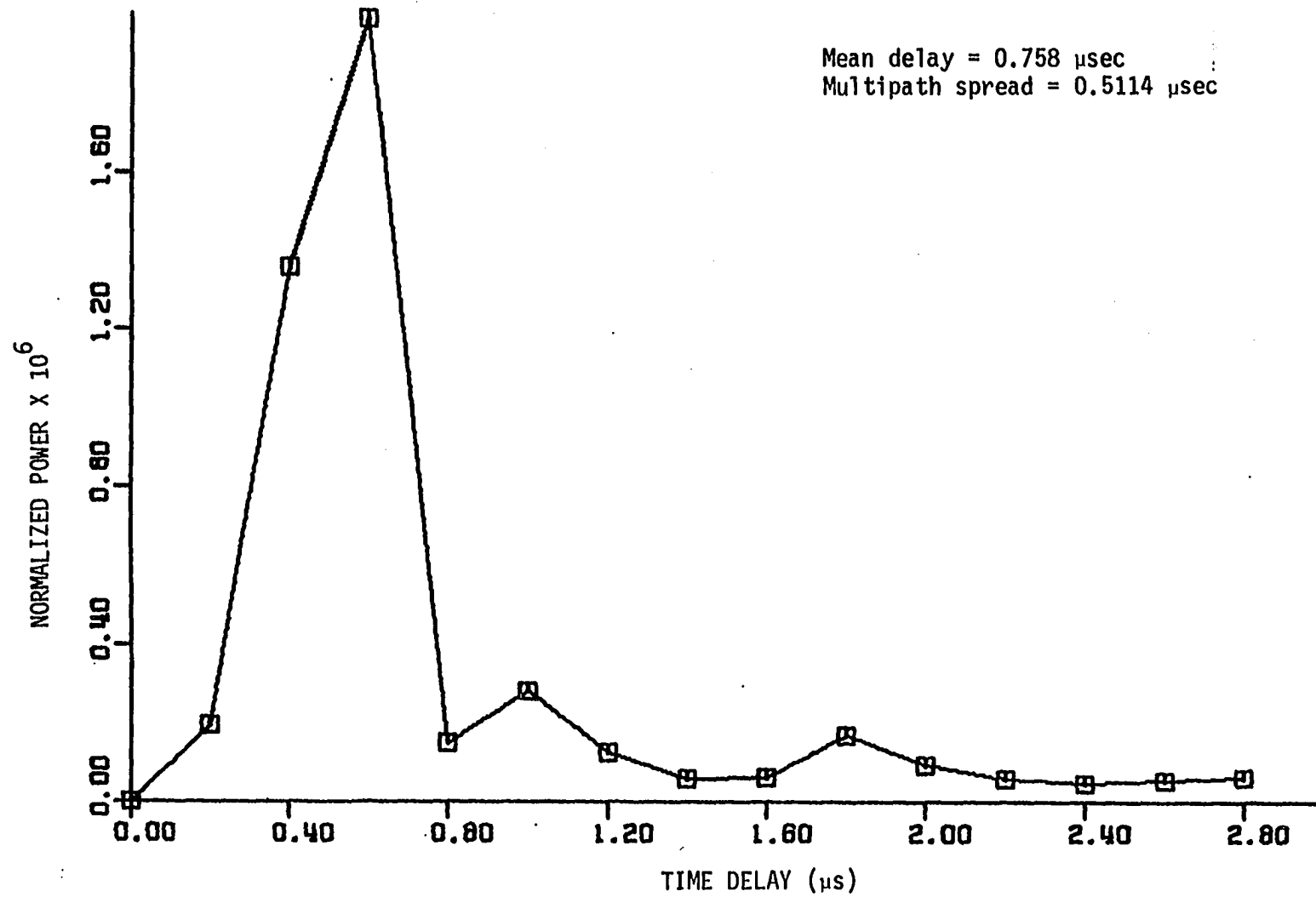


Figure 4.11. Measured delay power spectra of November 20, 1981

conditions according to the $-11/3$ spectrum using Equation 4.9.

Table 4.2 summarizes the mean delay and multipath spread parameters for the measured data and calculations based on isotropic scattering conditions for the above-mentioned dates.

Looking at Table 4.2, it is apparent that the measured mean delay of April 2, November, 20, 1981 and April 6, 1982 are larger than those theoretically calculated based on isotropic conditions; while for that of March 11, 1982, the measured mean delay is less than the calculated one. The multipath spread parameter shows measured values that are less than the theoretically calculated ones for the day of March 11 and April 6, 1982. The measured and calculated values are in close agreement for the April 2, 1981 data. The day of November 20, 1981 shows an increased measured value relative to the theoretically calculated one.

At this point, it is useful to mention the expected variations between the measured and calculated values of the multipath parameters. The anisotropic model was presented in Chapter III, together with the typical behavior of the anisotropy coefficient, which tends to increase with delay, then levels off. According to the data of the variation of the anisotropy coefficient with height (or tap number) shown in Figures 3.10 through 3.13 for the previously mentioned dates, we expect that the measured value should be larger than the calculated values based on isotropic scattering. It was mentioned earlier that the increase in the anisotropy coefficient with delay tends to increase both the multipath spread and the mean delay parameters.

Table 4.2. Comparison between the measured and calculated mean delay and multipath spread parameter

	April 2, 1981		Nov. 20, 1981		March 11, 1982		April 6, 1982	
	ξ_0 μsec	Δ μsec	ξ_0 μsec	Δ μsec	ξ_0 μsec	Δ μsec	ξ_0	Δ
Measured	0.69	0.33	0.76	0.51	0.83	0.38	1.11	0.38
Calculated, based on the -11/3 spectrum	0.461	0.349	0.461	0.349	1.02	0.581	0.831	0.521
Linear anisotropy model	- ^a	- ^a	0.611	0.438	- ^a	- ^a	- ^a	- ^a

^aThe anisotropic model is not used for this situation.

The data reported in Table 4.2 show only one day, November 20, 1981, that has the above-mentioned characteristics of increased measured value relative to the theoretically calculated ones. The measured values exhibit increases of 40% and 32% (the percentage is with respect to the measured value) in the mean delay and multipath spread, respectively. The anisotropic model is introduced in the calculations to account for this increase. A linear least square fit to the data of November 20, 1981, is done and the resulting anisotropy profile is inserted into the calculations of the delay power spectra. The result is shown in Table 4.2 for that day. The difference between the measured and calculated value is now smaller. It is 19% and 14% for the mean delay and the spread parameter, respectively, which is an improvement in the proper direction. This situation indicates that the anisotropic model could indeed account for this type of difference between the measured and calculated delay power spectra characteristics.

The anomalies reported in the remaining dates of April 2, 1981 and March 11, April 6, 1982 could be attributed to a number of sources. The first source is that the values of the anisotropy coefficient shown in Figures 3.10 through 3.13 are indeed considered to be instantaneous values where the data from one tap are taken over a short period (about one minute) and this, which could result in values of the anisotropy coefficient having the characteristic variation of the anisotropy with height (or delay), does not in fact give an absolute value of the anisotropy coefficient. In order to get good estimates for the anisotropy coefficient, an average over longer time periods is

required, which means more data is still required to give a typical anisotropy variation with height for the specific link. The second source that could account for the anomalies is the high sensitivity of the delay power spectra calculations on the elevation angles of both the transmitter and receiver. Also, the delay power spectra are very sensitive to variations in the half power beam width. A half power beam width of 2.6° was used in these calculations. However, there is some evidence to indicate that the half power beam width of the transmitting antenna is somewhat less than that. Accurate measurements of the true elevation angles of the antennas used in the ISU-UW troposcatter link have not been accomplished. Another source of error is the use of a forecasted wind instead of the actual cross path wind which needs to be used in extracting the anisotropy coefficient.

In spite of the fact that the experimental data are somewhat limited, this study shows that the measurements of the anisotropy of the atmosphere can be made. The results of trying to relate the experimental measurements of the anisotropy profiles to the multipath parameters indicate that more information on the physical parameters of the troposcatter link are needed. The results are encouraging, however.

V. CONCLUSION

This dissertation has dealt with atmospheric anisotropy and its effect on the delay power spectra of the troposcatter communication links. Not enough information about the atmospheric anisotropy exists in the literature, and even direct measurements for the atmospheric anisotropy have not been attempted. This is due to difficulties in measuring small scale three-dimensional refractivity fluctuations simultaneously in time and space. A simplified model has been presented to estimate the atmospheric anisotropy coefficient indirectly by processing the Doppler spectrum for each tap delay. This has been shown to be a good approximation to the anisotropic scattering model based on turbulence induced fluctuations in the refractive index of the atmosphere. The model offers definite advantages for extracting the anisotropy coefficient. One advantage is that the anisotropy coefficient can be evaluated using data from a single time delay shell. The anisotropy coefficient determined by this process is an average taken over the scattering volume of the time delay shell. The second advantage lies in the relative ease of implementing the inversion process. The Doppler spectrum of the received signal is fit to the Gaussian shaped scattering model. This process can be accomplished by linear regression done on a digital computer.

Having determined the anisotropy coefficient for each time delay shell, the impact of the anisotropy on the troposcatter channel as a communication link is studied. Bello's model for the troposcatter channel is modified to include the effect of the anisotropy on the delay

power spectra of the troposcatter signals. It has been found that the anisotropy will result in increased multipath spread and mean delay parameters relative to those resulting from isotropic scattering. Different theoretical anisotropy profiles based on the general experimentally observed changes in the anisotropy coefficient with delay are used in this study. The different characteristics of the delay power spectra are calculated for each anisotropy profile. The effect of anisotropy on the probability density function of the intermodulation distortion has been shown to be very slight. However, its effect on binary communication systems is to increase the bit error rate by an order of magnitude or more.

This study could be extended for future work in two areas. The first area is that of improving the characterization of the atmospheric anisotropy by extending the anisotropic model to be applicable to wider varieties of atmospheric conditions. More carefully planned measurements are still needed in this field. The model presented for determining the anisotropy depends on the accuracy of the wind measurements at the common volume. In our calculations, a forecasted wind aloft near midpath is used. These are estimated values and are of questionable accuracy. Also, the weather service estimates are given at a few discrete heights, so the coverage is incomplete. In fact, this problem arises whenever one attempts to use Doppler frequency information to determine the anisotropy coefficient and is independent of the scattering model employed in the process.

The second possible area that needs more investigation is the accuracy of Bello's model to accurately predict the delay power spectra of short troposcatter links and their frequency correlation functions. Daniel and Reinman [20] presented a modification to Bello's model by correlating the exponent of the scattering angle with the path length. This, of course, is not based on a physical model of scattering. Pusone and Hoag [21] also introduced a troposcatter channel model which is based on meteorological measurements. Their model predicts results closer to the measured values of the frequency correlation function. We believe that by considering the scattering process to be described by an anisotropic scattering model and its characteristic increase with height, the reduction in the correlation bandwidth which has been reported experimentally can be accounted for.

VI. BIBLIOGRAPHY

1. H. T. Friis, A. B. Crawford and D. C. Hogg. "A Reflection Theory for Propagation Beyond the Horizon." Bell Sys. Tech. Journal, 36 (May 1957):627-644.
2. H. G. Booker and W. E. Gordon. "A Theory of Radio Scattering in the troposphere." Proc. I.R.E., 38 (April 1950):401-412.
3. V. I. Tatarski. Wave Propagation in a Turbulent Medium. New York: McGraw Hill, 1961.
4. W. P. Birkemeier. "A Comparison of RAKE Scattering Layer Signatures with Radiosonde Data." Rome Air Development Center RADC-TR-74-17.
5. P. A. Bello. "A Troposcatter Channel Model." IEEE Trans. on Comm. Tech., 17 (April 1969:130-137).
6. P. A. Bello and B. D. Nelin. "The Effect of Frequency Selective Fading on Intermodulation Distortion and Subcarrier Phase Stability in Frequency Modulation Systems." IEEE Trans. on Comm. Systems, 12 (March 1964):87-101.
7. P. A. Bello and L. Ehrman. "Error Rates in Diversity FDM-FM Digital Troposcatter Transmission." IEEE Trans. on Comm. Tech., 17 (April 1969):183-191.
8. W. P. Birkemeier, P. F. Duvoisin, A. B. Fontaine and D. W. Thompson. "Indirect Atmospheric Measurements Utilizing Tropospheric Scatter Techniques." Part II: Radiometeorological Interpretation of RAKE Channel-sounding Observations. Proceedings of the IEEE 36, No. 3, (April 1969):552-559.
9. A. Ishimaru. Wave Propagation and Scattering in Random Media. Volumes I and II. New York: Academic Press, 1978.
10. M. T. Badr. "Microwave Propagation and Surface Conditions." Ph.D. Thesis. Cairo University, Cairo, Egypt, 1973.
11. M. Dolukhanov. Propagation of Radio Waves. Translated by B. Kuzentsov. Moscow, U.S.S.R.: Mir Publisher, 1971.
12. N. Cianos. "Atmospheric Structure, Transhorizon Propagation and Their Relationship to Remote Sensing." IEEE Trans. on Antennas and Prop., 26, No. 2 (1978):333-340.
13. R. Price and P. E. Green. "A Communication Technique for Multipath Channels." Proceedings of the I.R.E., 46 (1958):555-570.

14. D. R. Bitzer, D. A. Chesler, R. Ivers and S. Stein. "A RAKE System for Tropospheric Scatter." IEEE Trans. on Comm. Tech. Com., 14 (August 1966):499-506.
15. B. B. Barrow, L. G. Abraham, W. M. Cowan and R. M. Gallant. "Indirect Atmospheric Measurements Utilizing RAKE Tropospheric Scatter Techniques." Part I: The RAKE Tropospheric Scatter Technique. Proceeding of IEEE, 57, No. 4 (April 1969):537-551.
16. K. S. Gage, W. P. Birkemeier and W. H. Jaspersen. "Atmospheric Stability Measurements at Tropopause Altitudes Using Forward-Scatter CW Radar." Journal of Applied Meteor., 12 (October 1973):1205-1212.
17. R. E. Post and H. M. Ibrahim. "A Simplified Model for Interpreting the Doppler Spectrum of Forward-Scatter Radar Signals." Accepted for publication in IEEE Trans. on Antennas and Propagation, 1982.
18. A. B. Crawford, C. D. Hogg and W. H. Kummer. "Studies in Tropospheric Propagation Beyond the Horizon." Bell Sys. Tech. Journal, 38, No. 5 (September 1959):1067-1178.
19. W. P. Birkemeier, A. B. Fontaine, K. S. Gage, S. A. Gronemeyer, W. H. Jaspersen and F. S. Sechrist. "Wind Measurement Using Forward-Scatter CW Radar." Journal of Applied Meteor., 12 (1973): 1044-1053.
20. L. D. Daniel and R. A. Reinman. "Performance Prediction for Short-Range Troposcatter Links" IEEE Trans. on Comm., (June 1976): 670-672.
21. Ezio Pusone and Den Hoag. "A Channel Model for Prediction of Delay and Doppler Power Spectra and Frequency Correlation Function for Troposcatter Communication Links." International Zurich Seminar on Digital Communication Transmission in Wireless systems, Zurich, Switzerland, March 1980, D4.1-d4.5.
22. E. D. Sunde. "Intermodulation Distortion in Analog FM Troposcatter System." Bell Sys. Tech. Journal, 43 (January 1964):399-435.
23. E. D. Sunde. "Digital Troposcatter Transmission and Modulation Theory." Bell Sys. Tech. Journal, 43 (January 1964): 143-214.
24. P. A. Bello. "Characterization of Randomly Time Variant Channel." IEEE Trans. on Comm. System, CS-II (December 1963):360-393.
25. P. A. Bello. "Some Techniques for the Instantaneous Real Time Measurement of Multipath and Doppler Spread." IEEE Trans. on Comm. Tech., 13, No. 3 (September 1965):285-292.

26. P. Beckmann. Probability in Communication Engineering. New York: Harcourt, Brace & World, 1967.
27. A. B. Crawford and W. C. Jakes. "Selective Fading of Microwaves." *Bell Sys. Tech. Journal*, 31 (January 1952):69-89.
28. F. P. Panter. Communication Systems Design. New York: McGraw Hill, 1972.
29. A. D. Whalen. Detection of Signals in Noise. New York: Academic Press, 1971.

VII. ACKNOWLEDGMENTS

The author expresses his deep and heartfelt gratitude to his major professor, Dr. R. E. Post, for his continuous discussion, valuable comments, and assistance during the work leading to this thesis.

The author wishes to thank Dr. W. P. Birkemeier at the University of Wisconsin for all the kind help he offered, for both the experimental work and his valuable discussions.

Thanks to my colleague Mr. L. Bacon for his help in the experimental work. Thanks to the Department of Electrical Engineering at Iowa State University for providing the research facilities required for this thesis.

Finally, special thanks to my wife, Nagwa, for her sacrifice, patience, encouragement and understanding, without which this work would not have been possible.

VIII. APPENDIX A: PARAMETERS OF THE ISU-UW
TROPOSCATTER LINK

Table 8.1 summarizes the important characteristics of the ISU-UW tropospheric scatter radio link.

Table 8.1. Summary of the characteristics of the ISU-UW forward scatter radar

Parameter	Value or location
Transmitter location	ISU Fick-Observatory, Moingona, IA
Receiver location	UW Agricultural Farm, Arlington, WI
Transmitter power	10 Kw (cw)
Carrier frequency	940 MHz
Bandwidth	10 MHz
Transmitting antenna	8.53 m paraboloid
Receiving antenna	8.53 m paraboloid
Antenna half-power beamwidth	2.6°
Receiver noise figure	6dB
Distance	406 Km
Basic path loss	156 dB
Minimum propagation time from trans. to rec.	1.354 ms
Modulation	pseudorandom binary code 2^{16} /bits per code word at a bit rate of 10^7 bits/sec

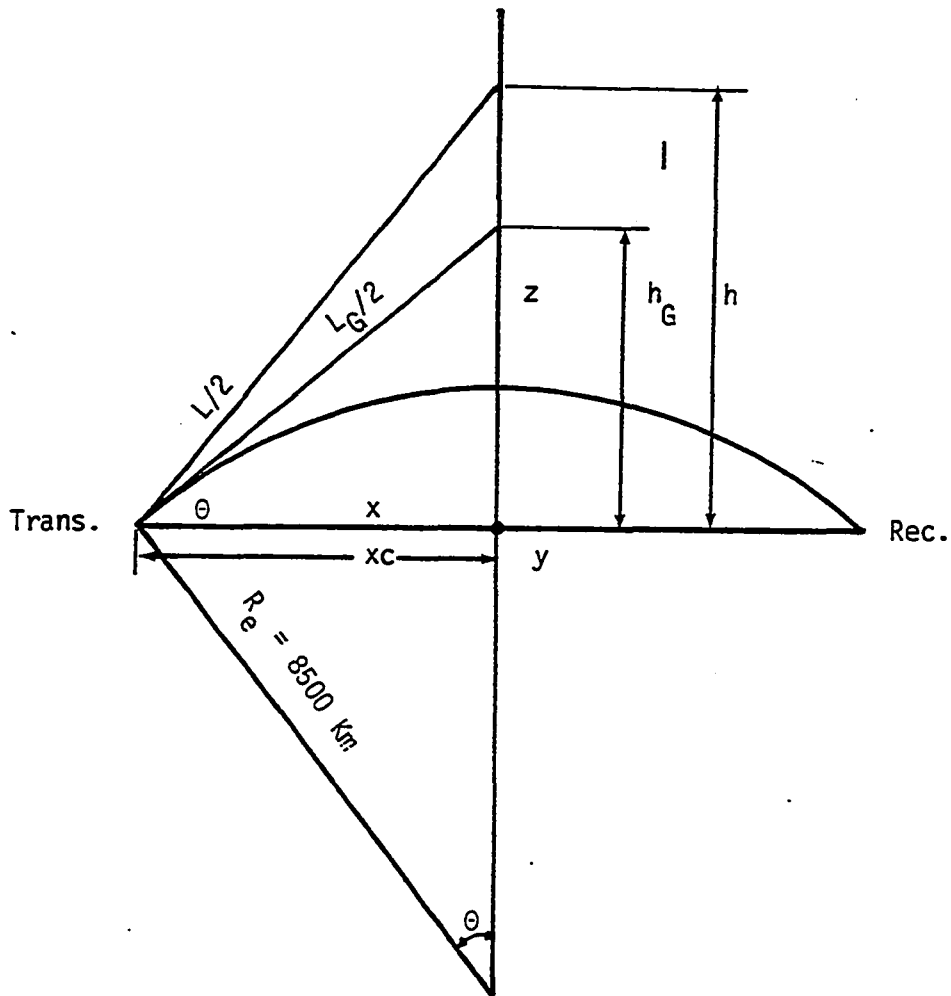


Figure 8.1. Geometry for height delay relations at midpath

The height-delay relations can be deduced from the geometry of Figure 8.1. The time delay is usually taken relative to the grazing ray. Let L denote the path length and h the height at midpath. L and h are the corresponding values at the horizon (grazing ray). The following relations can be written:

$$L - L_G = c\Delta t, \quad L = L_G + c\Delta t \quad 8.1$$

$$L = 2(h^2 + x_c^2)^{1/2} \quad 8.2$$

$$\theta = \text{arc tan } (d/R_e) \quad 8.3$$

$$L_G = 2R_e \tan \theta \quad 8.4$$

$$x_c = R_e \sin \theta. \quad 8.5$$

From Equations 8.1 and 8.2, one can write

$$h = \left[\left(\frac{L_G + c\Delta t}{2} \right)^2 - x_c^2 \right]^{1/2} . \quad 8.6$$

Substituting for L_G and x_c in terms of θ and R_e , and putting $c = 0.3 \text{ Km}/\mu\text{s}$ results in

$$h = \left[(R_e \tan \theta + 0.15 \Delta t)^2 - (R_e \sin \theta)^2 \right]^{1/2} \quad 8.7$$

In Equation 8.7, when Δt is in microseconds and R_e is in Km, h will be in Km. Equation 8.7 is used to calculate the midpath height corresponding to the different delays. Figure 8.2 shows a cross section at midpath depicting the different delay shells and their relative height for $0.2 \mu\text{s}$ resolution. Tables 8.2 and 8.3 list the shell height for 0.1 and 0.2 microseconds delays. The mid-shell height is usually used in our calculations. Tables 8.2 and 8.3 list distances from the chord and from the surface, as well as the shell thickness.

The Doppler frequency, given by Equation 2.27, can be written for the ISU-UW link as

$$f_d \approx - 0.031 \text{ vy} . \quad 8.8$$

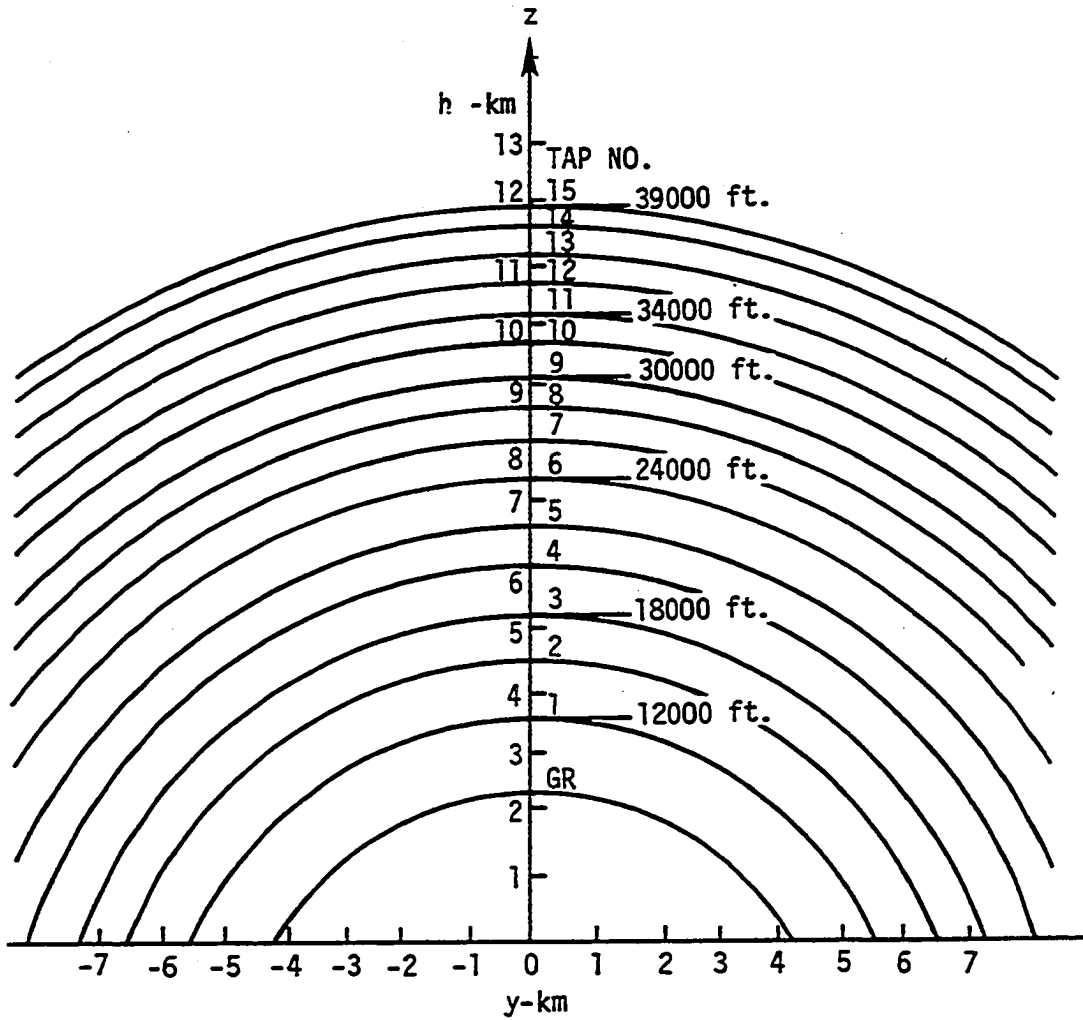


Figure 8.2. Contours of $0.2 \mu\text{s}$ increments of constant time delay in the midpath plane

Table 8.2. Delay heights (in Km) for 0.1 μ s resolution

Tap #	Time delay	Mid height ZMC	Mid height ZMS	Shell thickness
1	0.1000	5.1450	2.7192	0.5929
2	0.2000	5.7082	3.2824	0.5334
3	0.3000	6.2198	3.7940	0.4899
4	0.4000	6.6924	4.2666	0.4553
5	0.5000	7.1336	4.7078	0.4271
6	0.6000	7.5488	5.1230	0.4034
7	0.7000	7.9423	5.5165	0.3836
8	0.8000	8.3174	5.8916	0.3666
9	0.9000	8.6763	6.2505	0.3512
10	1.0000	9.0207	6.5950	0.3378
11	1.1000	9.3526	6.9268	0.3260
12	1.2000	9.6731	7.2473	0.3150
13	1.3000	9.9833	7.5575	0.3054
14	1.4000	10.2842	7.8584	0.2965
15	1.5000	10.5766	8.1508	0.2883
16	1.6000	10.8611	8.4353	0.2807
17	1.7000	11.1383	8.7125	0.2737
18	1.8000	11.4088	8.9830	0.2672
19	1.9000	11.6730	9.2473	0.2614
20	2.0000	11.9315	9.5057	0.2555
21	2.1000	12.1844	9.7587	0.2504
22	2.2000	12.4323	10.0066	0.2454

Table 8.2. Continued

Tap #	Time delay	Mid height ZMC	Mid height ZMS	Shell thickness
23	2.3000	12.6753	10.2495	0.2405
24	2.4000	12.9137	10.4879	0.2362
25	2.5000	13.1479	10.7221	0.2322
26	2.6000	13.3780	10.9522	0.2280
27	2.7000	13.6042	11.1784	0.2243
28	2.8000	13.8268	11.4010	0.2209
29	2.9000	14.0459	11.6201	0.2173
30	3.0000	14.2615	11.8357	0.2139
31	3.1000	14.4739	12.0481	0.2109
32	3.2000	14.6833	12.2576	0.2079
33	3.3000	14.8898	12.4640	0.2050
34	3.4000	15.0934	12.6677	0.2023
35	3.5000	15.2944	12.8686	0.1996
36	3.6000	15.4928	13.0670	0.1972
37	3.7000	15.6886	13.2628	0.1946
38	3.8000	15.8821	13.4563	0.1923
39	3.9000	16.0733	13.6475	0.1900
40	4.0000	16.2621	13.8364	0.1877
41	4.1000	16.4489	14.0231	0.1857
42	4.2000	16.6335	14.2078	0.1837
43	4.3000	16.8163	14.3905	0.1818
44	4.4000	16.9970	14.5712	0.1797

Table 8.2. Continued

Tap #	Time delay	Mid height ZMC	Mid height ZMS	Shell thickness
45	4.5000	17.1758	14.7500	0.1779
46	4.6000	17.3528	14.9270	0.1761
47	4.7000	17.5280	15.1022	0.1743
48	4.8000	17.7015	15.2757	0.1727
49	4.9000	17.8733	15.4475	0.1710
50	5.0000	18.0435	15.6177	0.1694
51	5.1000	18.2121	15.7864	0.1678
52	5.2000	18.3792	15.9534	0.1663
53	5.3000	18.5448	16.1190	0.1649
54	5.4000	18.7090	16.2832	0.1634
55	5.5000	18.8717	16.4459	0.1621
56	5.6000	19.0330	16.6073	0.1606
57	5.7000	19.1931	16.7673	0.1596
58	5.8000	19.3519	16.9261	0.1580
59	5.9000	19.5092	17.0835	0.1568

Table 8.3. Delay heights (in Km) for 0.2 μ s resolution

Tap #	Time delay	Mid height ZMC	Mid height ZMS	Shell thickness
1	0.2000	5.4117	2.9859	1.1263
2	0.4000	6.4475	4.0217	0.9451
3	0.6000	7.3353	4.9095	0.8305
4	0.8000	8.1256	5.6998	0.7502
5	1.0000	8.8452	6.4194	0.6889
6	1.2000	9.5101	7.0843	0.6410
7	1.4000	10.1315	7.7057	0.6018
8	1.6000	10.7169	8.2911	0.5690
9	1.8000	11.2719	8.8461	0.5410
10	2.0000	11.8008	9.3750	0.5169
11	2.2000	12.3071	9.8814	0.4958
12	2.4000	12.7934	10.3676	0.4768
13	2.6000	13.2620	10.8362	0.4604
14	2.8000	13.7147	11.2889	0.4450
15	3.0000	14.1528	11.7271	0.4313
16	3.2000	14.5779	12.1521	0.4188
17	3.4000	14.9909	12.5651	0.4073
18	3.6000	15.3930	12.9672	0.3968
19	3.8000	15.7848	13.3590	0.3869
20	4.0000	16.1671	13.7413	0.3778
21	4.2000	16.5407	14.1149	0.3694
22	4.4000	16.9061	14.4803	0.3615

Table 8.3. Continued

Tap #	Time delay	Mid height ZMC	Mid height ZMS	Shell thickness
23	4.6000	17.2639	14.8381	0.3540
24	4.8000	17.6143	15.1886	0.3470
25	5.0000	17.9580	15.5322	0.3404
26	5.2000	18.2954	15.8696	0.3344
27	5.4000	18.6267	16.2009	0.3283
28	5.6000	18.9522	16.5264	0.3227
29	5.8000	19.2722	16.8464	0.3173
30	6.000	19.5871	17.1613	0.3124
31	6.2000	19.8970	17.4712	0.3074
32	6.4000	20.2021	17.7764	0.3029
33	6.6000	20.5029	18.0771	0.2985
34	6.8000	20.7993	18.3735	0.2943
35	7.0000	21.0916	18.6658	0.2902
36	7.2000	21.3799	18.9541	0.2864
37	7.4000	21.6644	19.2386	0.2826
38	7.6000	21.9452	19.5195	0.2791
39	7.8000	22.2227	19.7969	0.2758
40	8.0000	22.4967	20.0710	0.2724
41	8.2000	22.7675	20.3417	0.2691
42	8.4000	23.0351	20.6093	0.2661
43	8.6000	23.2996	20.8738	0.2630
44	8.8000	23.5612	21.1355	0.2602

Table 8.3. Continued

Tap #	Time delay	Mid height ZMC	Mid height ZMS	Shell thickness
45	9.0000	23.8201	21.3943	0.2574
46	9.2000	24.0761	21.6503	0.2547
47	9.4000	24.3294	21.9037	0.2521
48	9.6000	24.5803	22.1545	0.2496
49	9.8000	24.8286	22.4028	0.2470
50	10.0000	25.0744	22.6486	0.2447
51	10.2000	25.3180	22.8922	0.2424
52	10.4000	25.5593	23.1335	0.2402
53	10.6000	25.7983	23.3725	0.2379
54	10.8000	26.0352	23.6094	0.2358
55	11.0000	26.2700	23.8442	0.2337
56	11.2000	26.5027	24.0769	0.2317
57	11.4000	26.7334	24.3076	0.2298
58	11.6000	26.9622	24.5364	0.2278
59	11.8000	27.1891	24.7633	0.2259

IX. APPENDIX B: WATFIV COMPUTER PROGRAM FOR CALCULATING
THE DISTRIBUTION OF THE DIFFERENTIAL
ISOTROPIC SCATTERED POWER VS CROSSPATH
DISTANCE

```

C *****
C *
C *           MAIN PROGRAM #1 USED FOR UNEQUAL
C *           ANTENNAS ELEVATION
C *
C * PURPOSE
C *
C *   THIS PROGRAM IS USED TO CALCULATE THE DISTRIBUTION OF
C *   THE DIFFERENTIAL ISOTROPIC SCATTERED POWER AS A FUNCTION OF
C *   THE CROSSPATH DISTANCE FOR EACH TIME DELAY SHELL IN A
C *   TROPOSPHERIC SCATTER LINK UTILIZING RAKE RECEIVER . THE
C *   PROGRAM APPROXIMATES THE TIME DELAY SHELLS AS A CONFOCAL
C *   CYLINDERS NEAR MIDPATH . ONLY THE POWER CONFINED TO THE 3-DB
C *   BOUNDARIES OF BOTH THE TRANSMITTING AND RECEIVING ANTENNAS
C *   IS CALCULATED.
C *
C *   A CROSS SECTION OF THE 3-DB ANTENNAS PATTERNS IN THE
C *   Y-Z PLANE AT THE MIDPATH CAN BE APPROXIMATED BY A CIRCLE,
C *   WHICH INTERSECTS WITH EACH TIME DELAY SHELL . THE 3-DB
C *   BOUNDARIES ALONG-THE-PATH AND CROSSPATH ARE FOUND FOR EACH
C *   TIME DELAY SHELL . AT ANY CROSSPATH DISTANCE ,A LINEAR
C *   RELATIONSHIP BETWEEN THE ALONG-THE-PATH AND CROSSPATH
C *   BOUNDARIES IS ASSUMED . THE SCATTERED POWER AT ANY
C *   CROSSPATH DISTANCE Y IS CALCULATED USING EQUATION 3.22 WITH
C *   ASSUMPTIONS GIVEN IN SECTION III.C.1 . THE CLACULATED POWER
C *   IS THEN NORMALIZED TO THE POWER SCATTERED FROM THE GREAT
C *   CIRCLE PLANE . A GAUSSIAN LEAST SQUARE FIT IS ALSO CALCULATED
C *   . IT SHOULD BE NOTICED THAT THE ELEVATIONS ARE ALWAYS REFERED
C *   TO THE CHORD JOINING THE TRANSMITTER AND THE RECEIVER . THE
C *   ORIGIN OF THE COORDINATE SYSTEM IS CHOSEN TO BE AT THE
C *   RECEIVER LOCATION FOR CONVENIANCE . THE PROGRAM ASSUMES THAT
C *   THE DIFFERENCE IN THE ANTENNAS ELEVATION NO MORR THAN .5 DEG.
C *
C * DESCRIPTION OF PARAMETERS
C *
C *   D           : PATH LENGTH
C *   THPW        : HALF POWER BEAMWIDTH OF THE ANTENNAS .
C *               IDENTICAL TRANSMITTING AND RECEIVING ANTENNAS
C *               ARE ASSUMED .
C *   PHT,PHR    : ELEVATION OF THE TRANSMITTING AND RECEIVING
C *               ANTENNAS RESPECTIVELY
C *   TAU(N)     : DIFFERENTIAL DELAY
C *   ZMC(N),ZMS(N) : MID SHELL HEIGHTS FROM THE CHORD AND THE

```

```

C      *          SURFACE RESPECTIVELY          *
C      *  DZ(N)    : SHELL THICKNESS            *
C      *  YP(J)    : CROSSPATH DISTANCE         *
C      *  PD(J)    : DIFFERENTIAL ISOTROPIC SCATTERED POWER *
C      *          CORRESPONDING TO CROSSPATH DISTANCE YP(J) *
C      *  X1P(J),X2P(J) : THE X-BOUNDARIES OF TIME DELAY SHELL *
C      *          CORRESPONDING TO CROSSPATH DISTANCE YP(J) *
C      *  Z1P(J),Z2P(J) : THE Z-BOUNDARIES OF TIME DELAY SHELL *
C      *          CORRESPONDING TO CROSSPATH DISTANCE YP(J) *
C      *
C      * SUBROUTINE CALL  UNEQU                  *
C      * SUBROUTINE CALL  POWER                 *
C      *
C      *****
C      REAL ZC(130),ZS(130),TAU(130),DZ(130),PD(30),ZMC(130),X1(130),
+X2(130),YP(30),ZP(30),Z1P(30),Z2P(30),X1P(30),X2P(30),PL(30),
+YP2(30)
      PI=3.14159265
      D=406.0
      THPW=2.6*PI/180
      HPW=THPW/2
      PHR=D/17000.+1.0*PI/180.
      PHT=D/17000.+2.5*PI/180.
      TN=TAN(D/17000.)
      SN= SIN(D/17000.)
      RG=8500.*TN
      XC=8500.*SN
      ZGC=XC*TN
      ZSC=8500.-XC/TN
      DELTA=0.2
      TAU(1)=0.0
      ZC(1)=ZGC
      ZS(1)=ZC(1)-ZSC
      PRINT 1
1  FORMAT('1','TAP #',2X,'TIME DELAY',2X,'MID HEIGHT ZMC',2X,
+'MID HEIGHT ZMS',2X,'SHELL THICKNESS',/)
      DO 10 I=2,101

```

```

TAU(I)=TAU(I-1)+DELTA
ZC(I)=SQRT((RG+.15*TAU(I))**2-XC**2)
ZS(I)=ZC(I)-ZSC
DZ(I-1)=ZC(I)-ZC(I-1)
ZMC(I-1)=(ZC(I-1)+ZC(I))*0.5
ZMS=ZMC(I-1)-ZSC
PRINT 2,I-1,TAU(I),ZMC(I-1),ZMS,DZ(I-1)
FORMAT(' ',I3.6X,F7.4,6X,3(F7.4,12X))
CONTINUE
CALL UNEQU(D,HPW,PHR,PHT,ZMC,Z1,Z2,Z3,Z4,XZ2,XZ3,X1,X2)
Z1,Z2,Z3,Z4 ARE THE BOUNDARIES OF THE COMMON VOLUME IN THE
Z DIRECTION . XZ2, XZ3 ARE THE BOUNDARIES IN THE X DIRECTION
PRINT 5, Z1,Z2,Z3,Z4,XZ2,XZ3
FORMAT('1',2X,'Z1=',F8.4,3X,'Z2=',F8.4,3X,'Z3=',F8.4,3X,'Z4=',F8.4
+,3X,'XZ2=',F8.4,3X,'XZ3=',F8.4)
ZCA=D*SIN(PHT)*SIN(PHR)/SIN(PI-PHT-PHR)
XCA=ZCA/TAN(PHR)
RA=(Z4-Z1)/2
DO 20 K=1,90
IF((ZMC(K).GT.(ZCA-RA)).AND.(ZMC(K).LT.(ZCA+RA)))THEN
Y1T AND Z1T ARE THE Y AND Z INTERSECTION OF THE 3-DB ANTENNA
PATTERNS WITH TIME DELAY SHELL
Z1T=(ZMC(K)*ZMC(K)+ZCA*ZCA-RA*RA)/(2*ZCA)
Y1T=SQRT(ZMC(K)*ZMC(K)-Z1T*Z1T)
PHI=ARSIN(Y1T/ZMC(K))
DPHI=PHI/20
X1(K)=X1(K)-XCA
X2(K)=X2(K)-XCA
DO 30 J=1,21
YP(J)=ZMC(K)*SIN((J-1)*DPHI)
ZP(J)=ZMC(K)*COS((J-1)*DPHI)
X1P(J)=X1(K)*(PHI-(J-1)*DPHI)/PHI
X2P(J)=X2(K)*X1P(J)/X1(K)
X1P(J)=X1P(J)+XCA
X2P(J)=X2P(J)+XCA
Z1P(J)=ZP(J)+DZ(K)/2

```



```

Z2P(J)=ZP(J)-DZ(K)/2
30 CONTINUE
CALL POWER(D,THPW,PHR,PHT,X1P,X2P,Z1P,Z2P,YP,PO)
PRINT 3,K,ZMC(K),Z1T,Y1T,PO(1)
3 FORMAT('1',2X,I3,2X,4(F11.7,3X))
C NORMALIZING THE DIFFERENTIAL POWER TO THE GREAT CIRCLE POWER
YS=PO(1)
DO 40 J=1,21
PO(J)=PO(J)/YS
PRINT 4,YP(J),PO(J)
4 FORMAT('0',2X,2(F11.7,2X))
IF(J.NE.21)THEN
C PL(J) IS THE LOGARITHM OF THE DIFFERENTIAL SCATTERED POWER
C YP2(J) IS THE CROSSPATH DISTANCE SQUARED BOTH PARAMETERS ARE
C USE IN THE LEAST SQUARE GAUSSIAN FIT
PL(J)=ALOG(PO(J))
YP2(J)=YP(J)*YP(J)
ENDIF
40 CONTINUE
C GAUSSIAN LEAST SQUARE FIT TO THE DIFFERENTIAL SCATTERED POWER
SPL=0.0
SYP2=0.0
SPLY=0.0
SYP22=0.0
DO 55 I=1,20
SPL=SPL+PL(I)
SYP2=SYP2+YP2(I)
SPLY=SPLY+PL(I)*YP2(I)
SYP22=SYP22+YP2(I)*YP2(I)
55 CONTINUE
C AI IS THE REQUIRED PARAMETER TO BE USED EQUATION 3.21
AI=(SPLY-SPL*SYP2/20.0)/(SYP22-SYP2*SYP2/20.0)
BO=(SPL/20.0)-(AI*SYP2/20.0)
BO=EXP(BO)
PRINT,AI,BO

```

```

20      ENDIF
        CONTINUE
        STOP
        END
C      *****
C      * THE SUBROUTINE UNEQ CALCULATES THE GREAT CIRCLE X BOUNDARIES
C      * FOR EACH TIME DELAY SHELL . IT ALSO CALCULATES THE BOUNDARIES
C      * OF THE COMMON VOLUME .ITS INPUTS ARE THE PATH LENGTH,THE
C      * BEAMWIDTH,THE ANTENNA ELEVATIONS AND THE MID SHELL HEIGHT
C      *
C      *****
SUBROUTINE UNEQU(D,HPW,PHR,PHT,ZMC,Z1,Z2,Z3,Z4,XZ2,XZ3,X1,X2)
REAL ZMC(130),X1(130),X2(130)
SR=SIN(PHR)
ST=SIN(PHT)
CSR=COS(PHR)
CST=COS(PHT)
TS=TAN(HPW)
AR=SR*SR-(CSR*CSR)*(TS*TS)
AT=ST*ST-(CST*CST)*(TS*TS)
Z1=D*(TAN(PHR-HPW))*(TAN(PHT-HPW))/(TAN(PHT-HPW)+
+TAN(PHR-HPW))
Z2=D*(TAN(PHR-HPW))*(TAN(PHT+HPW))/(TAN(PHR-HPW)+
+TAN(PHT+HPW))
Z3=D*(TAN(PHR+HPW))*(TAN(PHT-HPW))/(TAN(PHR+HPW)+
+TAN(PHT-HPW))
Z4=D*(TAN(PHR+HPW))*(TAN(PHT+HPW))/(TAN(PHR+HPW)+
+TAN(PHT+HPW))
XZ2=Z2/TAN(PHR-HPW)
XZ3=Z3/TAN(PHR+HPW)
DO 30 I=1,100
X1(I)=0.0
X2(I)=0.0
IF((ZMC(I).GT.Z1).AND.(ZMC(I).LE.Z4))THEN

```

```

BR=-2*ZMC(I)*SR*CSR*(1+TS*TS)
CR=ZMC(I)*ZMC(I)*CSR*CSR-(SR*SR)*(TS*TS)
BT=2*ZMC(I)*ST*CST*(1+TS*TS)
CT=ZMC(I)*ZMC(I)*CST*CST-(ST*ST)*(TS*TS)
B1=BT
BT=B1-2*406*AT
CT=CT+406*406*AT-406*B1
XR1=(-BR+SQRT(BR*BR-4*AR*CR))/(2*AR)
XR2=(-BR-SQRT(BR*BR-4*AR*CR))/(2*AR)
XT1=(-BT+SQRT(BT*BT-4*AT*CT))/(2*AT)
XT2=(-BT-SQRT(BT*BT-4*AT*CT))/(2*AT)
IF((ZMC(I).GT.Z2).AND.(ZMC(I).LT.Z3))GO TO 200
IF(ZMC(I).LE.Z2)GO TO 100
IF(ZMC(I).GE.Z3)GO TO 300
IF(XR1.GT.XR2)THEN
  X11=XR1
ELSE
  X11=XR2
ENDIF
IF(XT1.GT.XT2)THEN
  X12=XT2
ELSE
  X12=XT1
ENDIF
GO TO 400
IF(XT1.GT.XT2)THEN
  X11=XT1
  X12=XT2
ELSE
  X11=XT2
  X12=XT1
ENDIF
GO TO 400
IF(XR1.GT.XR2)THEN
  X12=XR2
ELSE
  X12=XR1
ENDIF
100
200
300

```

```

      IF (XT1.GT.XT2) THEN
      X11=XT1
      ELSE
      X11=XT2
      ENDIF
400  X1(I)=X11
      X2(I)=X12
      ENDIF
30   CONTINUE
      RETURN
      END

C   *****
C   * THE SUBROUTINE POWER CALCULATES THE DIFFERENTIAL ISOTROPIC *
C   * SCATTERED POWER AT DISCRETE CROSSPATH DISTANCES FOR EACH *
C   * TIME DELAY SHELL . ITS INPUTS ARE THE X AND Z BOUNDARIES *
C   * FOR THE CORRESPONDING DISCRETE CROSSPATH DISTANCES TO BE USED *
C   * AS INTEGRATION LIMITS , THE HALF-POWER BEAMWIDTH,AND THE *
C   * ANTENNAS ELEVATIONS . THE PROGRAM UTILIZES A FIVE-POINT *
C   * GAUSS-LEGENDRE INTEGRATION TECHNIQUE . *
C   *****
      SUBROUTINE POWER(D,THPW,PHR,PHT,X1P,X2P,Z1P,Z2P,YP,PO)
      REAL X1P(30),X2P(30),Z1P(30),Z2P(30),X(5),Z(5),A(5),B(5),
+YP(30),PO(30)
      A(1)=.236926885
      A(2)=.47862867
      A(3)=.568889
      A(4)=A(2)
      A(5)=A(1)
      B(1)=-0.9061798
      B(2)=-0.5384693
      B(3)=0.0
      B(4)=-B(2)
      B(5)=-B(1)
      EX=2/((.85*THPW)**2)
      PHH=PHR**2+PHT**2

```

```

DO 60 M=1,21
PO(M)=0.0
YPP=YP(M)*YP(M)
DO 40 I=1,5
X(I)=.5*(X1P(M)-X2P(M))*B(I)+.5*(X1P(M)+X2P(M))
Z(I)=0.5*(Z1P(M)-Z2P(M))*B(I)+0.5*(Z1P(M)+Z2P(M))
CONTINUE
DO 45 I=1,5
DX=1/X(I)
DXX=DX*DX
DMX=1/(D-X(I))
DMXX=DMX*DMX
DO 50 J=1,5
FX=0.0
ARS=-EX*(PHH+(Z(J)*Z(J)+YPP)*(DXX+DMXX)-2*Z(J))*(PHT*DMX+PHR*DX)
R1=1/DXX+Z(J)*Z(J)+YPP
R2=1/DMXX+Z(J)*Z(J)+YPP
THS=.5*D*SQRT(Z(J)*Z(J)+YPP)*DMX*DX
FX=EXP(ARS)*1/((SIN(THS))*3.666667))*((1/R1))*((1/R2)
PD(M)=PO(M)+A(I)*A(J)*FX
CONTINUE
50 CONTINUE
45 CONTINUE
60 PO(M)=PO(M)*(X1P(M)-X2P(M))*(Z1P(M)-Z2P(M))/4
CONTINUE
RETURN
END
$ENTRY

```

```

C *****
C *                               MAIN PROGRAM #2 USED FOR EQUAL *
C *                               ANTENNAS ELEVATION *
C *
C * PURPOSE *
C * THIS PROGRAM IS USE TO CALCULATE THE DISTRIBUTION OF THE *
C * ISOTROPIC SCATTERED POWER AS A FUNCTION OF THE CROSSPATH *
C * DISTANCE FOR EACH TIME DELAY SHELL IN A TROPOSPHERIC SCATTER *
C * LINK UTILIZING RAKE RECEIVER . ALL THE PARAMETERS AND THE *
C * COMMENTS EXPLAINED IN MAIN PROGRAM #1 FOR UNEQUAL ELEVATIONS*
C * CARRY THE SAME INTERPRETATION IN THIS PROGRAM AND WILL NOT *
C * BE EXPLAINED HERE . THE COORDINATE SYSTEM IS CONVENIENTLY *
C * CHOSEN TO BE AT MIDPATH . IT SHOULD BE NOTICED THAT THE *
C * ANTENNAS ELEVATION IS EQUAL . *
C *
C * SUBROUTINE CALL EQUAL *
C * SUBROUTINE CALL POWER *
C *
C *****
REAL ZC(130),ZS(130),TAU(130),DZ(130),PO(30),ZMC(130),X1(130),
+X2(130),YP(30),ZP(30),Z1P(30),Z2P(30),X1P(30),X2P(30),PL(30),
+YP2(30)
PI=3.14159265
D=406.0
THPW=2.6*PI/180
HPW=THPW/2
PHR=D/17000.+HPW
PHT=PHR
TN=TAN(D/17000.)
SN= SIN(D/17000.)
RG=8500.*TN
XC=8500.*SN
ZGC=XC*TN
ZSC=8500.-XC/TN
DELTA=0.2
TAU(1)=0.0

```

```

ZC(I)=ZGC
ZS(I)=ZC(I)-ZSC
PRINT 1
FORMAT('1','TAP #','2X','TIME DELAY','3X','MID HEIGHT ZMC','3X',
+ 'MID HEIGHT ZMS','3X','SHELL THICKNESS',/)
DO 10 I=2,101
TAU(I)=TAU(I-1)+DELTA
ZC(I)=SORT((RG+.15*TAU(I))*2-XC**2)
ZS(I)=ZC(I)-ZSC
DZ(I-1)=ZC(I)-ZC(I-1)
ZMC(I-1)=(ZC(I-1)+ZC(I))*0.5
ZMS=ZMC(I-1)-ZSC
PRINT 2,I-1,TAU(I),ZMC(I-1),ZMS,DZ(I-1)
FORMAT(' ','13.6X,F7.4,6X,3(F7.4,10X))
CONTINUE
CALL EQUAL(D,HPW,PHR,ZMC,Z1,Z2,Z3,Z4,XZ2,XZ3,X1,X2)
PRINT 5, Z1,Z2,Z3,Z4,XZ2,XZ3
FORMAT('1','2X','Z1=',F8.4,3X,'Z2=',F8.4,3X,'Z3=',F8.4,3X,'Z4=',F8.4,
+ ,3X,'XZ2=',F8.4,3X,'XZ3=',F8.4)
ZA=(D/2)*TAN(PHR)
RA=(D/4)*(TAN(PHR+HPW)-TAN(PHR-HPW))
DO 20 K=1,90
IF((ZMC(K).GT.Z1).AND.(ZMC(K).LT.Z4))THEN
Z1T=(ZMC(K)+ZMC(K)+ZA*ZA-RA*RA)/(2*ZA)
Y1T=SORT(ZMC(K)*ZMC(K)-Z1T*Z1T)
PHI=ARSIN(Y1T/ZMC(K))
DPHI=PHI/20
DO 30 J=1,21
YP(J)=ZMC(K)*SIN((J-1)*DPHI)
ZP(J)=ZMC(K)*COS((J-1)*DPHI)
X1P(J)=X1(K)*(PHI-(J-1)*DPHI)/PHI
X2P(J)=X2(K)*X1P(J)/X1(K)
Z1P(J)=ZP(J)+DZ(K)/2
Z2P(J)=ZP(J)-DZ(K)/2
CONTINUE

```

30

```

CALL POWER(D,THPW,PHR,PHT,X1P,X2P,Z1P,Z2P,YP,PO)
PRINT 3,K,ZMC(K),Z1T,Y1T,PO(1)
3  FORMAT('1',2X,I3,2X,4(F11.7,3X))
   YS=PO(1)
   DO 40 J=1,21
   PO(J)=PO(J)/YS
   PRINT 4,YP(J),PO(J)
4  FORMAT('0',2X,2(F11.7,2X))
   IF(J.NE.21)THEN
   PL(J)=ALOG(PO(J))
   YP2(J)=YP(J)*YP(J)
   ENDIF
40  CONTINUE
   SPL=0.0
   SYP2=0.0
   SPLY=0.0
   SYP22=0.0
   DO 55 I=1,20
   SPL=SPL+PL(I)
   SYP2=SYP2+YP2(I)
   SPLY=SPLY+PL(I)*YP2(I)
   SYP22=SYP22+YP2(I)*YP2(I)
55  CONTINUE
   AI=(SPLY-SPL*SYP2/20.0)/(SYP22-SYP2*SYP2/20.0)
   BO=(SPL/20.0)-(AI*SYP2/20.0)
   BO=EXP(BO)
   PRINT,AI,BO
   ENDIF
20  CONTINUE
   STOP
   END
C  *****
C  * THE SUBROUTINE EQUAL CALCULATES THE X AND Z BOUNDARIES *
C  * OF EACH TIME DELAY SHELL CORRESPONDING TO THE GREAT CIRCLE *
C  * PATH . IT ALSO CALCULATES THE BOUNDARIES OF THE COMMON *
C  * VOLUME . *
C  *****

```



```

SUBROUTINE EQUAL(D,HPW,PHR,ZMC,Z1,Z2,Z3,Z4,XZ2,XZ3,X1,X2)
REAL X1(130),X2(130),ZMC(130)
S=SIN(PHR)
CS=COS(PHR)
TS=TAN(HPW)
A1=S*S-(CS*CS)*(TS*TS)
Z1=(D/2)*TAN(PHR-HPW)
Z2=D*(TAN(PHR-HPW)*TAN(PHR+HPW))/(TAN(PHR-HPW)+TAN(PHR+HPW))
Z3=Z2
Z4=(D/2)*TAN(PHR+HPW)
XZ2=Z2/TAN(PHR+HPW)
XZ3=Z2/TAN(PHR-HPW)
DO 20 I=1,100
X1(I)=0.0
X2(I)=0.0
IF((ZMC(I).GT.Z1).AND.(ZMC(I).LT.Z4))THEN
B1=-2*ZMC(I)*S*CS*(1+TS*TS)
C1=ZMC(I)*ZMC(I)*(CS*CS-(S*S)*(TS*TS))
X11=(-B1+SQRT(B1*B1-4*A1*C1))/(2*A1)
X12=-(B1/A1)-X11
X11=ABS(X11-D/2)
X12=ABS(X12-D/2)
IF(X11.GT.X12)THEN
X11=X12
ENDIF
X1(I)=X11
X2(I)=-X11
ENDIF
CONTINUE
RETURN
END

```

20

```

C *****
C SUBROUTINE POWER CALCULATES THE DIFFERENTIAL SCATTERED POWER
C CORRESPONDING TO A DIFFERENTIAL CROSSPATH DISTANCE. ITS
C INPUTS ARE ; THE PATH LENGTH, THE HALF-POWER BEAMWIDTH, THE
C THE ANTENNAS ELEVATION, AND THE X AND Z BOUNDARIES OF THE
C CORRESPONDING CROSSPATH DISTANCE. THE SUBROUTINE UTILIZES A
C FIVE-POINT GAUSS-LEGENDRE NUMERICAL INTEGRATION TECHNIQUE.
C
C
C *****
C SUBROUTINE POWER(D,THPW,PHR,PHT,X1P,X2P,Z1P,Z2P,YP,PO)
C REAL X1P(30),X2P(30),Z1P(30),Z2P(30),X(5),Z(5),A(5),B(5),
C +YP(30),PO(30)
C A(1)=.236926885
C A(2)=.47862867
C A(3)=.568889
C A(4)=A(2)
C A(5)=A(1)
C B(1)=-0.9061798
C B(1)=-0.9061798
C B(2)=-0.5384693
C B(3)=0.0
C B(4)=-B(2)
C B(5)=-B(1)
C EX=2/((.85*THPW)**2)
C PHH=PHR**2+PHT**2
C DO 60 M=1,21
C PO(M)=0.0
C YP=YP(M)*YP(M)
C DO 40 I=1,5
C X(I)=.5*(X1P(M)-X2P(M))*B(I)+.5*(X1P(M)+X2P(M))
C Z(I)=0.5*(Z1P(M)-Z2P(M))*B(I)+0.5*(Z1P(M)+Z2P(M))
C CONTINUE
C DO 45 I=1,5
C DMX=.25*D*D-X(I)*X(I)
C DX=DMX+2*X(I)*X(I)
C DMXX=DMX*DMX
40

```

```

DP=0.5#D+X(I)
DN=DP-2#X(I)
DPP=DP#DP
DNN=DN#DN
DO 50 J=1.5
FX=0.0
ARS=-EX*(PHH+2*(Z(J)**2+YPP)*DX/DMXX-2*PHR#Z(J)/DP-2*PHT#Z(J)/DN)
R1=DNN+Z(J)#Z(J)+YPP
R2=DPP+Z(J)#Z(J)+YPP
T=HS=.5#D#SQRT(Z(J)#Z(J)+YPP)/DMX
FX=EXP(ARS)*((1/(SIN(THS)))**3.666667))*(1/R1)*(1/R2)
PO(M)=PO(M)+A(I)#A(J)#FX
CONTINUE
CONTINUE
PO(M)=PO(M)#X1P(M)*(Z1P(M)-Z2P(M))/2
CONTINUE
RETURN
END
$ENTRY
50
45
60

```

X. APPENDIX C: WATFIV COMPUTER PROGRAM FOR CALCULATING
THE DELAY POWER SPECTRA BASED ON AN
ANISOTROPIC SCATTERING MODEL

```

C *****
C *
C *           MAIN PROGRAM
C *
C * PURPOSE
C *   TO EVALUATE THE DELAY POWER SPECTRA OF TROPOSCATTER LINKS*
C *   NORMALIZED TO UNIT AREA. ALSO THE PROGRAM CALCULATES THE
C *   DIFFERENT PARAMETERS OF MULTIPATH SPREAD, MEAN DELAY, SKEW
C *   ,AND EXCESS. IT CALCCULATE THE DELAY POWER SPECTRA BASED ON
C *   AN ANISOTROPIC SCATTERING MODEL PRESENTED IN CHAPTER IV .
C *
C * DESCRIPTION OF PARAMETERS
C *
C *   N           : NUMBER OF POINTS FOR WHICH THE DELAY POWER
C *               SPECTRUM IS CALCULATED . IT IS CHOSEN TO BE
C *               EVEN INTEGER
C *   D           : PATH LENGTH IN KM
C *   R           : EFFECTIVE EARTH RADIUS IN KM
C *   HPBW        :HALF POWER BEAMWIDTH OF THE ANTENNAS . IDENTICAL
C *               TRANSMITTING AND RECEIVING ANTENNAS ARE ASSUMED
C *   DELTA       :RESOLUTION OF THE DELAY POWER SPECTRUM
C *   GRT, GRR    :GRAZING ELEVATIONS OF BOTH THE TRANSMITTER AND
C *               THE RECEIVER ABOVE THE CHORD RESPECTIVELY
C *   ELT, ELR    :ELEVATIONS OF TRANSMITTING AND RECEIVING ANTENNA
C *               BEAMS ABOVE THE CHORD
C *   TAU(N)      :IS THE TIME DELAY WITH RESPECT TO THE HORIZON
C *   X(N)        :IS A NORMALIZED DELAY PARAMETER
C *   P(N)        :IS THE VALUE OF THE DELAY POWER SPECTRA CORRESP-
C *               ONDING TO DELAY TAU(N)
C *
C * SUBROUTINE CALL : POWER
C * SUBROUTINE CALL : SIMPSN
C *
C *****
C
C   REAL P(512),X(512),PT(512),PT2(512),PT3(512),PT4(512),TAU(512),
+ANIS(512)

```

```

N=128
M=7
N1=N-1
N2=(2*M)/2
PI=3.141592654
D=406.0
R=8500.0
HPBW=2.6*PI/180.0
C THE MINIMUM NORMALIZED DELAY BASED ON SMOOTH EARTH HORIZONS
DMIN=D*D/(8*R*R)
DELTA=0.02
C GRAZING ELEVATIONS ABOVE THE CHORD BASED ON SMOOTH EARTH
C HORIZONS
GRT=D/(2*R)
GRR=D/(2*R)
ELT=GRT
ELR=GRR
DO 10 I=1,N
TAU(I)=(I-1)*DELTA
10 X(I)=DMIN+0.3*TAU(I)/D
C THE AN ANISOTROPY PROFILE IS INSERTED HERE AS THE MATRIX
C ANIS(N) CALCULATED FOR EACH TIME DELAY
DO 200 I=1,N
200 ANIS(I)=1+8*TAU(I)
C CALL TO SUBROUTINE POWER TO CALCULATE THE DELAY POWER SPECTRA
C
CALL POWER(HPBW,X,ELT,ELR,GRT,GRR,N,P,ANIS)
PRINT 1
1 FORMAT('1','POINT#',4X,'NORMLAIZED DELAY',15X,'ZDPOWER')
DO 20 I=1,N
PRINT 3,I,X(I),P(I)
3 FORMAT(' ',I3,6X,E14.5,14X,E14.5)
20 CONTINUE
C CALL TO SUBROUTINE SIMPSN TO CALCULATE THE AREA UNDER THE DELAY

```

```

C    POWER SPECTRA
    CALL SIMPSN(P,DELTA,N1,SP)
    PRINT,'AREA UNDER DELAY POWER SPECTRA', SP
    PRINT 5
5    FORMAT('1','POINT#',2X,'TIME DELAY',9X,'NORMALIZED DELAY',13X,
+ 'NORMALIZED ZDPOWER')
    DO 30 I=1,N
    P(I)=P(I)/SP
    PT(I)=P(I)*TAU(I)
    PRINT 7,I,TAU(I),X(I),P(I)
7    FORMAT(' ',I3,6X,F5.3,14X,E14.5,14X,E14.5)
30   CONTINUE
    CALL SIMPSN(P,DELTA,N1,SP)
    CALL SIMPSN(PT,DELTA,N1,SP1)
    DO 40 I=1,N
    XSP=TAU(I)-SP1
    PT2(I)=P(I)*(XSP**2)
    PT3(I)=P(I)*(XSP**3)
40   PT4(I)=P(I)*(XSP**4)
    PRINT 9
9    FORMAT('1','AREA',10X,'CENTROID',8X,'2ND MOMENT',5X,' SKEW ',
+5X,' EXCESS ',5X,'MULTIPATH SPREAD')
    CALL SIMPSN(PT2,DELTA,N1,SP2)
    CALL SIMPSN(PT3,DELTA,N1,SP3)
    CALL SIMPSN(PT4,DELTA,N1,SP4)
C    THE MULTIPATH SPREAD PARAMETER
    PSP=SQRT(SP2)
C    THE SKEW PARAMETER WHICH MEASURE THE ASYMMETRY OF THE DELAY
C    POWER SPECTRA
    BETA3=(SP3/SP2**1.5)
C    THE EXCESS PARAMETER WHICH MEASURE THE PEAKNESS OF THE DELAY
C    POWER SPECTRA
    EXCESS=(SP4/SP2**2)
    PRINT 11,SP,SP1,SP2,BETA3,EXCESS,PSP

```

11 FORMAT(' ',/,'6(F9.6,6X))

STOP

END

C *****

C * THE SUBROUTINE POWER CALCULATES THE DELAY POWER SPECTRA FOR *

C * TROPOSCATTER LINKS . ITS INPUTS ARE THE ANTENNA HALF POWER BEAM-

C * WIDTH, THE GRAZING ELEVATIONS, THE CENTER BEAM ELEVATIONS, *

C * THE ANISOTROPY PROFILE MATRIX , AND THE NUMBER OF DELAY POINTS *

C * THE ANTENNAS ARE ASSUMED TO BE GAUSSIAN IN SHAPE. THE SUBROUTINE*

C * POWER UTILIZES A GAUSS-LEGENDRE SIX-POINT NUMERICAL INTEGRATION *

C * TECHNIQUE .

C *

C *****

C SUBROUTINE POWER(HPBW,X,ELT,ELR,GRT,GRR,N,P,ANIS)

C REAL P(512),X(512),A(10),B(10),ANIS(512)

C CONSTANTS OF THE NUMERICAL INTEGRATION

A(1) = .4679139346

A(2) = .3607615730

A(3) = .1713244924

A(4) = A(3)

A(5) = A(2)

A(6) = A(1)

B(1) = .2386191861

B(2) = .6612093865

B(3) = .9324695142

B(4) = -B(3)

B(5) = -B(2)

B(6) = -B(1)

EX = 1 / (0.36 * HPBW * HPBW)

T = 11.0 / 3.0

P(1) = 0.0

ELV = ELT * ELT + ELR * ELR

DO 20 K = 2, N

P(K) = 0.0


```

SQ=SQRT(2*X(K))
AL=GRT/SQ
BL=SQ/GRR
DO 30 I=1,6
XIP=0.5*(BL-AL)*B(I)+0.5*(BL+AL)
X1=1/XIP
X2=XIP+X1
X22=XIP*XIP+X1*X1
ARS=-EX*(SQ*SQ*X22-2*SQ*(ELR*X1+ELT*XIP)+ELV)
FX=EXP(ARS)*X1*(1/X2**(T-2))
P(K)=P(K)+A(I)*FX
30 CONTINUE
P(K)=P(K)*(1/X(K)**(1+T/2))*((BL-AL)/2)*(ANIS(K)**2)
20 CONTINUE
RETURN
END
C *****
C * THE SUBROUTINE SIMPSN CALCULATES THE AREA UNDER A CERTAIN CURVE *
C * .IT UTILIZES SIMPSON NUMERICAL INTEGRATION METHOD .ITS INPUTS *
C * ARE THE VALUES OF THE FUNCTION,THE NUMBER OF POINTS, AND THE STEP *
C * SIZE *
C *
C *****
SUBROUTINE SIMPSN(P,DELTA,N1,SP)
REAL P(512)
K=N1-1
L=K-1
SPE=0.0
SPO=0.0
DO 10 I=2,K,2
10 SPE=SPE+P(I)
DO 20 I=3,L,2
20 SPO=SPO+P(I)
SP=(DELTA/3)*(P(1)+4*SPE+2*SPO+P(N1))
RETURN
END
$ENTRY

```